論文 / 著書情報
Article / Book Information

題目(和文)	Al-Mn合金の再結晶挙動に及ぼすMn含有分散粒子ならびに固溶Mn原子の影響
Title(English)	Effects of Mn Containing Dispersoids and Mn Solute Atoms on the Recrystallization Behavior of an Al-Mn Alloy
著者(和文)	LEEYONG-CHUL
Author(English)	YongChul Lee
出典(和文)	学位:博士（工学）, 学位授与機関:東京工業大学, 報告番号:甲第9615号, 授与年月日:2014年9月25日, 学位の種別:課程博士, 審査員:里　達雄,小林　郁夫,熊井　真次,中村　吉男,曽根　正人
Citation(English)	Degree:, Conferring organization: Tokyo Institute of Technology, Report number:甲第9615号, Conferred date:2014/9/25, Degree Type:Course doctor, Examiner:,,,,
学位種別(和文)	博士論文
Type(English)	Doctoral Thesis

Effect of Mn Containing Dispersoids and Mn Solute Atoms on the Recrystallization Behavior of an Al-Mn Alloy

by

Lee YongChul

Doctoral Thesis

Department of Metallurgy and Ceramics Science
Tokyo Institute of Technology

2014

Acknowledgements

My research and the present thesis could not be possible without following supports:

First and foremost, I would like to express my sincere gratitude to my supervisor, Prof. Tatsuo Sato, my vice supervisor, Prof. Equo Kobayashi and my assistant professor Hiroyasu Tezuka for their continuous support to my doctor study and research. I am grateful to Prof. Sato for his patience, motivation and immense knowledge in assisting my research. I would like to thank Prof. Kobayashi for his many useful suggestions and help all along during my life in Japan. I owe many thanks to assistant Prof. Tezuka for supporting many activities during my doctoral course.

I would like to express my thanks to Prof. Yoshio Nakamura, Prof. Shinji Kumai and Prof. Masato Sone for giving me valuable comments and ideas. With great points of three professors, I was able to enhance the value of this thesis throughout discussion and comments.

Moreover, I am profoundly grateful to Prof. Chun ByeongSeon at Chungnam National University in South Korea who gave me the great opportunity and encouraged me to study at Tokyo Institute of Technology.

I would like to thank my colleagues in Sato-Kobayashi Laboratory. I also thank Dr. Lee Hyunbom, Dr. Kim Yelim and Dr. Kim JaeHwang for their concern and encouragement and Kim SeongNyeong for her support and encouragement during staying in Japan.

I deeply appreciate scholarship and good dormitory from Japan Student Services Organization. I also deeply appreciate the financial support for research from Tokyo Institute of Technology Global COE program and The Light Metal Educational Foundation in Japan.

Finally, I am indebted to my parents and my younger sister SeulGi for their love and support.

August, 2014

Lee YongChul

Contents

Chapter 1

General introduction

1.1 Background

AA3xxx aluminum alloys contain manganese as a major alloying element and silicon and iron as minor alloying elements. The compositions of AA3xxx alloys are included in Table 1.1. The characteristic of these alloys is to have moderate mechanical strength, high ductility and excellent corrosion resistance. These alloys are widely used for architectural application, cooking utensils, bodies of beverage cans, packaging and heat exchanger by the sheet form [1-4]. The thermo-mechanical processes including homogenization, deformation and annealing treatments are generally applied to these alloys because the characteristics of microstructures such as the type, size, and distribution of constituent particles are greatly changed by each process [5-9]. Especially, during the homogenization treatment, a large amount of particles precipitate in the supersaturated matrix with Mn. These constituent particles have a significantly different size distribution, i.e. primary particles have a size of 1-5 μm and the precipitates of 50-200nm. It is established that larger particles (>1 μm) can act as the particle-stimulated nucleation (PSN) sites, which generally accelerate recrystallization. On the other hand, finer particles retard grain growth by pinning grain boundaries [10-

12] .The phenomena during thermo-mechanical processes are related very complicatedly. The Al-Mn alloy commonly referred to as the 3003 alloy is easy to understand these complicated phenomena in the 3xxx alloys.

1.2 Non-heat-treatable 3003 alloy

1.2.1 Al-Mn-Fe-Si phase diagrams

The equilibrium binary Al-Mn phase diagram is shown in Figure 1.2. The aluminum has the structure of Faced Center Cubic (FCC). The phase in equilibrium with Al is the orthorhombic Al_6Mn. This phase forms a eutectic with aluminum at 1.8 wt% and 658.5 °C. The Al_6Mn phase has the limited range of primary particle to 4.1 wt% Mn. The peritectic reaction of Al_4Mn occurs at above 4.1 wt% Mn. The Al_4Mn phase has a hexagonal structure [13-15].

In case of the Al-Fe-Mn, there are three kinds of primary phases such as Al, Al_3Fe and $Al_6(Mn,Fe)$ [15]. The maximum solubility of iron in aluminum is 0.03-0.04 wt%. Moreover, this is unchanged in the ternary alloys while the manganese solubility is decreased. The Al_3Fe phase has a monoclinic structure. In this ternary phase diagram, manganese can be replaced by iron due to similar lattice parameters between manganese and iron.

Figure 1.3 shows the equilibrium ternary Al-Mn-Si phase diagram. In case of the Al-Fe-Mn, a ternary phase is not formed while a ternary phase such as α-Al(Mn,Fe)Si is formed in the Al-Mn-Si ternary alloy. Relevant literature gives the stoichiometry of α-Al(Mn,Fe)Si as either α-$Al_{12}(Mn,Fe)_3Si$[17,19,21,23,24] or α-$Al_{15}(Mn,Fe)_3Si_2$[25]. These differences are probably due to Al atoms substituting for Si atoms [28].

Therefore, the following eutectic and peritectic reactions, as shown in Equation 1.1~1.4, may

occur during solidification depending on the chemistry of the alloy.

$$L \rightarrow Al(s) + Al_6(Mn,Fe) \quad (1.1)$$

$$L + Al_6(Mn,Fe) \rightarrow \alpha\text{-}Al(Mn,Fe)Si \quad (1.2)$$

$$L \rightarrow Al(s) + \alpha\text{-}Al(Mn,Fe)Si \quad (1.3)$$

$$Al_6(Mn,Fe) + Si \rightarrow \alpha\text{-}Al(Mn,Fe)Si + Al(s) \quad (1.4)$$

The crystal structures of Mn/Fe containing dispersoids are include in Table 1.2.

1.2.2 Intermetallic particles in 3003 aluminum alloy

Intermetallic compounds formed during the solidification of the alloy are generally referred to as constituent or insoluble particles, and usually have dimensions of 1-10 micrometers [16]. In as-cast 3003 ingots, the aluminum phase consists of the dendritic structure. Moreover, between dendrite arms the eutectic mixture containing the coarse Fe-rich intermetallic constituent particles is formed [17]. The particles are identified to be the orthorhombic $Al_6(Mn,Fe)$ and simple cubic α-Al(Mn,Fe)Si compounds [17-21]. The α-Al(Mn,Fe)Si phase has high hardness than the $Al_6(Mn,Fe)$ phase [20,22].

The nucleation, growth and coarsening of the small dispersoids in the intragranular regions also occur simultaneously with the evolution of constituent particles during homogenization. Particles precipitated from the solid solution matrix are usually referred to as secondary precipitates or dispersoid particles [18]. During homogenization in the as-cast 3xxx ingots, the supersaturated Mn, Fe, and Si in the matrix produce precipitates as fine dispersoid particles of α-Al(Mn,Fe)Si and/or $Al_6(Mn,Fe)$ [17]. Electrical conductivity measurement is considered as a simple method for indirect estimation of the dispersoids fraction because the

electrical conductivity can be correlated to the manganese in the solid solution [10-11].

1.3 Recovery and recrystallization

Recovery and recrystallization are thermally activated processes of restoring the structure after deformation. Recovery is the term referring to the changes in the properties of a deformed material, which occur prior to recrystallization. Recovery and recrystallization are competitive processes as they both are driven by the stored energy of the deformed state. In contrast to recrystallization, there is no clearly identifiable beginning or end of the recovery process.

1.3.1 Recovery

Recovery involves primarily changes in the dislocation structure of the material and may consist of a series of micro-mechanisms, i.e. cell formation, dislocation annihilation, sub-grain formation, and sub-grain growth. Obviously, the recovery rate is determined by the speed of which the dislocations can move in the crystal lattice. The glide of dislocations is usually so fast that the rate controlling mechanisms are the cross slip or climb. [12].

1.3.2 Recrystallization

As opposed to recovery, which is relatively homogenous in terms of space and time, recrystallization can be divided into nucleation and growth events. A recrystallization nucleus is defined as “a crystallite of low internal energy growing into deformed material from which it is separated by a high angle grain boundary”. Only a very few sub-grains or cells of the total amount will continue to grow into a new recrystallized grain. From numerous

investigations, it is clear that the nucleation of a new grain occurs in regions where a high angle boundary easily can be formed i.e. at heterogeneities in the microstructure like grain boundaries, shear hands and second phase particles (PSN). In commercial alloys, second phase particles are always present and they affect the recrystallization in three ways: i) the stored energy may increase, ii) large particles may act as nucleation sites (PSN) and iii) small particles may exert a pinning effect on both small angle and high angle grain boundaries. The first two effects tend to promote recrystallization whereas the last tend to hinder recrystallization [12].

1.4 Scope

In this study, experimental work is conducted on the AA3003 alloy. The chemical composition of this alloy is Mn 1.05, Fe 0.52 and Si 0.28 (wt %). The as-cast state, homogenization treatment, deformation (described in Section 2.2) and annealing treatment (described in Section 3.2) are examined. Deformation method is cold-rolling, because this thesis focuses mainly on the role of constituent particles. The schematic of whole process in this study is shown in Figure 1.4.

1.5 Objective of present thesis

The recrystallization behavior is strongly affected by thermo-mechanical histories such as homogenization and deformation. Many investigations have been done to study the precipitation behavior of dispersoids [7,8,27-33], the transformation of Al_6Mn phase to α-

Al(Mn,Fe)Si phase [30,34-38], and particle stimulated nucleation behavior. However, the quantitative studies on the relationship between the constituent particles and recrystallization behavior have been scarce and unclear. Therefore, the effects of characteristics of constituent particles in the recrystallization behavior are mainly discussed in the present thesis.

The objectives of this study are as follows:

1. To quantify the precipitation behavior during homogenization treatment, i.e. heating, holding and cooling stages.

2. To investigate the effects of different constituent particles in the recrystallization behavior, i.e. size of recrystallized grains, the rate of recovery and recrystallization behavior with annealing temperature and time.

3. To investigate the effects of Mn solute atoms after the homogenization treatment in the recovery and recrystallization behavior.

4. To evaluate the change of mechanical properties after annealing treatments.

1.6 Outline of the present thesis

The flow chart of the present thesis is shown in Figure 1.5.

The background of the non-heat-treatable AA3xxx alloys is introduced. Current problems and the objective of the present thesis are described in Chapter 1 '**General introduction**'.

The precipitation behavior during the designed homogenization treatments is investigated in the Al-Mn alloy in Chapter 2 '**Formation of Mn containing dispersoids with homogenization treatments and deformation microstructure in an Al-Mn alloy**'. The change of microstructure after homogenization and deformation and the characteristic of precipitates are discussed.

The relationship between the annealing conditions and recrystallization behavior with recovery is presented in Chapter 3 '**Effects of annealing temperature and time on the recrystallization behavior of an Al-Mn alloy**'. The influences of the annealing conditions as temperature and time on the recrystallization behavior are discussed.

The relationship between the precipitates with Mn solute atoms and recrystallization behavior with recovery is presented in Chapter 4 '**Combined effects of Mn containing dispersoids and Mn solute atoms on the recrystallization microstructures of an Al-Mn alloy**'. The

influences of the precipitates and Mn solute atoms on the recrystallization behavior are discussed.

The transition of mechanical properties during recrystallization with various homogenization conditions is presented in Chapter 5 '**Mechanical properties of specimens with different recrystallization microstructures in an Al-Mn alloy**'. The influence of homogenization conditions on the mechanical properties during recrystallization treatment is discussed.

Finally, the results and conclusions of the present thesis from Chapter 2 to 5 are summarized in Chapter 6 '**General conclusions**'.

Reference

1. S. H. Avner, *Introduction to Physical Metallurgy*, p. 481-489, McGraw-Hill, (1974).

2. I. J. Polmear, *Light Alloys: Metallurgy of the Light Metals*, p. 90-91, and 103-104, St Edmundsbury Press Ltd., Bristol, UK, (1995).

3. B. D. Craig, *Handbook of Corrosion Data*, p. 17, ASM International, Metals Park, USA, (1960).

4. W. D. Callister, *Materials Science and Engineering: An Introduction*, p. 372, John Wiley & Sons, Inc., USA, (1999).

5. E. Nes, Acta Metal, **24** (1976), 391.

6. Kwag Y. J. G. Morris, Mater. Sci. Eng., **77** (1986), 59.

7. J. Bottema, O. E. Grushko, W. S. Miller, L. M. Sheveleva. In: T. Sato, S. Kumai, T. Kobayashi, Y. Murakami (Eds.). ICAA-6. Toyohashi, Japan. Aluminum alloys: their physical and mechanical properties., (1998), p. 2143.

8. J. P. Sun, R. D. Doherty, P. A. Hollinshead. In: T. Sato, S. Kumai, T. Kobayashi, Y. Murakami (Eds.). ICAA-6. Toyohashi, Japan. Aluminum alloys: their physical and mechanical properties., (1998), p. 1203.

9. W. B. Hutchinson, A. Oscarsson, Å. Karlsson, Mater Sci Tech., **5** (1989), 1118.

10. Y. J. Li, L. Arnberg, Mater. Sci. Eng., A, **347** (2003), 130.

11. Y. J. Li, L. Arnberg, Acta Mater, **51** (2003), 3415.

12. F. J. Humphreys, M. Hatherly, Recrystallization and related annealing phenomena, Pergamon, Oxford, UK, (2004).

13. N. Krendelsberger, F. Weitzer, and J. C. Schuster, Metall. Mater. Trans. A, **33A** (2002), 3311.

14. J. L. Murray, A. J. McAlister, R. J. Schaefer, L. A. Bendersky, F. S. Biancaniello, and D. L. Moffat, Metall. Trans. *A,* **18A** (1987), 385.

15. Aluminum Vol.I, American Society for Metals, (1967), 375, 388, 393.

16. R. W. Cahn, P. Haasen, and E. J. Kramer, *Materials Science and Technology: A Comprehensive Treatment*, p. 242 and 267, 8, VCH, Germany, (1996).

17. A. K. Vasudevan and R. D. Doherty, *Aluminum Alloys-Contemporary Research and Applications*, p. 76, 137, Treatise on Materials Science and Technology, 31, H. Herman Editor. Academic Press, Inc., USA., (1989).

18. R. G. Kamat and S. Saimoto, in *Proceedings of The 3rd International Conference on ALUMINIUM ALLOYS (ICAA3): Their physical and mechanical properties*, Trondheim, Norway, **3** (1992), p. 291.

19. M. Zamin, Corrosion*,* **37** (1981), 627.

20. R. G. Kamat and S. Saimoto, Mater. Sci. Technol*,* **10** (1994), 215.

21. T. Z. Kattamis, H. D. Merchant, S. Skolianos, and G. Scharf, Aluminium, **65** (1989), 367.

22. D. L. Sun, S. B. Kang, and H.S.Koo, Mater. Chem. Phys., **63** (2000), 37.

23. N. C. W. Kuijpers, W. H. Kool, P. T. G. Koenis, K. E. Nilson, I. Todd, and S. van der Zwaag, Mater. Charact., **49** (2003), 409.

24. E. V. Koroleva, G. E. Thompson, G. Hollrigl, and M. Bloeck, Corros. Sci., **41** (1999), 1475.

25. L. F. Mondolfo, *Manganese in Aluminium Alloys*, Manganese Centre, Neuilly sur Seine, France, (1977).

26. D. T. L. Alexander and A. L. Greer, *Acta Materialia,* **50** (2002), 2571.

27. L. F. Mondolfo, *Manganese in Aluminium Alloys*, Manganese Centre, Neuilly sur Seine, (1977).

28. P. Furrer, Z. Metallkd. **70** (1979), 699.

30. F. J. Humphreys, Acta Metall. **25** (1977), 1323.

31. E. Nes, Acta Metall. **24** (1976), 391.

32. G. Hausch, P. Furrer, H. Warlimont, Z. Metallkd. **69** (1978), 174.

33. R. Sandstrom, Z. Metallkd. **71** (1980), 741.

34. P. Furrer, G. Hausch, Met. Sci. **13** (1979), 155.

35. J. Sanders, D.J. Lege, T.L. Hartman, Aluminium **65** (1989), 941.

36. E. Trømborg, A.L. Dons, L. Arnberg, in: L. Arnberg, O. Lohne, E. Nes, N. Ryum (Eds.), Aluminium Alloys: their Physical and Mechanical Properties, ICAA3, Trondheim, Norway, (1992), p.270.

37. X. Wang, R.G. Kamat, in: J.G. Morris, S.K. Das, H.S. Goodrich (Eds.), Aluminium Alloys for Packaging II, Warrendale, PA, TMS, (1996), pp. 209.

38. R.G. Kamat, J. Mater., **48** (1996), 34.

39. *International Alloy Designations and Chemical Composition Limits for Wrought Aluminum and Wrought Aluminum Alloys*, p. 3 and 17, The Aluminum Association, USA, (1998).

40. *The Properties of Aluminium and its Alloys*, p. 8, 20-21 and 84, Aluminium Federation Ltd., UK, (1998).

41. H. H. Uhlig, *Corrosion and Corrosion Control: an introduction to corrosionscience and engineering*, p. 295-306, John Wiley & Sons, Inc., USA, (1967).

42. D. B. Goel, P. Furrer, H. Warlimont, Aluminium, **50** (1974), 511.

43. E. Nes, S. E. Naess, R. Hoier, Z Metall., **63** (1972), 248.

44. V. Hansen, J. Gjønnes, B. Andersson, Mater Sci Lett., **8** (1989), 823.

45. M. Cooper, K. Robinson, Acta Cryst., **20** (1966), 614.

46. M. Cooper, Acta Cryst., **6** (1967), 287.

47. A. D. I. Nico, Acta Cryst., **6** (1953), 285.

48. L. K. Walford, Acta Cryst., **18** (1965), 287.

49. J. Adam, J. B. Rich, Acta Cryst., **7** (1954), 813.

Table 1.1 Compositions of non-heat-treatable wrought 3xxx alloys (wt%) [2,4,39-41]

	Si	Fe	Cu	Mn	Mg	Zn	Cr	Ti	Al
3003	0.6	0.7	0.05~0.20	1.0~1.5	–	–	–	–	Bal.
3103	0.5	0.7	0.10	0.9~1.5	–	–	–	–	Bal.
3004	0.3	0.7	0.25	1.0~1.5	0.8~1.3	0.25	–	–	Bal.
3005	0.6	0.7	0.30	1.0~1.5	0.2~0.6	0.25	0.10	–	Bal.
3105	0.6	0.7	0.30	0.3~0.8	0.2~0.8	0.40	0.20	0.10	Bal.

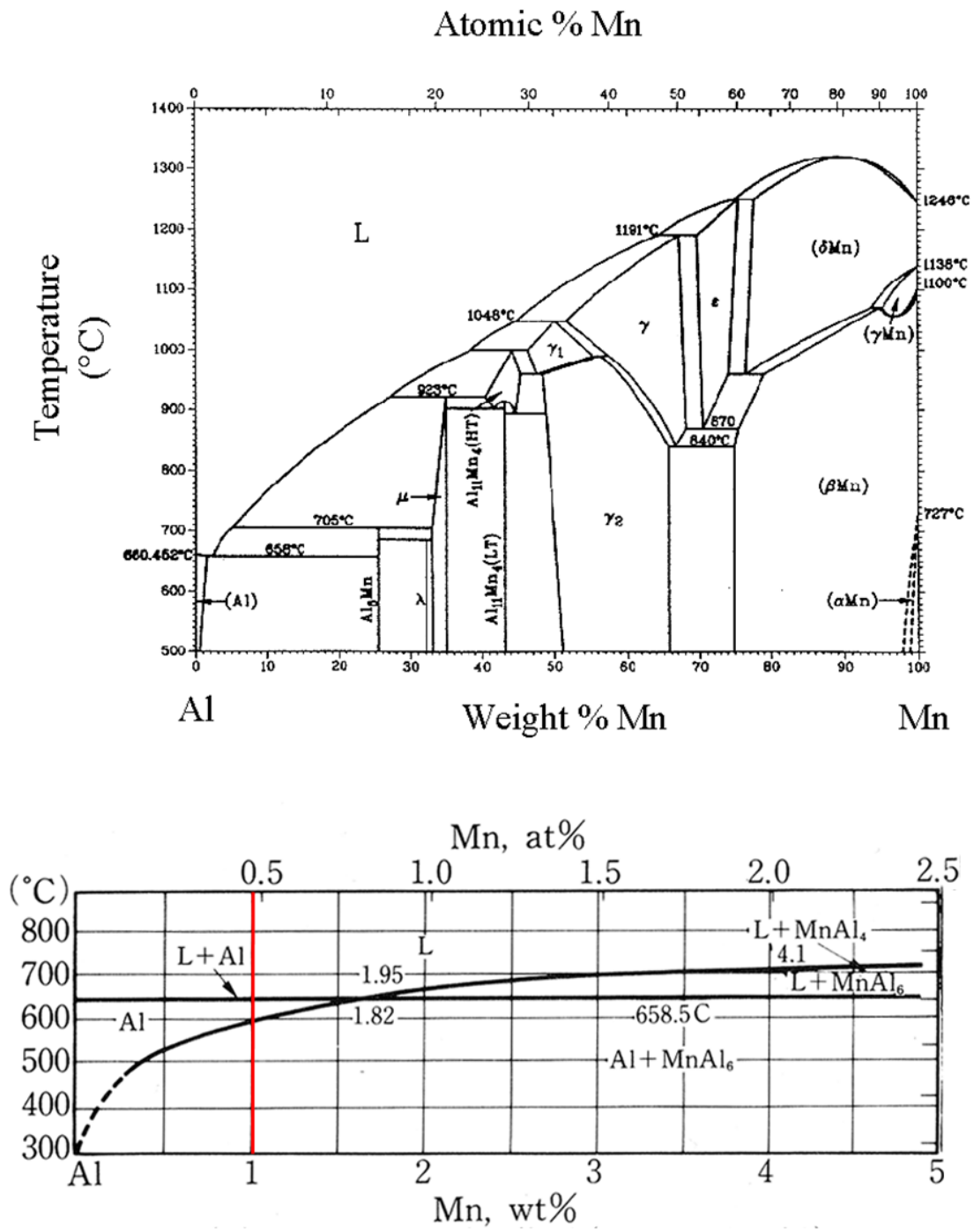

Figure 1.2 The binary Al-Mn phase diagrams.

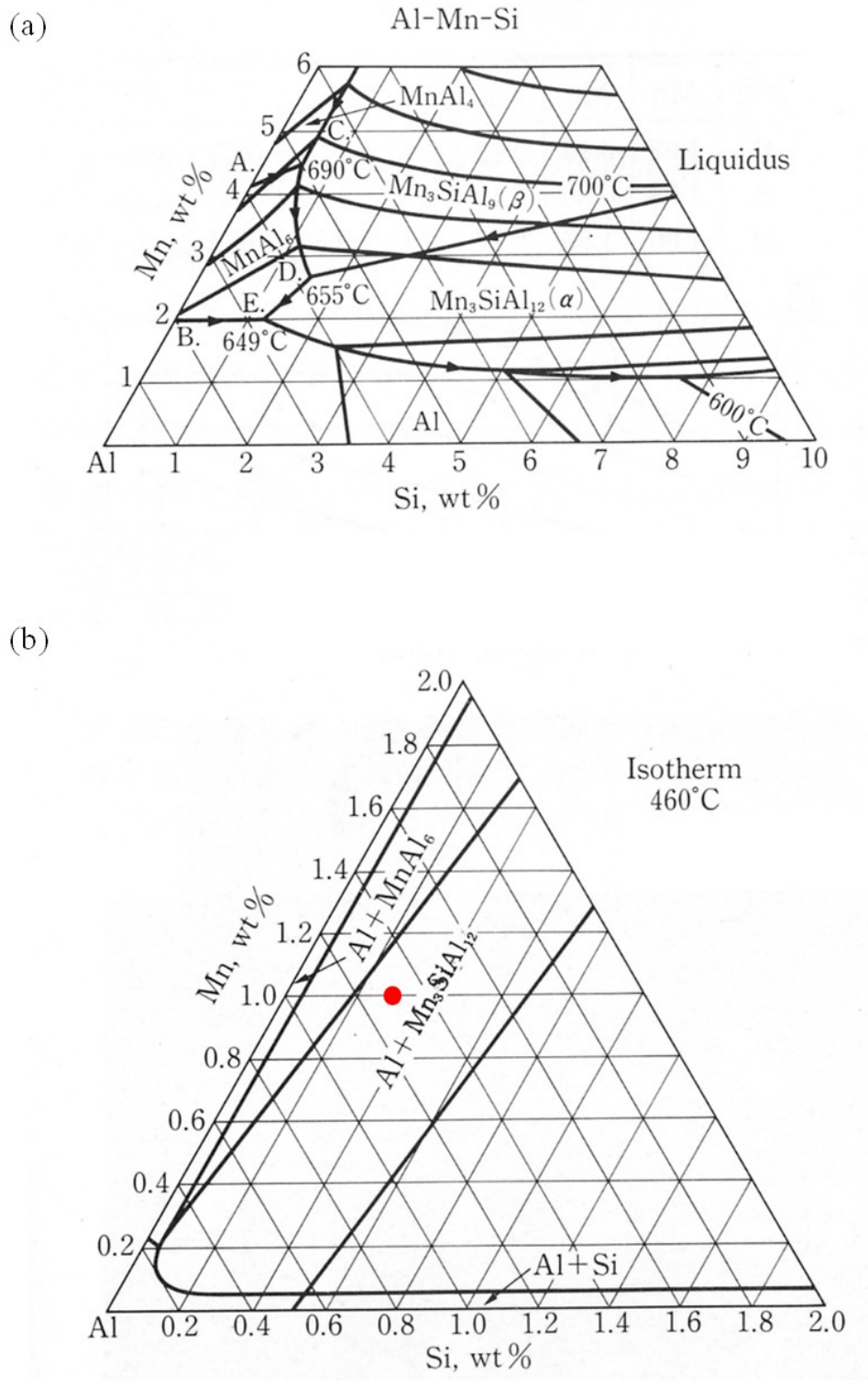

Figure 1.3 The ternary Al-Mn-Si phase diagrams. (a)Liquidus lines, (b)Isotherm at 460℃.

Table 1.2 Crystal structures of Mn/Fe containing dispersoids.

Name		Crystal	Space	Cell dimension (nm)			Reference
Symbol	Constitution	structure	group	a	b	C	
α Particle	α-AlFeSi	bcc	Im3	1.256	–	–	[45]
	α-AlMnSi	sc	$Pm\bar{3}$	1.265	–	–	[46]
	α-Al(Mn,Fe)Si	sc/bcc		1.256-1.265	–	–	
$Al_6(Fe,Mn)$	Al_6Fe	Orthorhombic	Cmcm	0.646	0.744	0.877	[47]
	Al_6Mn	Orthorhombic	Cmcm	0.650	0.755	0.887	[48]
G	$Al_{12}Mn$	sc		7.507	–	–	[42,43,49]
G2	Al_7Mn	Orthorhombic		0.251	2.48	3.03	[42]
α'	AlMnSi	Hexagonal		1.23	–	2.62	[43]
I	Al(Mn,Fe)Si	Icosahedral		–	–	–	[44]
G'	α-$Al_{12}Mn_3Si$	sc	Im3	1.275	–	–	[43]
G''	α-AlFeSi	Hexagonal		7.54	–	7.84	[43]

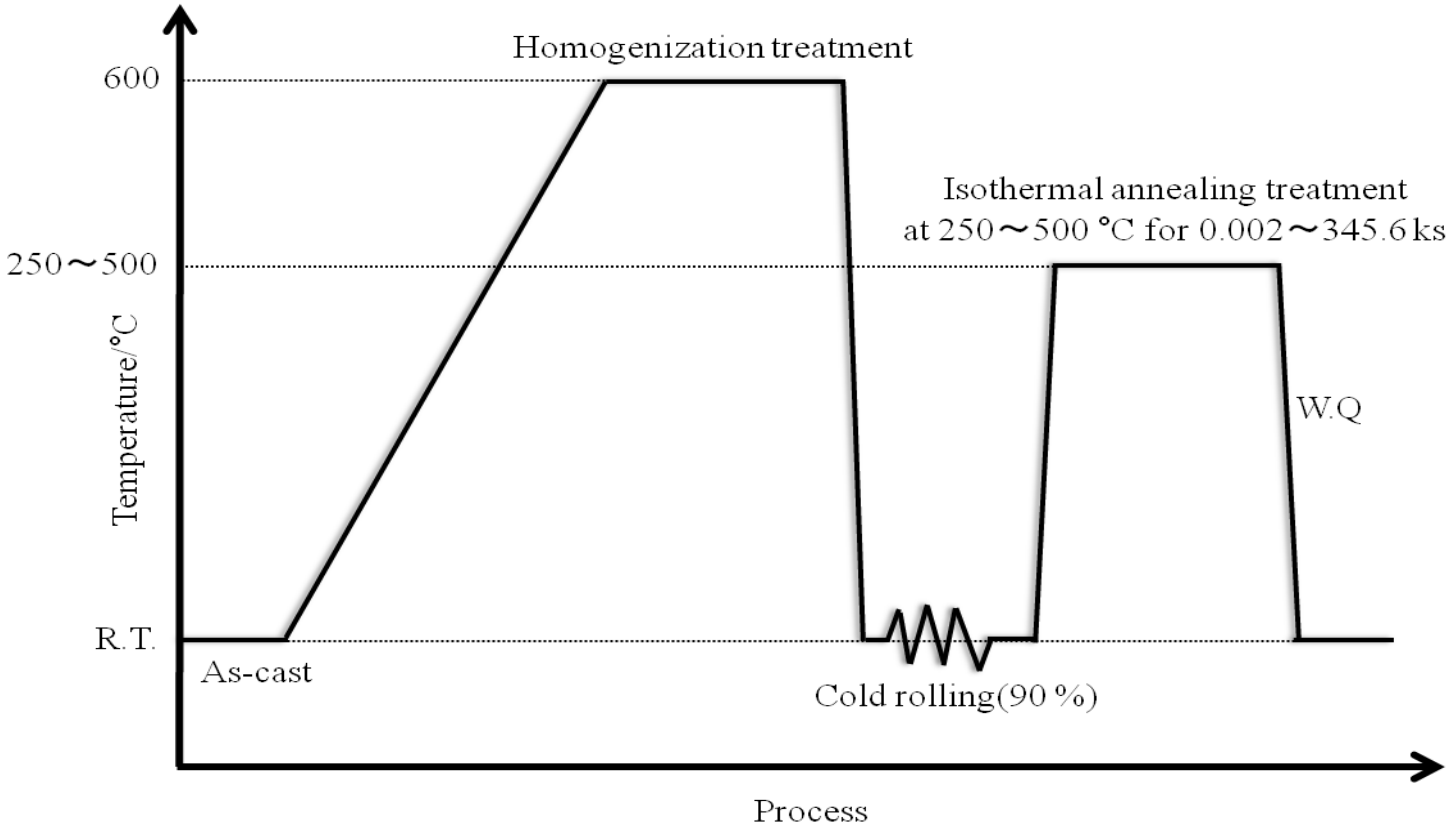

Figure 1.4 Schematic illustration of thermal-mechanical process in the Al-Mn alloys

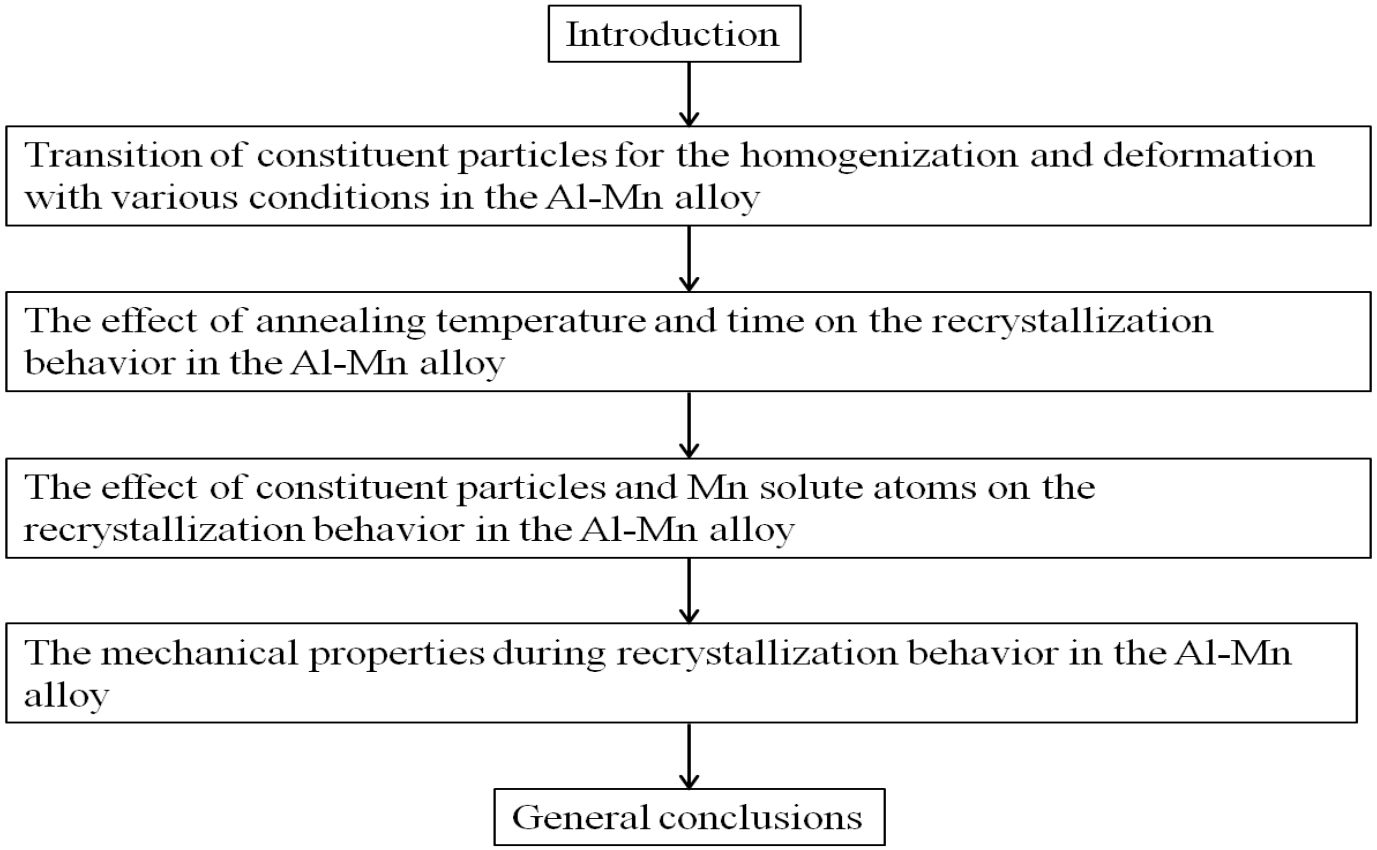

Figure 1.5 Outline of present study

Chapter 2

Formation of Mn containing dispersoids with homogenization treatments and deformation microstructure in an Al-Mn alloy

2.1 Introduction

For DC-cast ingots, homogenization must be conducted before thermo-mechanical processes such as cold-rolling and annealing treatment, due to reduce microsegregation and produce the right size, number density and distribution of constituent particles [1-6]. The characteristics of constituent particles formed during homogenization have strong influences on the deformation, recovery, recrystallization behavior and mechanical properties of wrought alloy in the 3xxx (Al-Mn-Fe-Si) series [7]. Large particles (> 1μm) promote recrystallization while fine dispersed particles that precipitates after homogenization called dispersoids retard recrystallization [8-9]. The transformation of Al_6Mn to α-Al(Mn,Fe)Si have investigated by Li and Arnberg, Alexander and Greer, [9-10]. The evolution of primary particles in a 3003 alloy also has investigated by Li and Arnberg [9]. Figure 2.1 shows the change of primary particle during homogenization treatment. Thus, the evolution of primary particle was investigated extensively. Some studies have discussed feasibility of precipitation hardening by heat treatment [12-13]. Some studies about the crystal structure or phase properties of the

precipitates have also been published [14-16]. However, quantitative studies on the size, distribution and volume fraction of precipitates and effect of Mn solute atoms in Al-Mn alloy have been scarce even though they have the strong influence on the recrystallization. Also the effect of cold-rolling by different reduction on the recrystallization behavior is clearly reported while the effect of different microstructure by cold-rolling with fixed reduction is unclear. Therefore, the objective is to investigate the transition of precipitates such as size and distribution and Mn solute atoms in the matrix by different homogenization treatments and deformation with the same reduction in this Chapter.

2.2 Experimental procedure

The material used in this study was a DC cast AA3003 alloy ingot. The chemical composition of the alloy was (wt. %): Mn 1.05, Fe 0.52, and Si 0.28. In order to investigate homogenization behavior during heating until 550 °C, differential scanning calorimetry (DSC) under Ar atmosphere is performed using the Rigaku DSC8230 ranging from room temperature to 550 °C with heating rate of 10 °C / min. In order to investigate the effect of the heat treatment condition on the homogenization behavior, three different homogenization treatments were conducted in an air circulation furnace. Their conditions are shown in Figure 2.2 and Table 2.1. Their specimens were cold-rolled with reduction of 90 % after homogenization treatment. Investigation of the microstructure was performed in an Olympus GX71 optical microscope. The specimens were ground and polished to 3μm surface finish and then polished in an OP-S suspension. Constituent particles were observed on the surface after etched by the Tucker's reagent (HF : HCl : HNO_3 : H_2O = 4.6 : 10.6 : 6 : 178.8). The Barker's reagent, i.e. 1.8% HBF_4, was employed to anodize specimens to reveal grain by

using polarized light of an optical microscope. Micro Vickers hardness measurements using Matsuzawa MMT-X3A were employed. Seven hardness measurements for each data point were acquired. The maximum and minimum values were discarded and the average of the remaining five was used. X-ray diffraction studies (XRD) were undertaken in order to identify the constituent particles such as primary particle and precipitate. X-ray diffraction studies were performed on a Rigaku Rint. The electrical conductivity measurements are performed using FD-102 by eddy current method.

2.3 Results

2.3.1 Formation behavior of precipitate during heating for homogenization

Figure 2.3 shows the DSC result of the as-cast current specimen with heating rate of 10 °C. The large exothermic peak appeared after 300 °C. Figure 2.4 shows the change of the electrical conductivity during heating stage of homogenization treatment. The electrical conductivity shows a small change after heating to 300 °C. After that, it increased rapidly to the maximum value around 520 °C and decreased with temperature. Figure 2.5 shows the XRD results of homogenization treatment from 300 °C to 600 °C. The peak of Al_6Mn existed from as- cast and the peak of α-Al(Mn,Fe)Si appeared after 400 °C.

2.3.2 Microstructure of the particles during homogenization treatment

Figure 2.6 shows the microstructure of the as-cast AA 3003 specimen. A large quantity of rod like, plate like and network eutectic primary particles are distributed in the interdendritic regions and on the grain boundaries. Figure 2.7 shows the microstructure of AA3003 specimens after designed homogenization treatments at the low magnification. A number of precipitates are distributed in the matrix. Figure 2.8 shows the back-scattered microstructure

of designed homogenization treatments at the high magnification. The number density and size of precipitates are different by homogenization conditions. Also precipitate free zones (PFZs) appear differently depending on the homogenization conditions. Figure 2.9 shows the size distribution of precipitates. The size of precipitates is largest in the Base specimen. The number density is high. The No-Holding specimen contains fine precipitates densely. In case of the Slow-Cooling, the size of precipitates is medium and the number density is low compared with other specimens.

2.3.3 Microstructure of the constituent particles after cold-rolling

Figure 2.10 shows the microstructure after homogenization and cold-rolling. The primary particles are fragmented and are arrayed toward the deformation direction. Precipitates are distributed uniformly and PFZs are reduced due to distortion by deformation. Figure 2.11 shows the microstructure of the deformed specimen by using the polarizing optical microscopy. In the deformed state, elongated bands were observed generally. It indicates the homogeneous deformation in all specimens.

2.4 Discussion

2.4.1 Transition of Mn Solute atoms during homogenization treatment

It is known that the electrical conductivity of the alloy has a linear relationship with the reciprocal of the concentration of an alloying element in the solid solution. The AA3003 alloy contains Mn, Fe and Si elements. However, the electrical conductivity is not particularly influenced by Fe and Si because the amount of contained Fe and Si is small in the present

alloy. Therefore, the change of electrical conductivity is mainly due to the variation of Mn in the solid solution. The electrical conductivity is converted to the resistance by equation (1)

$$\rho / n\Omega m = 1724.1 / \%IACS \quad (1)$$

The contribution of electrical resistivity, Δρ, between Mn, Mg solute atoms and Al matrix is 31 nΩm wt%$^{-1}$, 3.8~5.1 nΩm wt%$^{-1}$ and 26.5 nΩm wt%$^{-1}$, respectively at room temperature [17].

Therefore, the Mn concentration in the AA3003 is given by

$$\mathrm{Mn(wt\%)} = \frac{\rho_{\mathrm{measure}} - 26.5\,(\mathrm{wt\%})}{31} \quad (2)$$

The value of electrical conductivity, resistance and concentration of Mn solute atoms after homogenization treatment arrange in the Table 2.2. The volume fraction of precipitates can be estimated based on the concentration of Mn solute atoms. According to the results, Mn solute atoms are highest in the No-Holding specimen, while the Slow-Cooling specimen contains low Mn solute atoms compared with other specimens. It indicates that the Slow-Cooling specimen contains the largest volume fraction of precipitates and the No-Holding specimen contains lowest.

2.4.2 Effect of homogenization conditions on the precipitation behavior

The precipitation behavior and homogenization conditions are closely correlated. Firstly, the homogenization treatment is separated into the heating, holding and cooling stages.

During heating up to 600 °C in the No-Holding specimen, precipitates start to form at around 300 °C and constituent particles dissolve into the matrix at around 520 °C based on the DSC

and electrical conductivity results. Also α-Al(Mn,Fe)Si particles are formed at around 400 °C based on the XRD result. The reasons for the α-Al(Mn,Fe)Si development are the transformation of Al_6(Mn,Fe) to α-Al(Mn,Fe)[10] at the primary particles and the formation of α-Al(Mn,Fe)Si precipitates. It is found that during heating to 600 °C such as No-Holding specimen, the nucleation of precipitates and transformation and dissolution of primary particles occur mainly. Therefore, the size of precipitates is smallest and the number density is high.

During holding at 600 °C such as Base specimen, precipitates grow up and dissolve until the equilibrium state of solubility [9]. Thus, the size of precipitates becomes larger and number density becomes lower compared with the No-holding specimen.

At the cooling in the furnace such as the Slow-Cooling specimen, precipitates are formed due to the reducing of Mn solubility with decreasing temperature. In the Slow-Cooling specimen, the number density of precipitate becomes higher compared with Base specimen. Also, the size of precipitate becomes smaller slightly compared with the Base specimen due to the nucleation of new precipitates during cooling. The results of size distributions on the dispersoids in the specimens correspond to the phenomena occurring at each stage. The characteristic of precipitates in all specimens is shown in Table 2.3.

Based on the results, Figure 2.12 shows the schematic illustration of the precipitation behavior during the homogenization treatment.

2.4.3 The change of microstructure after cold-rolling

The change of electrical conductivity is shown in Figure 2.13. The value of electrical conductivity decreases compared with that after homogenization treatment in all specimens. It indicates that the generated dislocations by cold-rolling affect the electrical conductivity.

However, the decrement of the conductivity in each specimen is different. It means that the amount of generated dislocations is different with homogenization conditions. Especially, the decrement in the Slow-Cooling specimen is largest due to the large size of precipitates with high number density compared with other specimens.

2.5 Conclusions

Effects of homogenization conditions such as heating, holding and cooling on the precipitation behavior in Al-Mn alloy are examined. The optical microscope, scanning electron microscope, DSC, electrical conductivity measurement and XRD are applied in order to investigate the precipitation behavior of dispersoids. The obtained results are summarized as follows.

1. The formation of precipitates occur at around 300 °C and they dissolve at above 530 °C during heating of the homogenization treatment based on the DSC, electrical conductivity results.

2. Fine precipitates are formed with high number density, while low volume fraction during heating to 600 °C in the No-Holding specimen, because the nucleation of precipitates mainly occurs. The concentration of the Mn solute atoms is as high as 0.64 wt% in the matrix.

3. The growth with the partial dissolution of dispersoids is the dominant phenomena during holding at 600 °C. Therefore, the large precipitates are formed with low number density in the Base specimen. The volume fraction is higher and concentration of Mn solute atoms is lower, 0.57 wt%, than the No-holding specimen.

4. The fine precipitates are reformed with high number density during cooling to room temperature in the Slow-Cooling specimen. The volume fraction is highest and the concentration of the Mn solute atoms is lowest as 0.40 wt%, compared with other specimens.

Reference

1. E. Nes, Acta Metall Sin., **24** (1976), 391.

2. F. J. Humphreys, Acta Metall Sin., **25** (1977), 1323.

3. Y. Kwag, J. G. Morris, Mater. Sci. Eng, 77, 59 (1986).

4. J. Bottema, O. E. Grushko, W. S. Miller, L. M. Sheveleva, In:T. Sato, S. Kumai, T. Kobayashi, Y. Murakami (Eds.) ICAA-6. Toyohashi, Japan. Aluminum alloys: their physical and mechanical properties. (1998). p. 2143.

5. J. P. Suni, R. D. Doherty, P. A. Hollinshead, In: T. Sato, S. Kumai, T. Kobayashi, Y. Murakami (Eds.) ICAA-6. Toyohashi, Japan. Aluminum alloys: their physical and mechanical properties. (1998). p. 1203.

6. W. B. Hutchinson, A. Oscarsson, Å. Karlsson. Mater Sci Tech , **5** (1989),1118.

7. Y.J.Li, A.M.F.Muggerud, A.Olsen, T. Furu. Acta Mater., **60** (2012), 1004.

8. A. L. Dons, Y. J. Li, S. Benum, C.J. Simensen, A. Johansen, and E.K. Jensen, Aluminium, **81** (2005), 1038.

9. Y. J. Li and L. Arnberg, Mater. Sci. Eng A, **347** (2003), 130.

10. D. T. L. Alexander and A. L. Greer, Acta., **50** (2002), 2571.

11. Y. J. Li and L. Arnberg, , Mater. Sci. Eng. A, **347** (2003), 130.

12. T. Inaba, E. Usui, N. Shinano, JJILM **39** (1989), 3.

13. T. Inaba, E. Usui, R-D Kobe Steel Eng., **41** (1991), 77.

14. E. Nes, S. E. Naess, R. Hoier, Z Metallkd., **63** (1972), 248.

15. P. Furrer, Z Metallkd., **70** (1979), 699.

16. Y. J. Li, L. Arnberg, Acta Mater., **51** (2003), 3415.

17. S. Komatsu, S. Fujikawa, Mater. Trans., **47** (1997), 170

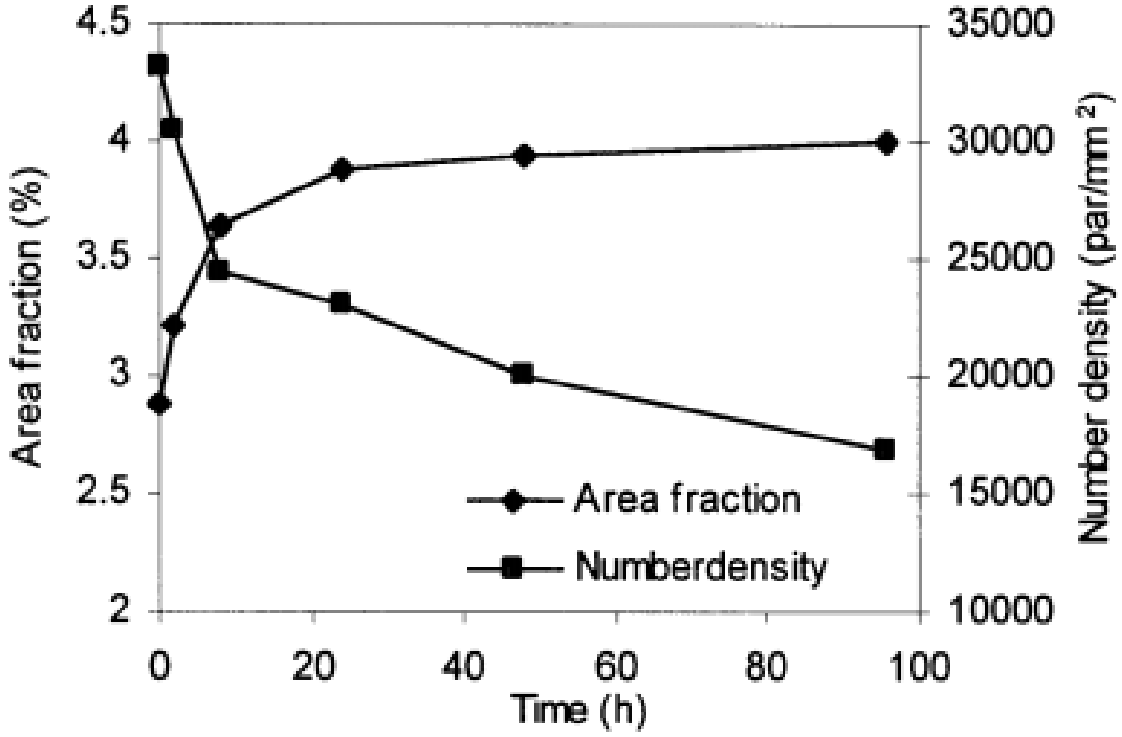

Figure 2.1 Evolution of primary particles during homogenization treatment in the Al-Mn alloy.

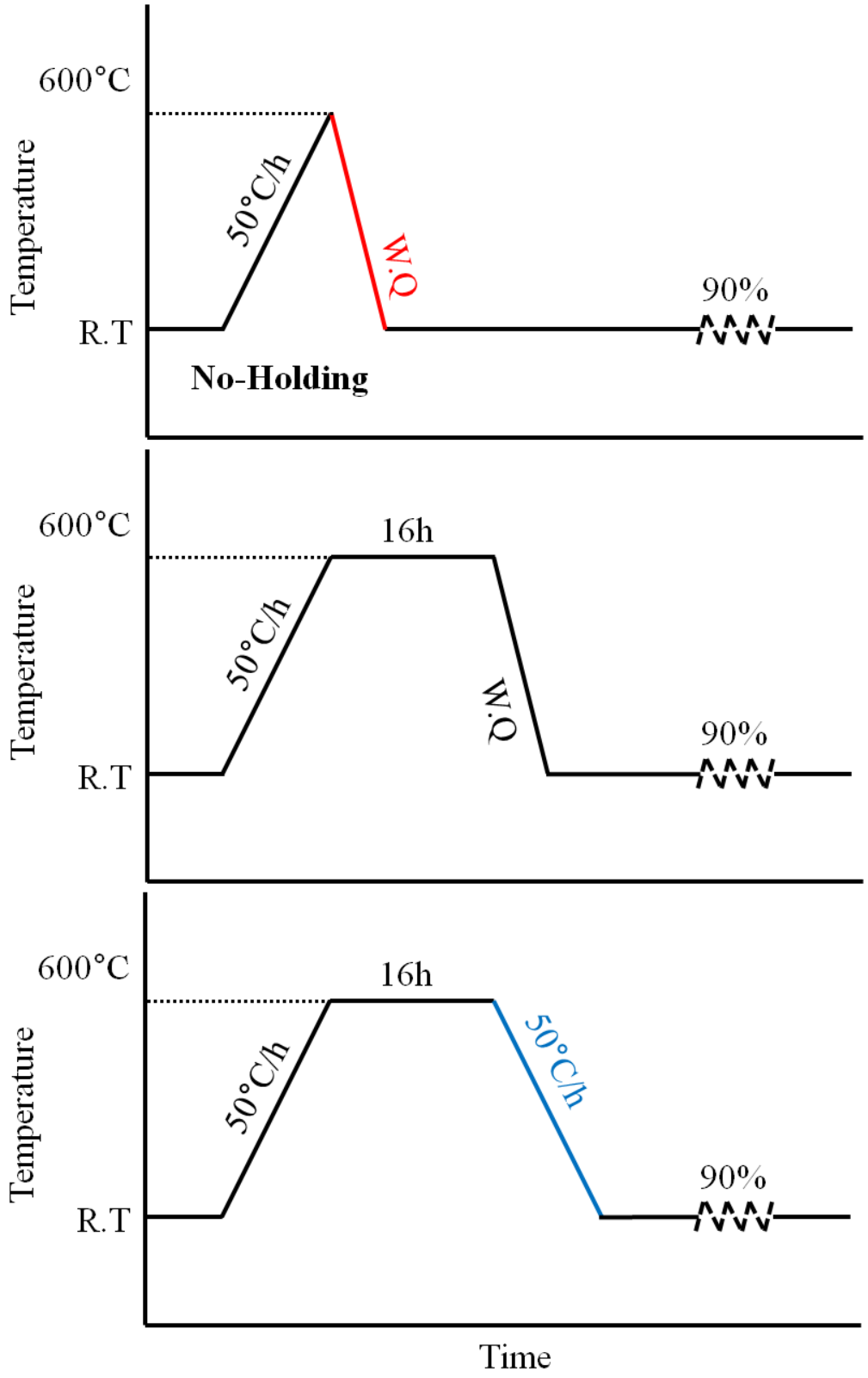

Figure 2.2 Schematic illustrations of homogenization treatments.

Table 2.1 Conditions of homogenization treatment.

The name of condition	Heating rate	Holding time	Cooling rate
Base	50 °C/h	16 h	W.Q.
No-Holding(NH)	50 °C/h	0 h	W.Q.
Slow-Cooling(SC)	50 °C/h	16 h	Furnace-Cooled

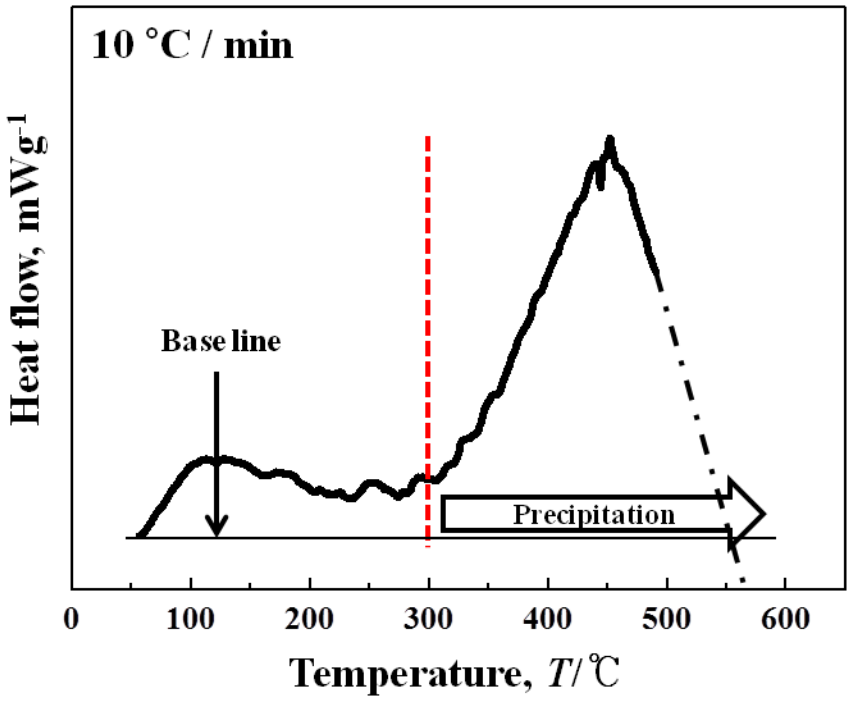

Figure 2.3 Evolution of precipitate during heating to 500 °C by DSC results in the Al-Mn alloy.

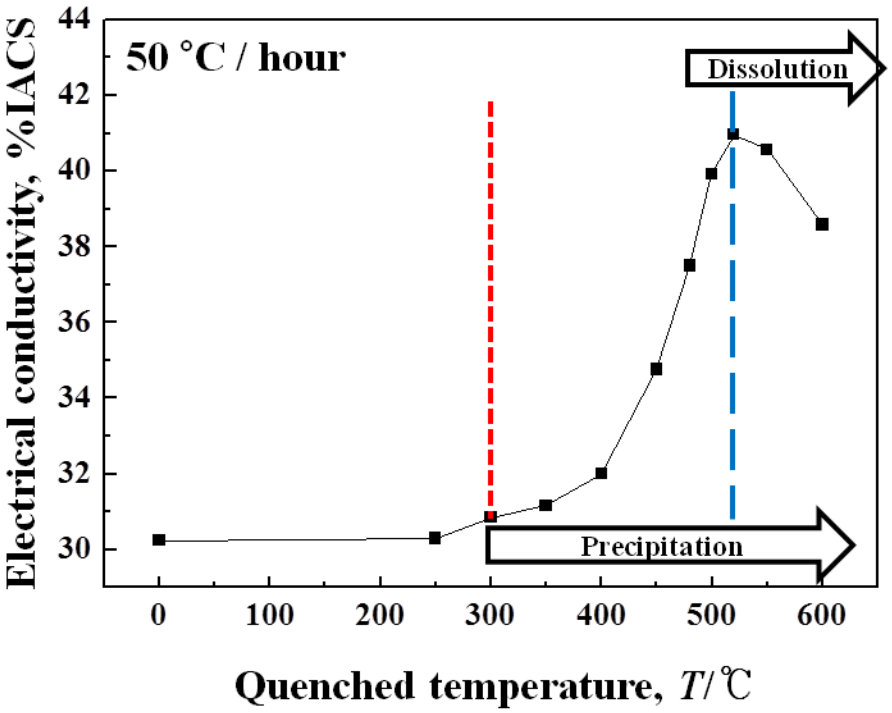

Figure 2.5 Change of electrical conductivity in the Al-Mn alloy.

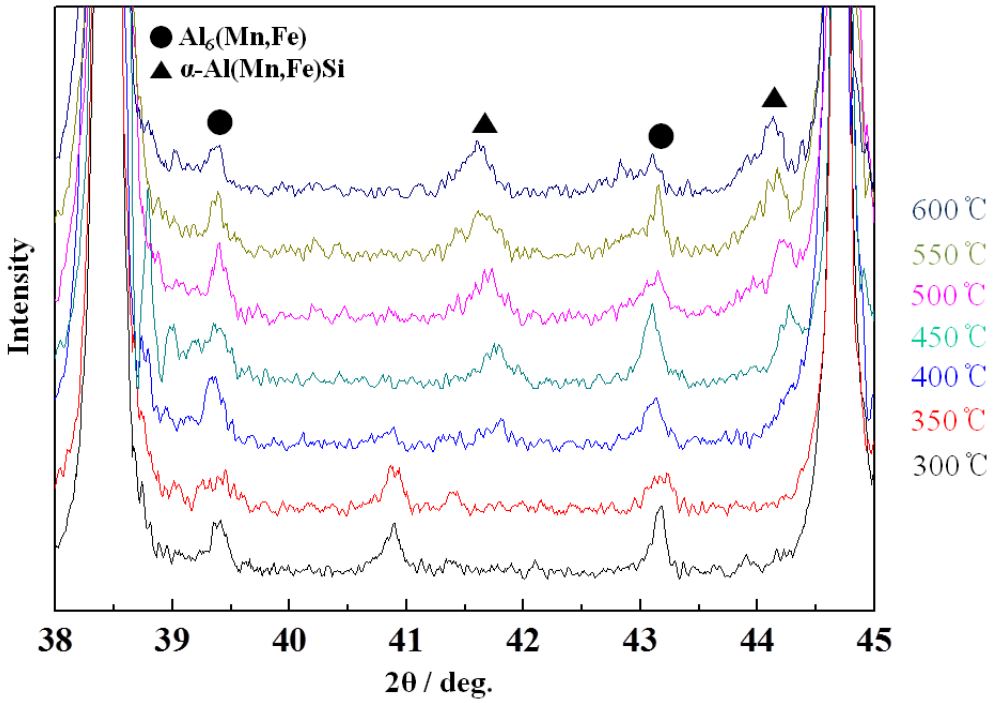

Figure 2.5 Evolution of phase transformation by XRD results in the Al-Mn alloy.

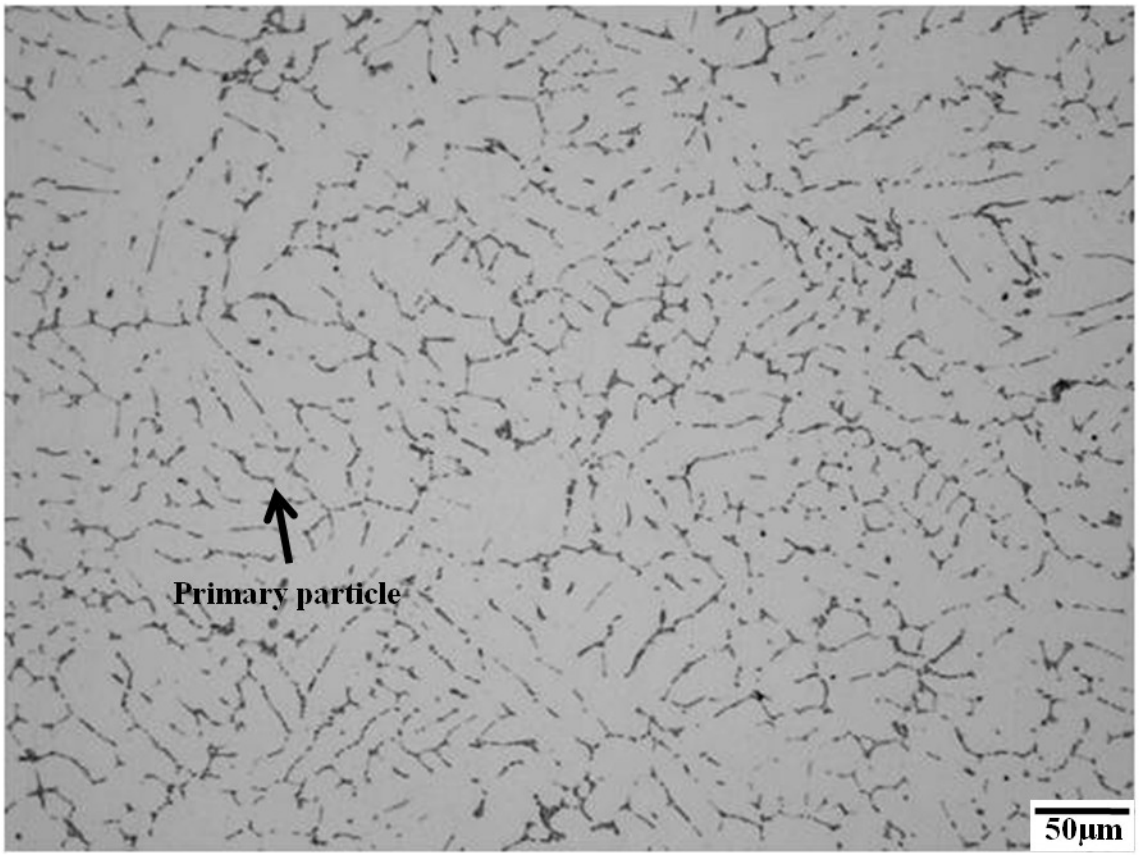

Figure 2.6 Microstructure at low magnification of as-cast Al-Mn alloy

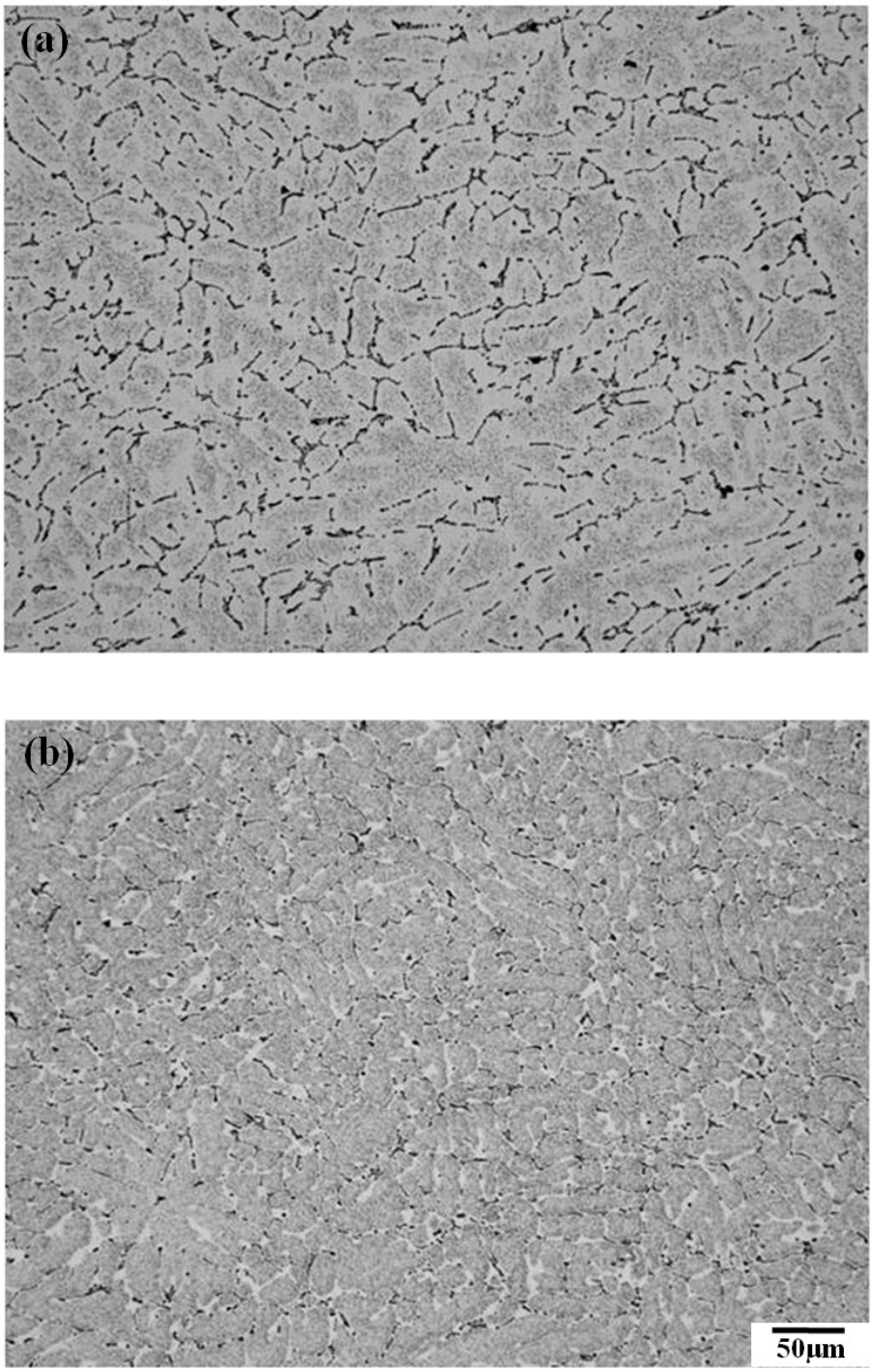

Figure 2.7 Microstructure at low magnification of the Al-Mn alloy with (a) Base condition, (b) No-Holding condition and (c) Slow-Cooling condition.

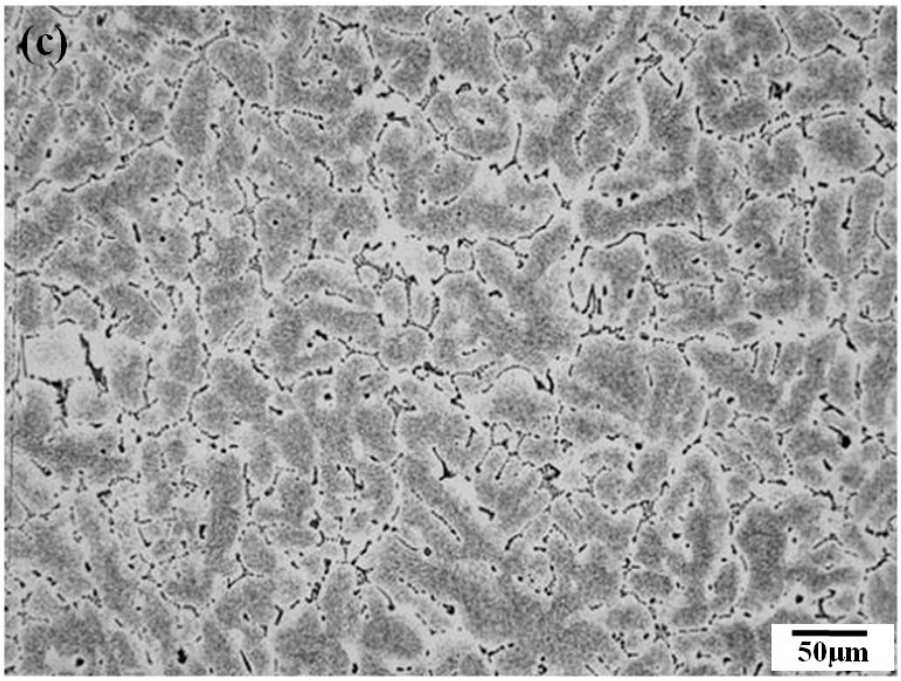

Figure 2.7 Continued

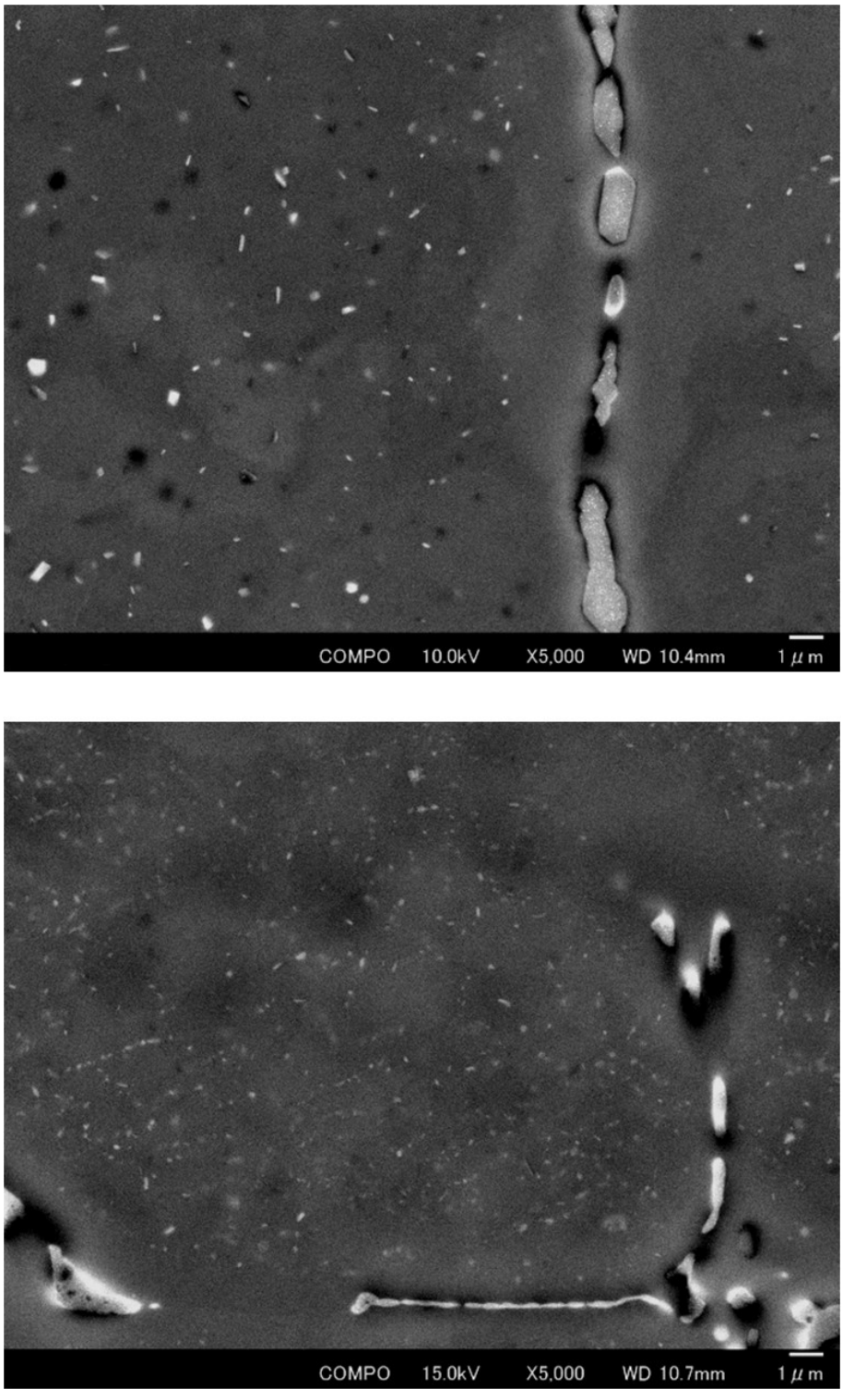

Figure 2.8 Back scattered images of the Al-Mn alloy with (a) Base, (b) No-Holding and (c) Slow-Cooling condition.

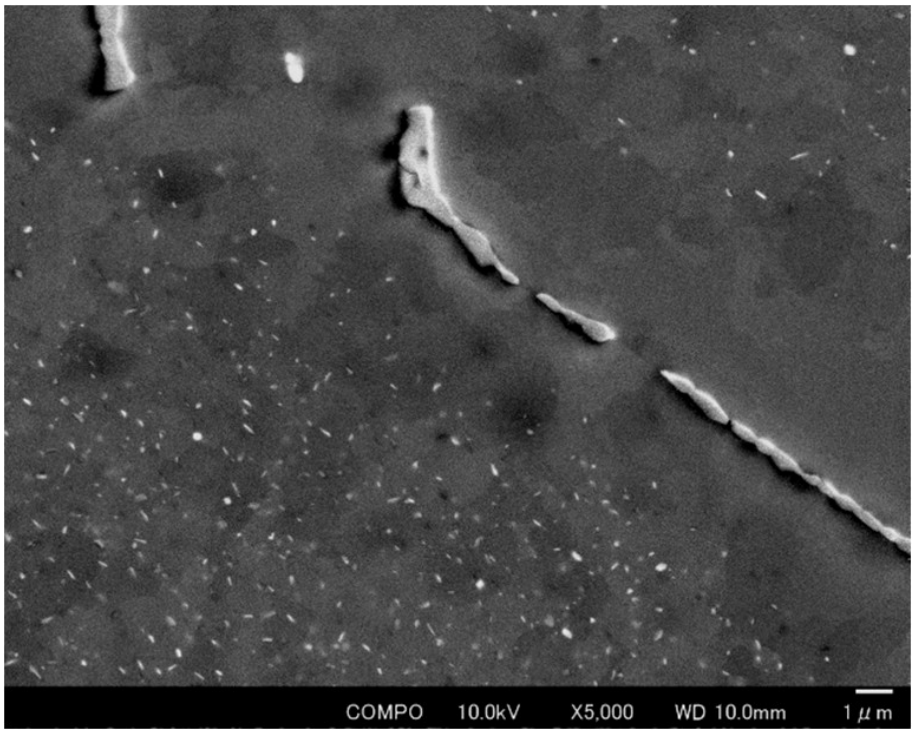

Figure 2.8 Continued

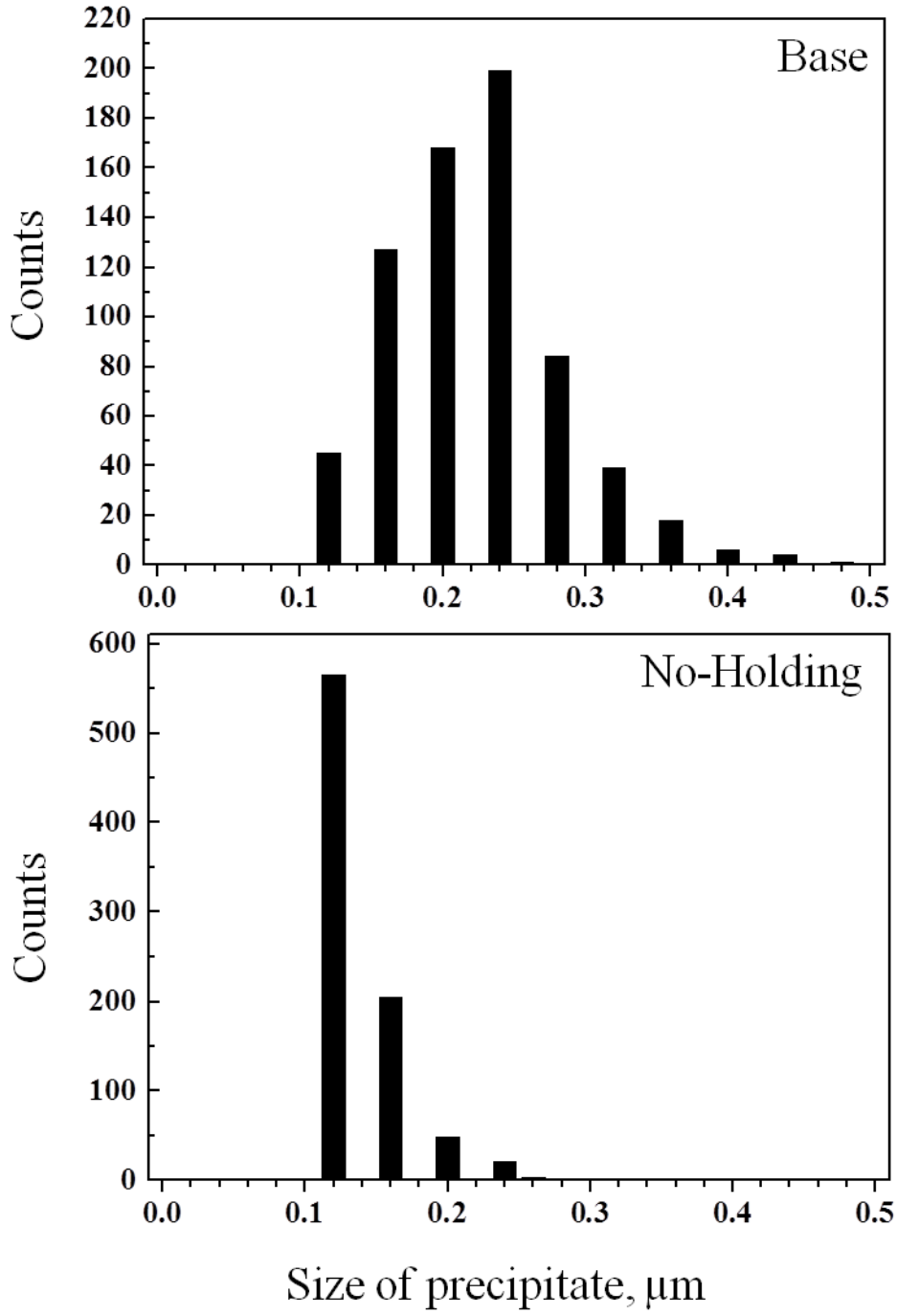

Figure 2.9 The size distribution of precipitates with designed homogenization conditions.

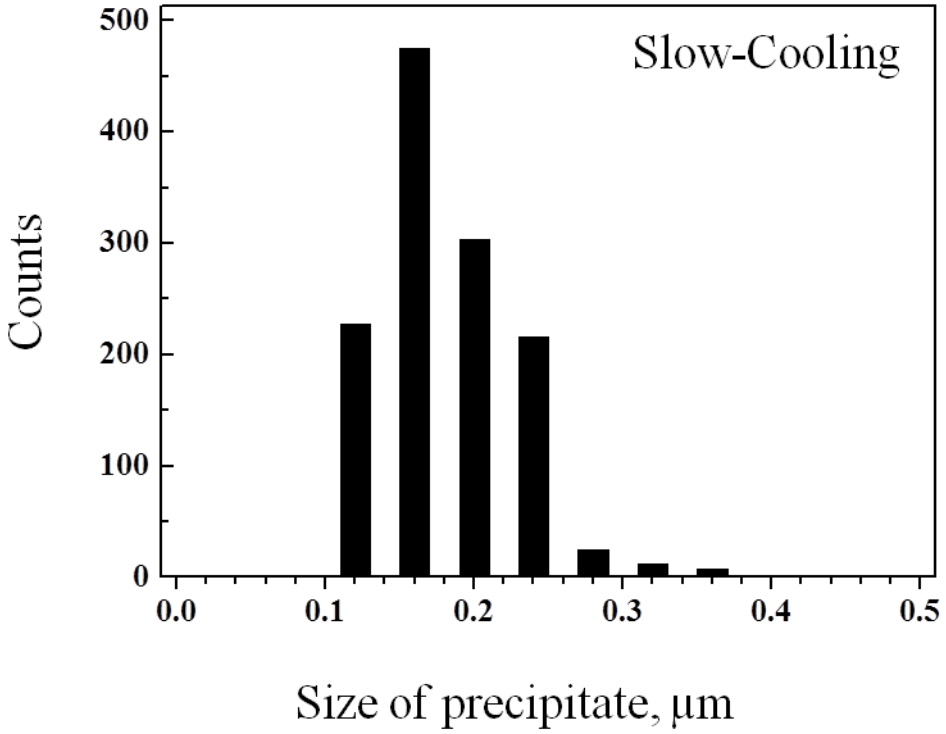

Figure 2.9 Continued

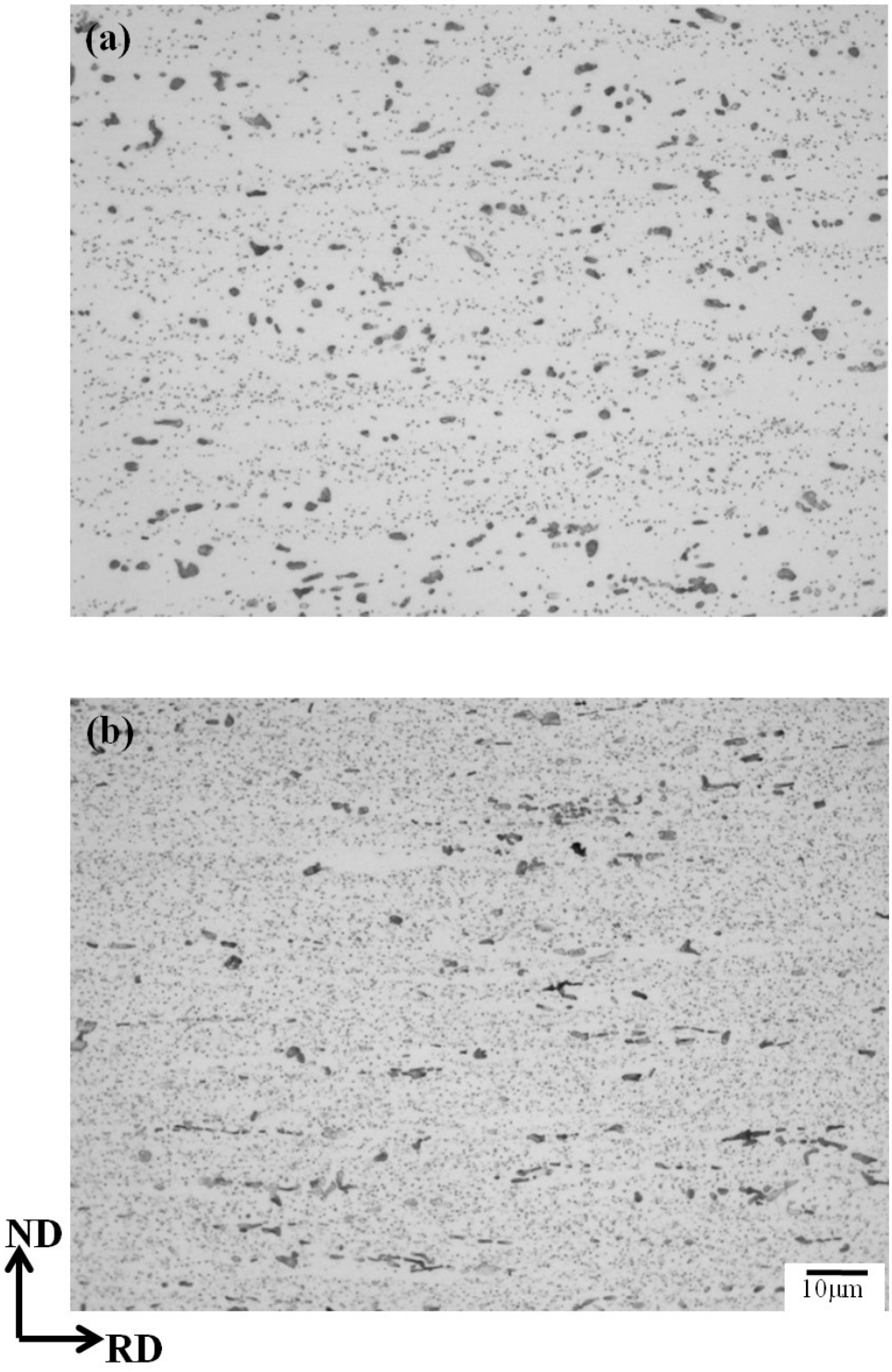

Figure 2.10 Microstructures after cold rolling with 90% reduction of (a) Base, (b) No-Holding and (c) Slow-Cooling specimen.

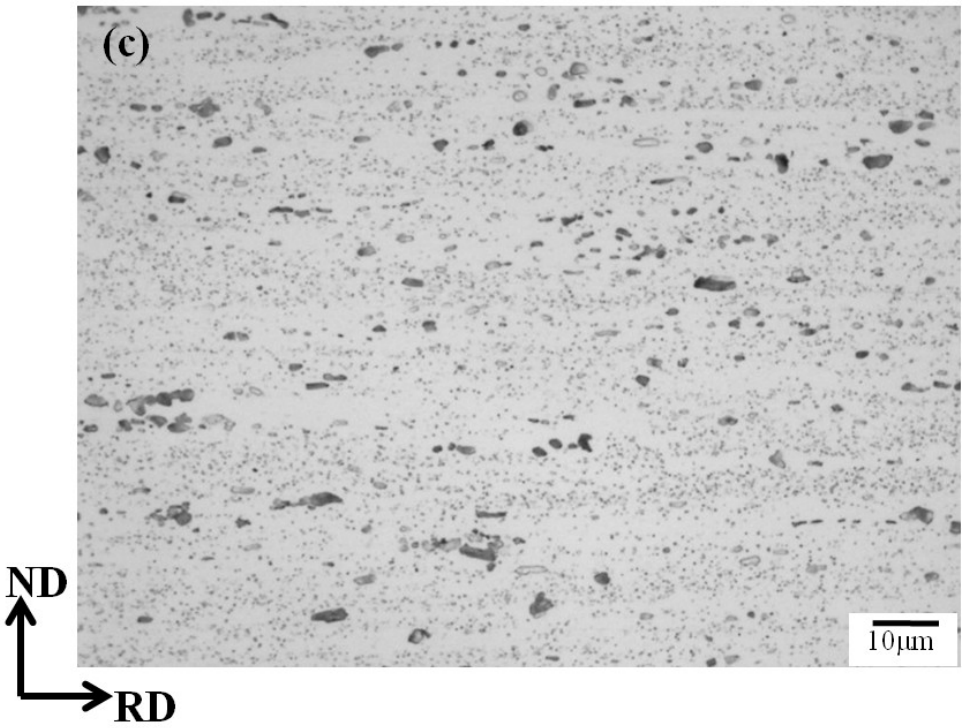

Figure 2.10 Continued

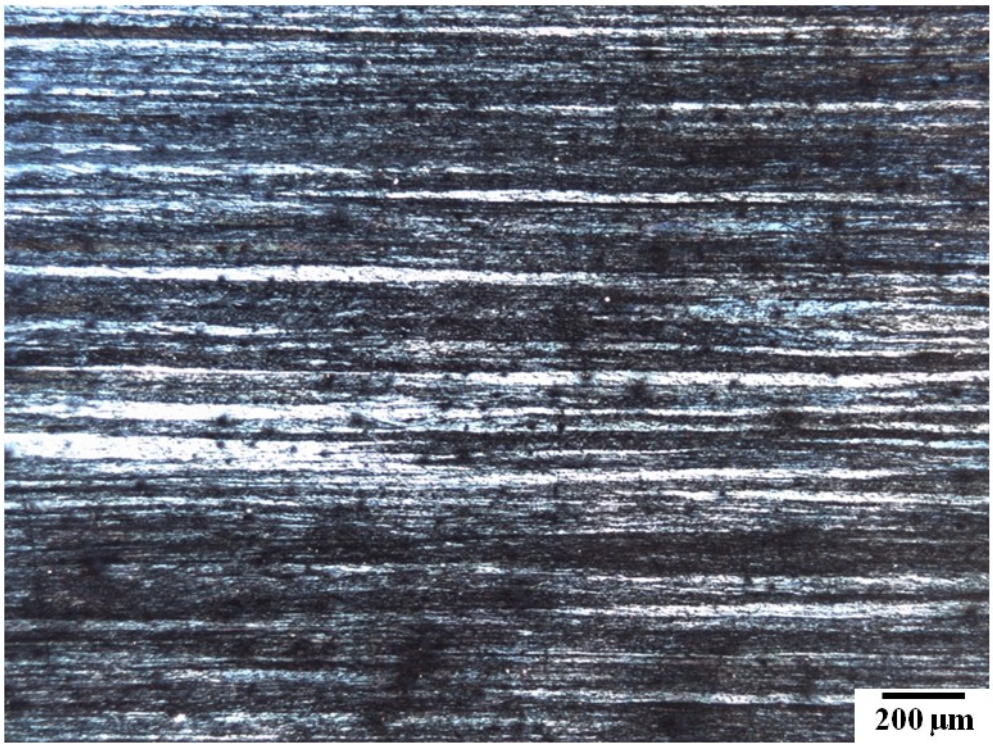

Figure 2.11 Polarized microstructure of Base specimen after cold-rolling

Table 2.2 Values of the electrical conductivity, resistivity and concentration of Mn solute atoms after homogenization treatments.

	Electrical conductivity (%IACS)	Electrical resistivity (nΩm)	Mn concentration (wt %)
Base	39.1	44.1	0.57
NH	37.1	46.5	0.64
SC	44.5	38.8	0.40

Table 2.3 Characteristic of precipitates after homogenization treatments

	Base	NH	SC
Volume fraction	Medium	Low	High
Number density	Low	High	High
Average size (μm)	0.22	0.14	0.18
Mn solute atom (wt %)	Medium (0.57)	High (0.64)	Low (0.40)

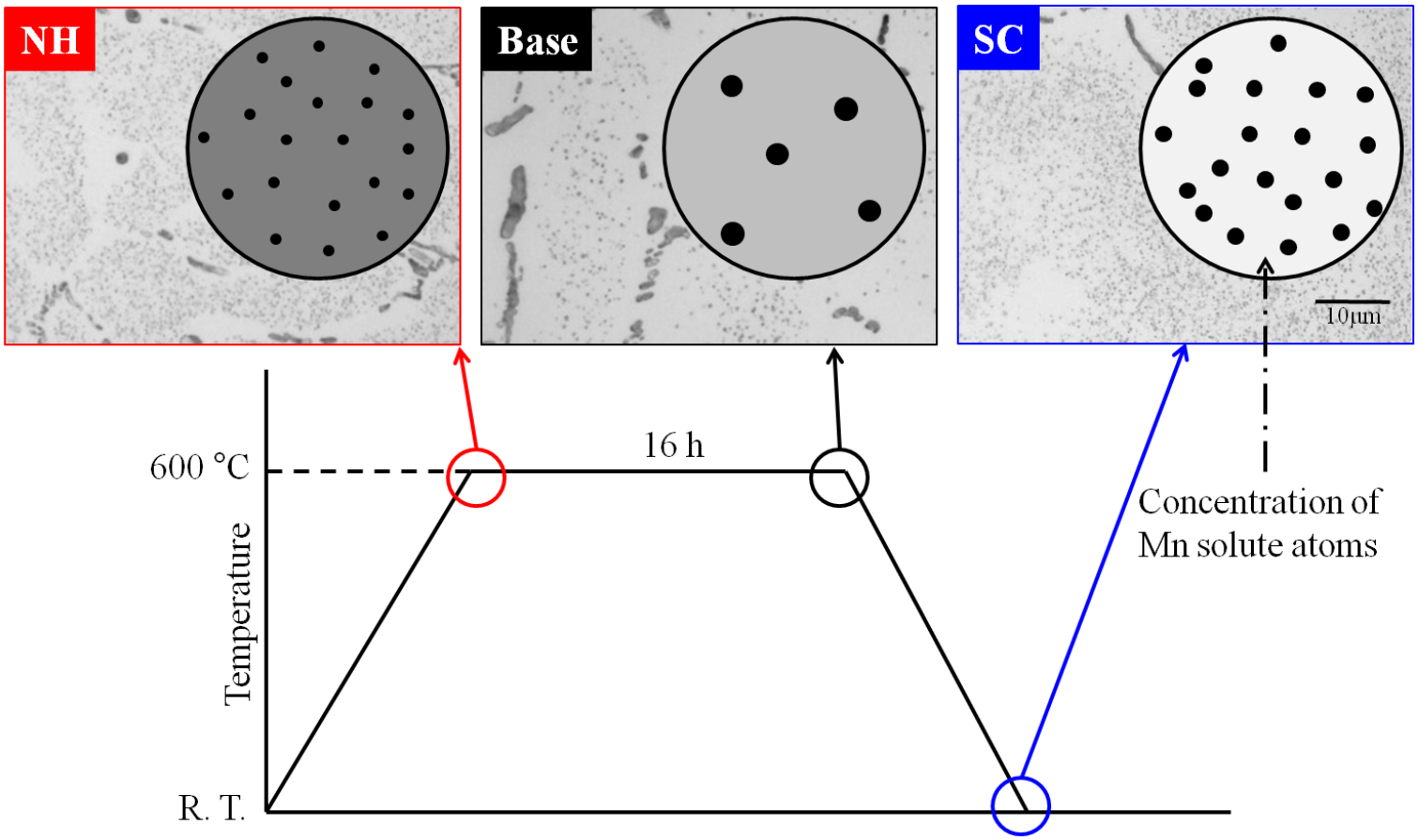

Figure 2.12 Schematic illustration of precipitation behavior during homogenization treatment.

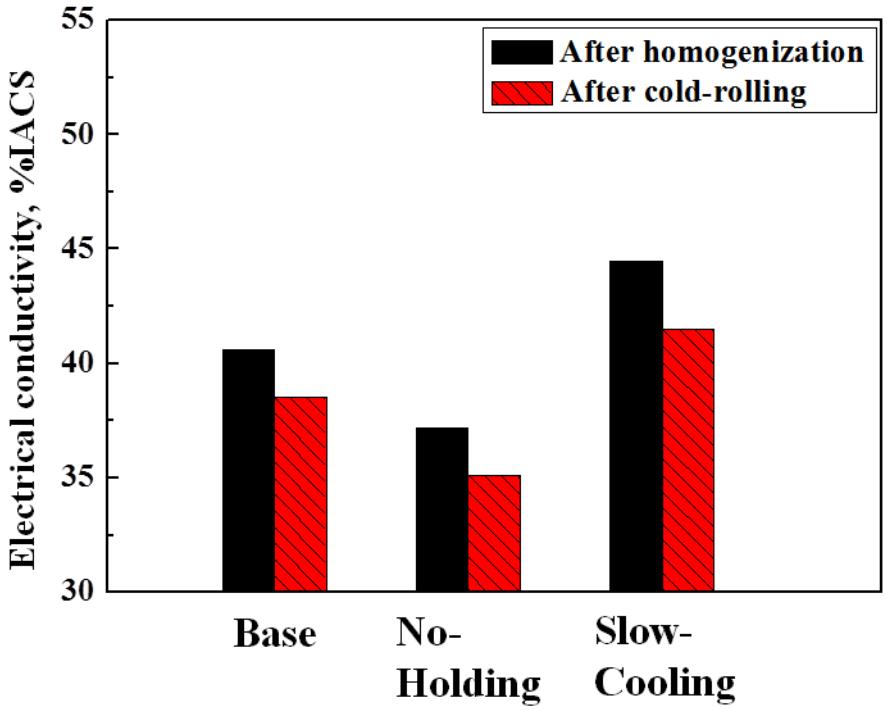

Figure 2.13 Change of the electrical conductivity before and after cold-rolling.

Chapter 3

Effects of annealing temperature and time on the recrystallization behavior of an Al-Mn alloy

3.1 Introduction

Recrystallization and recovery are two competing softening processes in deformed materials. Recrystallization is a process that involves the formation of a new grain structure in a deformed material by the formation and migration of high angle grain boundaries (HAGB) with the misorientation angles above 15 ° in aluminum [1]. Recovery can be defined as all annealing processes occurring in deformed materials without the migration of high angle grain boundaries (HAGB), i.e. dislocation rearrangement to lower the strain energy through the formation of sub-grains. Nucleation of recrystallized grains is typically found when high angle grain boundaries are produced, i.e. in the regions with lattice misorientation, deformation zones and shear bands. The nucleated new grains continue to grow with the rate depending on the grain boundary mobility. Grain growth normally appears as normal grain or abnormal grain growth [2]. Investigation on the deformed state is considered to be critical for studying recrystallization. Successful cases have been reported by many researchers [3-9] in which characterization of subgrain structures in the deformed states are carried out to

investigate the recrystallization mechanisms. Recrystallization is a thermally activated process; therefore temperature greatly influences the recrystallization rate. Heating rate can also be important and rapid heating may result in less time for recovery to occur which means that there is a lower reduction in the internal energy from recovery and hence recrystallization is more rapid [2]. The amount of strain affects the rate of recrystallization by changing the amount of stored energy. Increasing the strain rate of deformation prior to recrystallization increases the rate of recrystallization. Davenport et al. has been carried out on the strain path effect on recrystallization and they are primarily focused on cold worked aluminum [10]. The objective of this Chapter is to investigate the changes of recrystallization time and temperature depending on the different homogenized microstructures.

3.2 Experimental procedure

Same alloys after designed homogenization treatments are used in this study. In order to investigate the temperature dependence of recrystallization behavior with designed homogenization treatment, the isochronal annealing treatment was conducted at temperatures from 250 to 500 °C for 1 h in the salt bath after cold-rolled. The isothermal annealing treatment also conducted at 350 °C in order to investigate the time dependence. The thermo-mechanical processes in this study are schematically illustrated in Figure 3.1. Microstructure observations and hardness measurements are performed in a same way with Chapter 2.

3.3 Results

3.3.1 Softening phenomena with annealing temperature for 1 hour

Figure 3.2 shows the softening curves during isochronal annealing at each temperature for 1 hour. The hardness of the Slow-Cooling specimen is dropped at low temperature and the No-Holding specimen is dropped at high temperature to around 35 HV compared with the Base specimen.

Figure 3.3 shows the microstructure of the Base specimen during isochronal annealing at each temperature for 1 hour. The recrystallized grains are generated and increased gradually with increasing annealing temperature.

Figure 3.4 shows the microstructure of the Base, No-Holding, and Slow-Cooling specimens after isochronally annealed for 1 hour at low temperature. The deformation microstructure was observed clearly in all of specimens.

Figure 3.5 shows the microstructure of all specimens after isochronally annealed for 1 hour at 500 °C. All of the specimens exhibit recrystallization microstructures. However, the size of recrystallized grains is large in the No-Holding specimen compared with other specimens.

3.3.2 Softening phenomena with annealing time at 350 °C

Figure 3.6 shows the softening curves during isothermal annealing at 350 °C. The results are similar to the results of isochronal annealing treatment. The hardness of the Slow-Cooling specimen is dropped at the short time and the No-Holding specimen is dropped at the long time to around 35 HV compared with the Base specimen. Moreover, the recrystallization time is extremely delayed in the No-Holding specimen.

Figure 3.7 shows the microstructures of the Base specimen after isothermal annealing at

350 °C for 60s, 300s, and 345.6ks, respectively. The deformation bands were displaced by the recrystallized grains with annealing time. Moreover the recrystallized grains slightly grew up.

Figure 3.8 shows the microstructures of the No-Holding specimen after isothermal annealing at 350 °C for 1.8ks, 18ks, and 345.6ks, respectively. The deformation bands grew gradually with annealing time.

Figure 3.9 shows the microstructures of the Slow-Cooling specimen after isothermal annealing at 350 °C for 10s, 60s, and 345.6ks, respectively. The deformation bands were rapidly displaced by recrystallized grains. The grain size is smallest compared with other specimens. However, the growth of the recrystallized grains is not observed.

Figure 3.10 shows the microstructure of the Base, No-Holding and Slow-Cooling specimens after isothermal annealing for 0.3ks, 18ks, and 60s, respectively. The deformation bands were displaced by the recrystallized grains in the Slow-Cooling specimens and partially remained deformation bands in the Base specimen. However, the growth of deformation bands appeared in the No-Holding specimen. The size of the recrystallized grains is large in the Base specimen compared with the Slow-Cooling specimens.

Figure 3.11 shows the microstructure of the Base, No-Holding and Slow-Cooling specimens after isothermal annealing for 345.6 ks (4 days). The recrystallized grains were formed completely in the Base and Slow-Cooling specimens. However, the deformation bands more grew up in the No-Holding specimen.

3.4 Discussion

3.4.1 Effect of the annealing temperature on the recrystallization behavior

The rate of recovery and recrystallization behavior and size of recrystallized grains are strongly influenced by annealing temperature. The hardness values of all specimens decrease from around 70HV to 35HV with increasing annealing temperature in Figure 3.2. Then, the hardness of each specimen remains almost constant with the value of around 35HV. The temperature at which the hardness becomes 35HV indicates that the recrystallization behavior is completed at this temperature. The temperature is designated as T_R in the present thesis. The temperature T_R is different with different homogenized microstructures. Based on the Figure 3.2, in the Slow-Cooling specimen the recovery and recrystallization occur at low temperature compared with that of the Base specimen. On the other hand, in the No-Holding specimen the recovery and recrystallization occur at high temperature compared with those in the Base specimen. The microstructure at lower temperature than T_R exhibited deformation bands in Figure 3.4. The recrystallized grains of the Base specimen were generated with increasing annealing temperature for 1 hour in Figure 3.3. It indicates that the recovery and recrystallization behavior are accelerated at high annealing temperature in the same homogenized specimens. The size of the recrystallized grains also decreased with increasing annealing temperature such as Figure 3.3 (d) and Figure 3.5 (A). In case of the Base and Slow-Cooling specimens, the size of recrystallized grain corresponds with the distribution of precipitates. However, in case of the No-Holding specimen, large recrystallized grain appeared at high temperature compared with other specimens even though the number density of precipitates is high. It will be mentioned at Chapter 4.

3.4.2 Effect of the annealing time on the recrystallization behavior

The recrystallization time also is different with different homogenized microstructures even though the specimens are the same alloy. The hardness of the Base, No-Holding, and Slow-Cooling specimens at 350 °C decreased with increasing annealing time from the beginning to about 30 s, 600 s and 4.3×10^5 s, respectively, in Figure 3.6. The time when the hardness becomes almost constant of 35HV is designated as t_R in the present thesis. The hardness of each specimen remains almost constant after longer annealing time than t_R. The figure 3.7, 3.8 and 3.9 shows the change the microstructure of specimens during isothermal annealing at 350 °C. When the hardness reached to 35HV in the Base and Slow-Cooling specimens, the recrystallized grains are almost generated. In other word, the recrystallization behavior in the Base, Slow-Cooling specimens are finished at around 300s and 60s, respectively. On the other hand, the recrystallized grains were not observed while the elongated grains were observed in the No-Holding specimen even though the value of hardness dropped certainly. Moreover, the elongated grains grew with increasing annealing time in the No-Holding specimen. In case of low temperature, the size of recrystallized grains corresponds to the distribution of precipitates even though grain growth occurred slightly compared with the case of high temperature. However, in the No-Holding specimen, the Zenner pinning effect by precipitates does not work even though the No-Holding specimen contains high number density of fine precipitates. Figure 3.10 shows the comparison of microstructures at around t_R. The different recrystallization behavior is revealed between the No-Holding and other specimens definitely. This phenomenon will be discussed in Chapter 4.

3.4.3 Separation between recovery and recrystallization behaviors.

Usually, the recrystallization behavior can be defined as recovery, nucleation and grain growth stages. However, in this thesis, the recrystallization behavior would define as recovery, nucleation, grain growth, and coarsening stages by using hardness results and microstructures. Because, the driving force between the grain growth and coarsening stages is different. The grain growth occurs during the drop of the hardness. It means that the grain growth consumes the strain energy until impingement of grains. However, all strain basically disappeared at the coarsening stage. In case of this stage, the grain boundary energy is main driving force for the coarsening of grain. Therefore, grain growth and coarsening stage can be separated clearly. Figure 3.12 shows the schematic illustration for the separation of recrystallization behavior and the results of each specimen are summarize in the Table 3.1.

3.5 Conclusions

Effects of annealing temperature and time on the recrystallization behavior in the Al-Mn alloy are discussed. The optical microscope and hardness measurement were applied in order to investigate the recrystallization behavior. Obtained experimental results are summarized as follows.

1. The recrystallization temperature, T_R, is different with different homogenized microstructures. The Slow-Cooling specimen has the low recrystallization temperature while the No-Holding specimen has the high recrystallization temperature.

2. At high temperatures, recrystallization occurred completely in all specimens. However, the

size of recrystallized grains is different. The recrystallized grains are largest in the No-Holding specimen compared with other specimens.

3. The recrystallization time, $t_{R,}$ is also different with different homogenization conditions. The Slow-Cooling specimen has short recrystallization time while the No-Holding specimen has long recrystallization time.

4. At low temperatures, recrystallization occurred completely in the Slow-Cooling and Base specimens. However, the elongated grains appeared and grew up in the No Holding specimen even though annealing time was extended.

References

1. P. Heilmann, W. A. T. Clark, and D. A. Rigney, Acta Metall Sin., **31** (1983), 1293 .

2. R. D. Doherty, D. A. Hughes, F. J. Humphreys, J. J. Jonas, D. Juul Jensen, M. E. Kassner, W. E. King, T. R. McNelley, H. J. McQueen, and A. D. Rollett, , Mater. Sci. Eng., A, **238** (1997), 219.

3. T. Hasegawa, and U. F. Kocks, Acta Metal.l Sin., **27** (1979), 1705.

4. N. Hansen, and B. Bay, Acta Metall. Sin., **29** (1981), 65.

5. M. Ferry, and P. R. Munroe, Scr. Mater., **33** (1995), 857.

6. S. Gourdet, and F. Montheillet, Mater. Sci. Eng., A, **283** (2000), 274.

7. Y. Huang, and F. J. Humphreys, Acta Mater., **45** (1997), 4491.

8. E. A. Holm, M. A. Miodownik, and A. D. Rollett, Acta Mater., **51** (2003), 2701.

9. H. Hu, L. Zhen, B. Zhang, L. Yang, and J. Chen, , Mater. Charact., **59** (2008), 1185.

10. S. B. Davenport, and R. L. Higginson, J. Mater. Process. Technol., **98** (2000), 267.

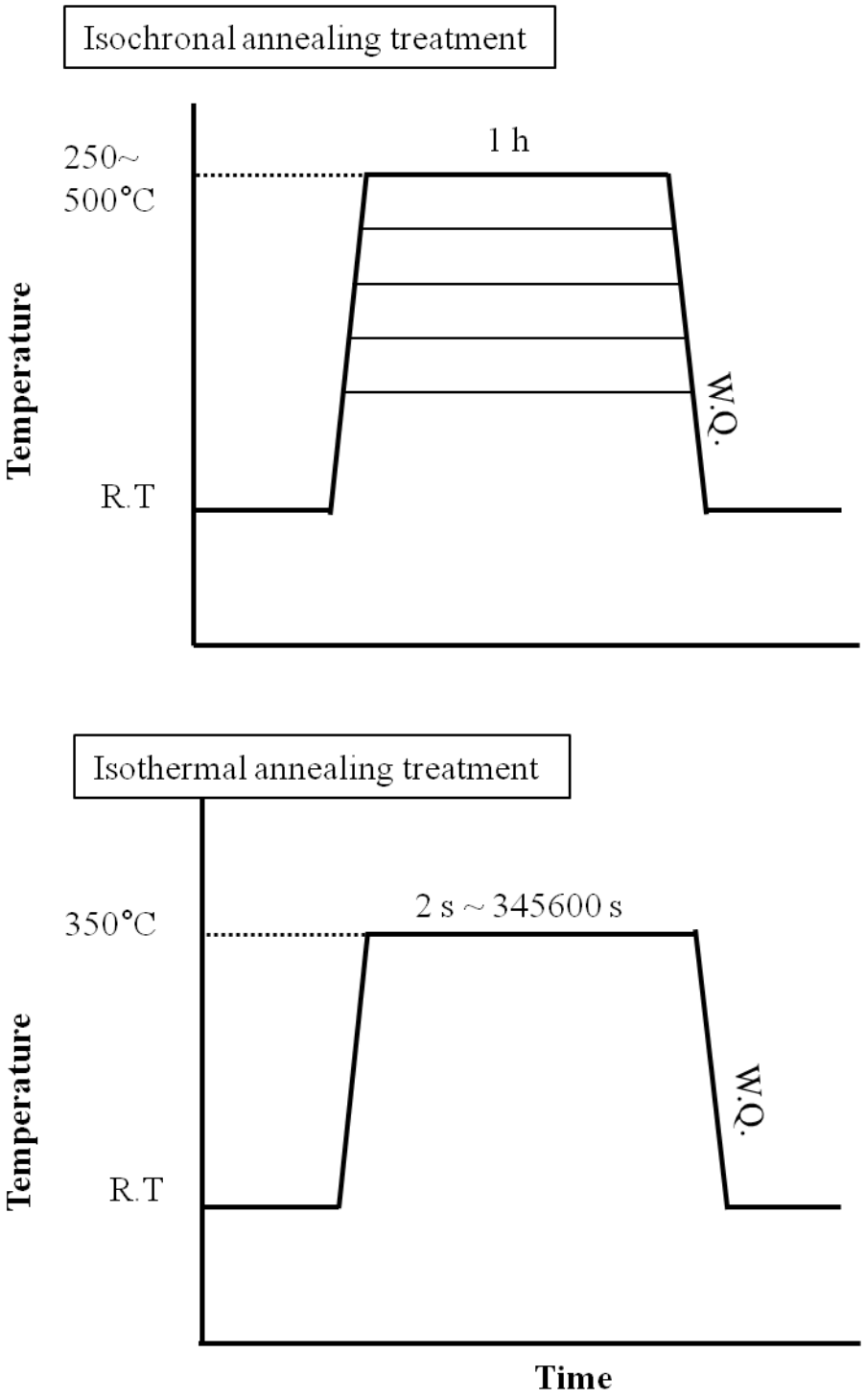

Figure 3.1 Schematic illustrations of annealing treatments.

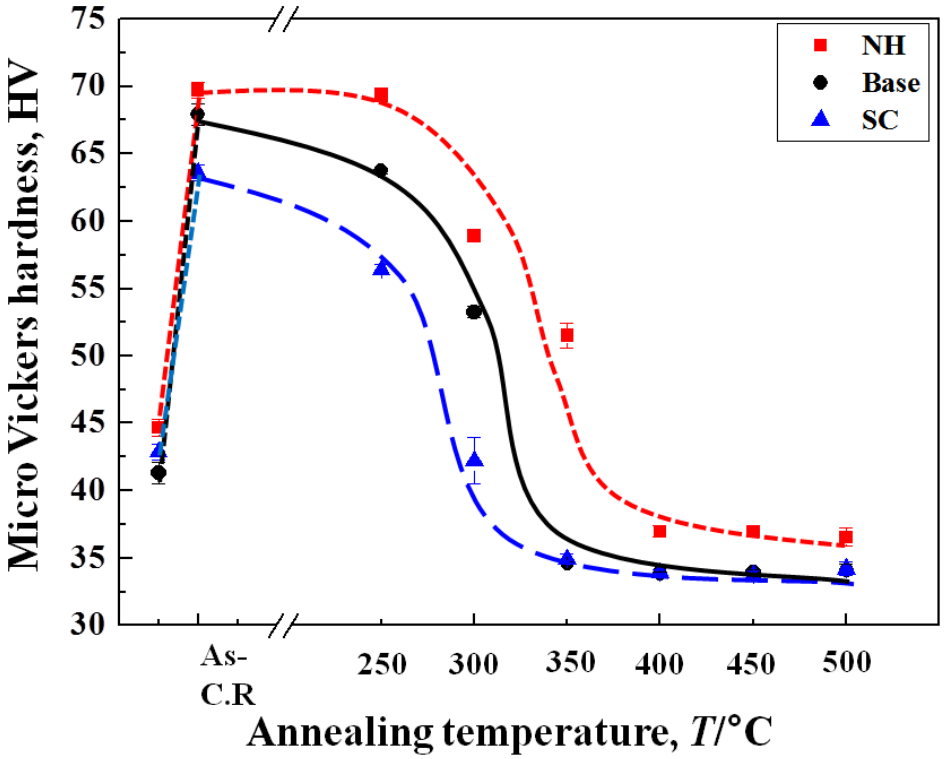

Figure 3.2 Changes of micro Vickers hardness during isochronal annealing at various temperatures for 1 hour.

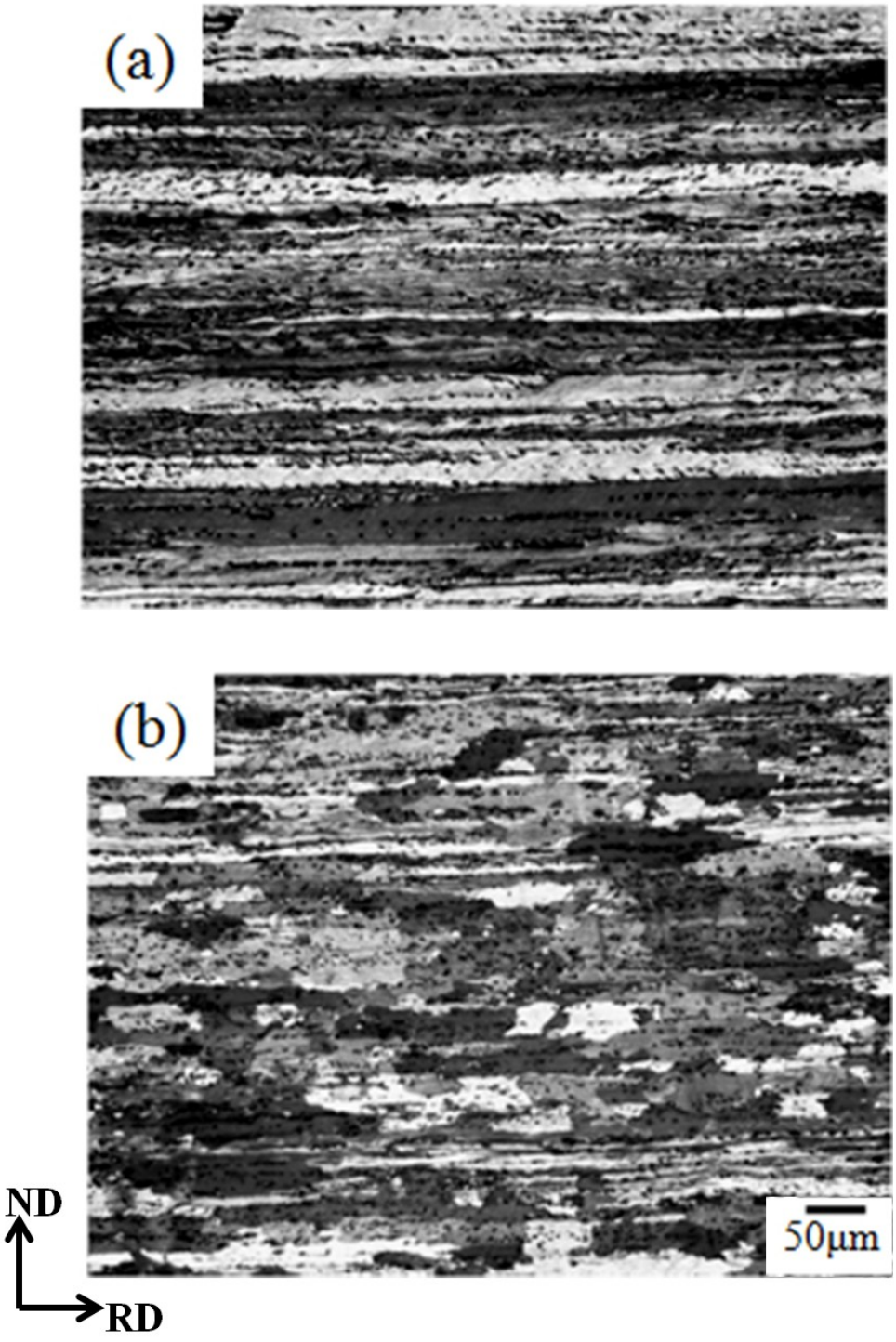

Figure 3.3 Microstructures of the Base condition specimen after isochronally annealed for 1 h at temperatures of (a) 300°C, (b) 325°C, (c) 350°C and (d) 400°C.

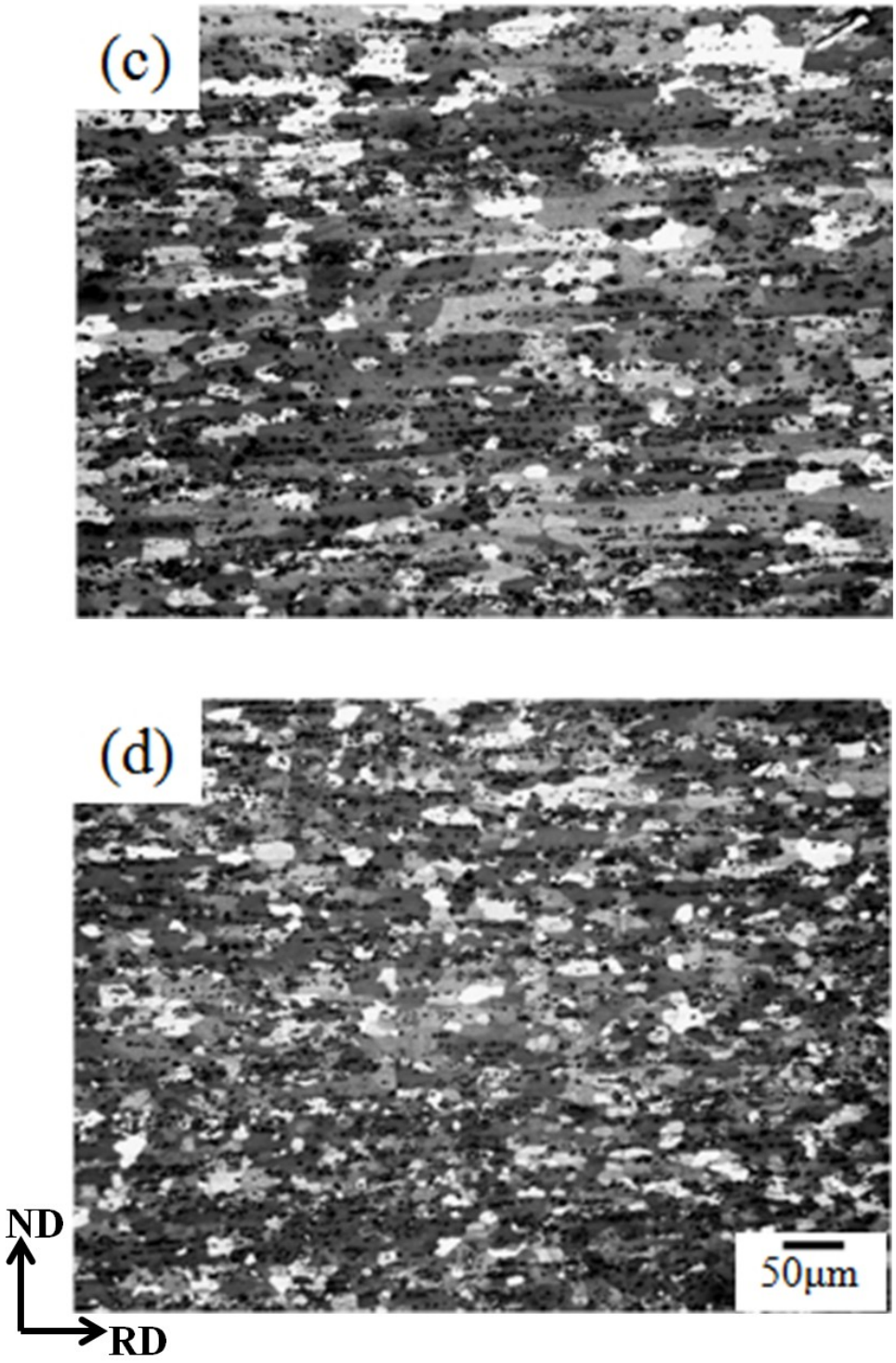

Figure 3.3 Continued.

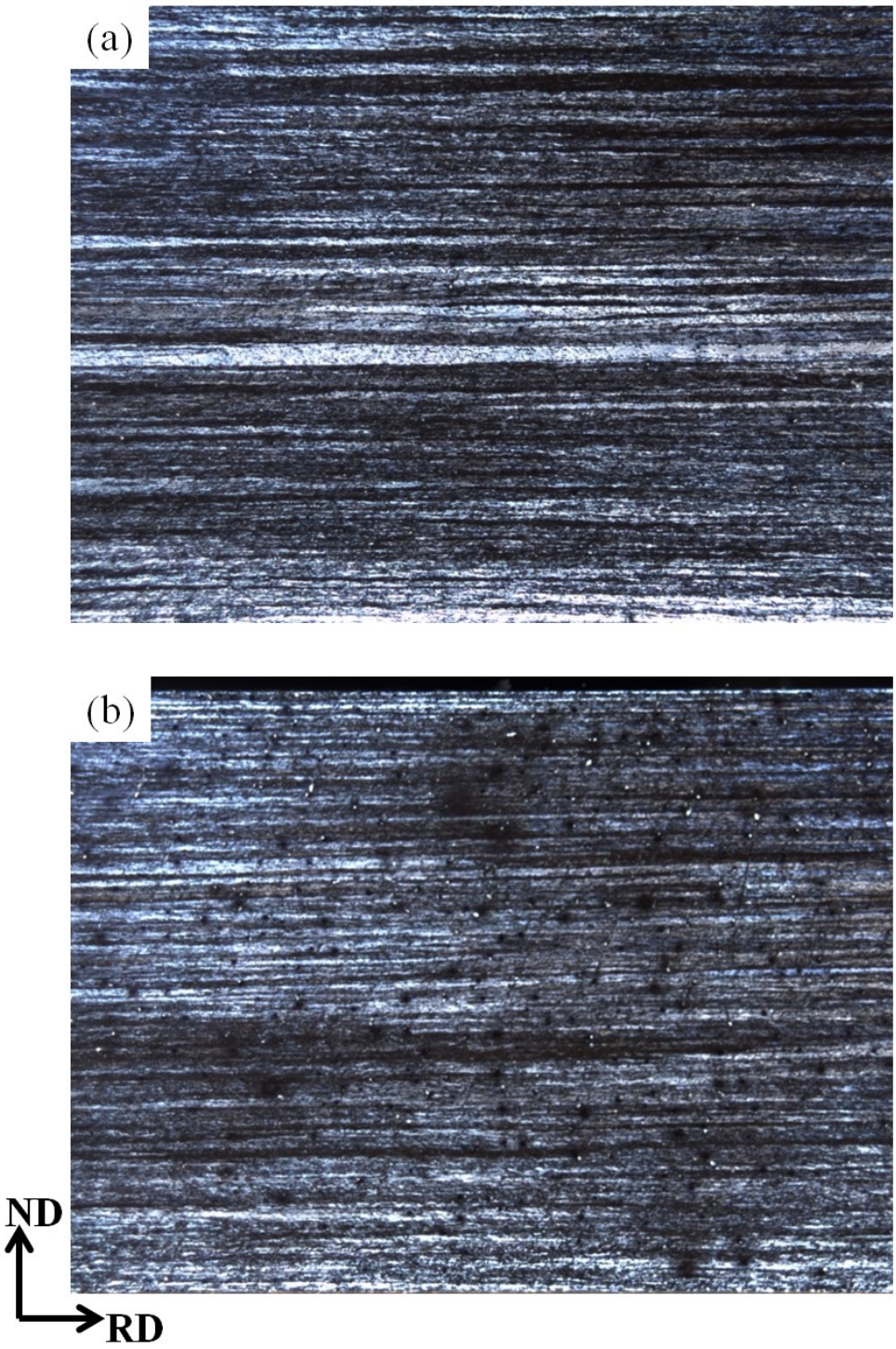

Figure 3.4 Microstructures after isochronally annealed for 1h at 300 °C of (a) Base, (b) No-Holding, and at 250 °C of (c) Slow-Cooling conditions.

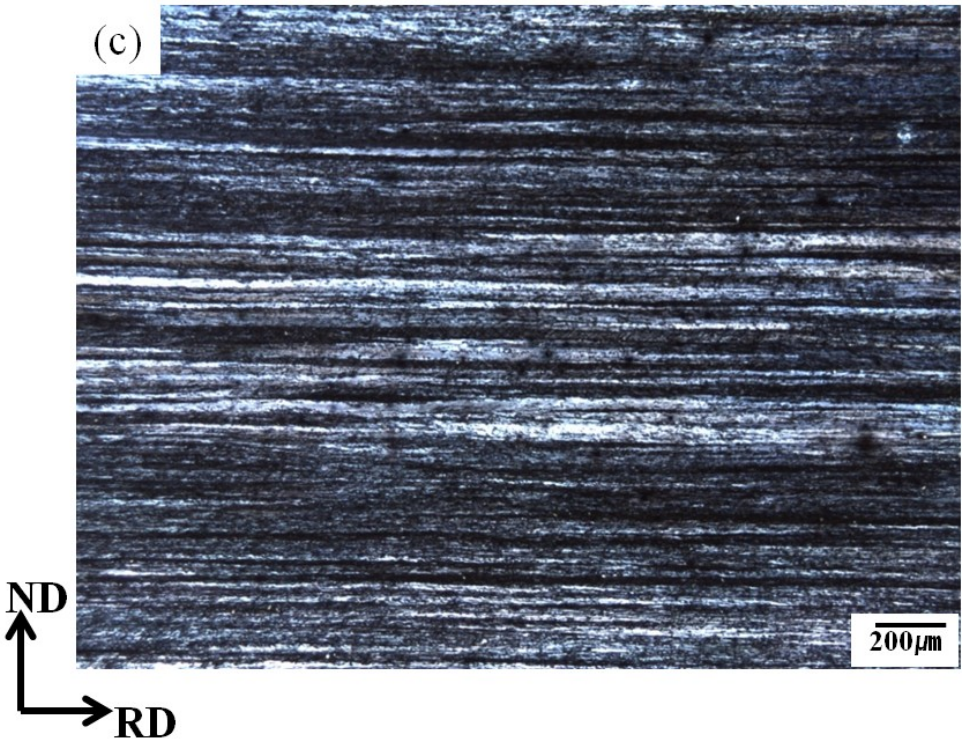

Figure 3.4 Continued.

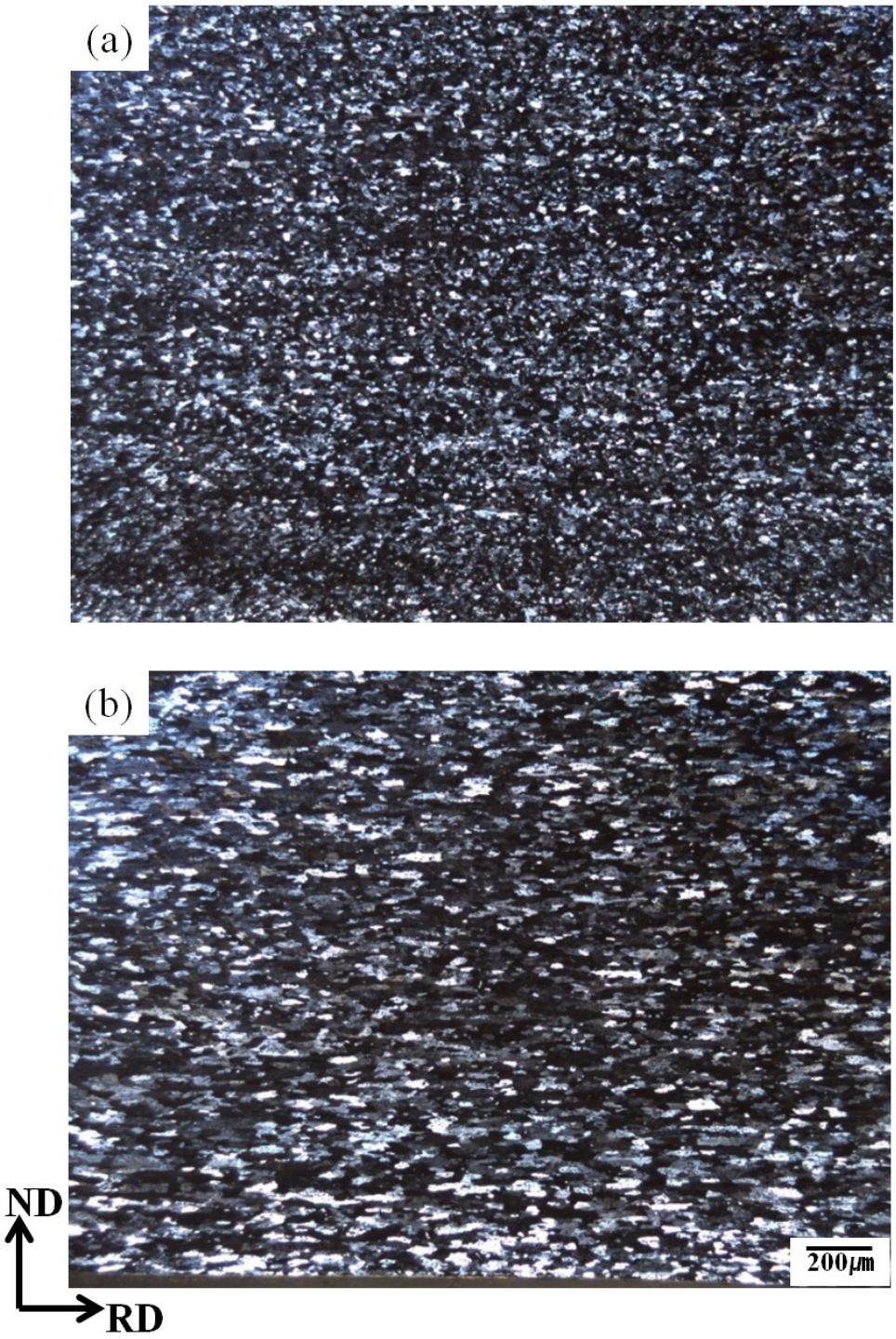

Figure 3.5 Microstructures after isochronally annealed for 1 h at 500 °C, (a) Base, (b) No-Holding, and (c) Slow-Cooling conditions.

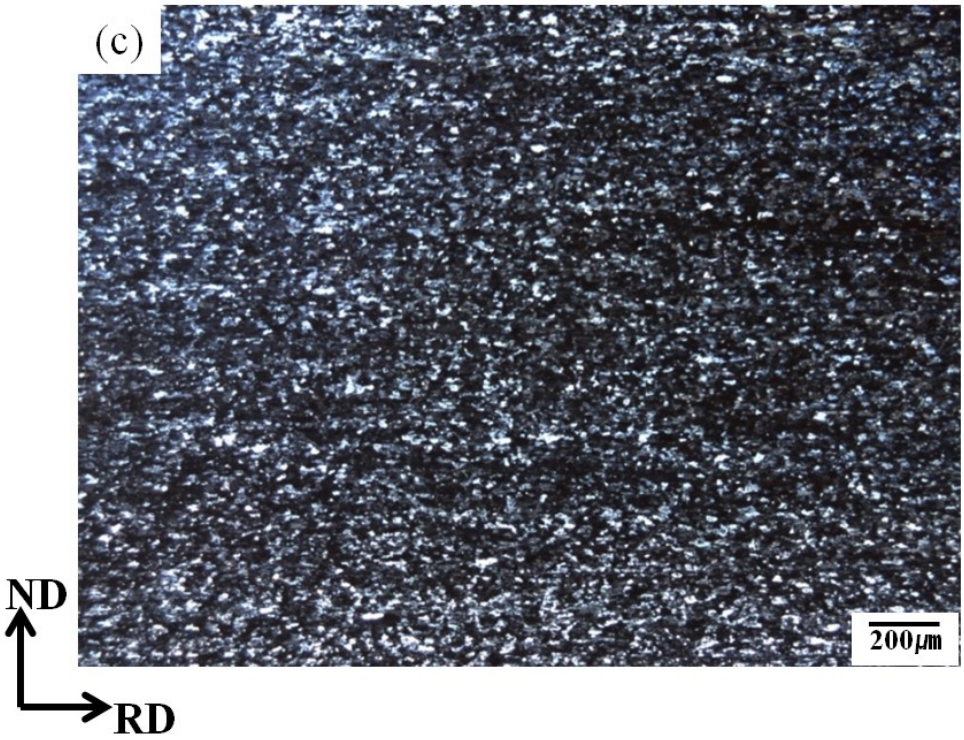

Figure 3.5 Continued.

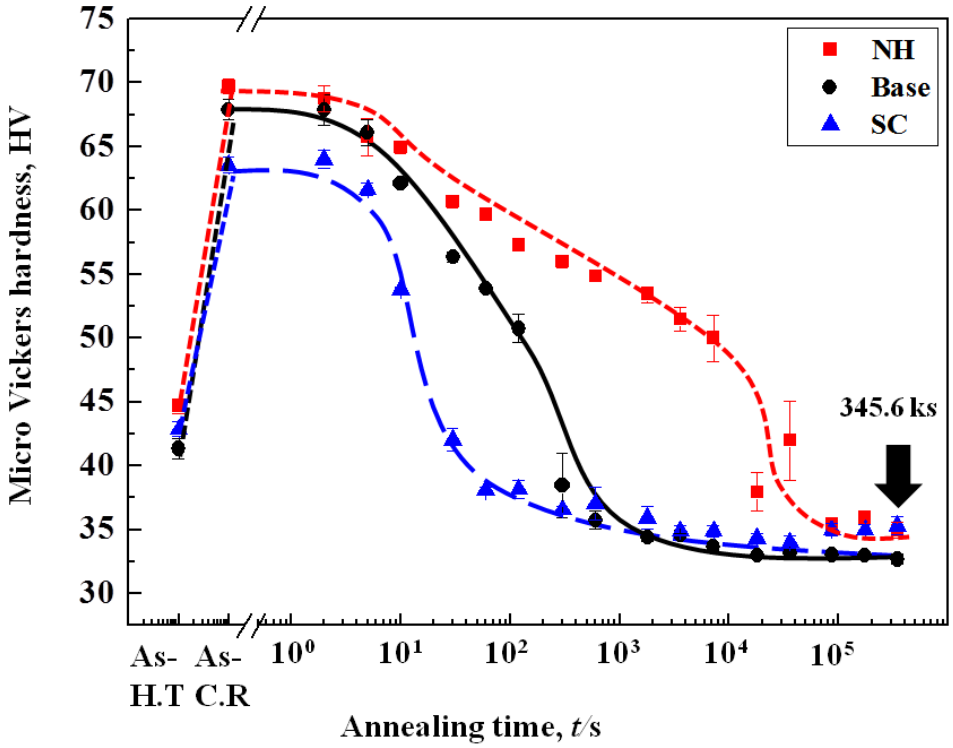

Figure 3.6 Changes of micro Vickers hardness for the specimens with the Base, NH and SC conditions during isothermal annealing at 350°C

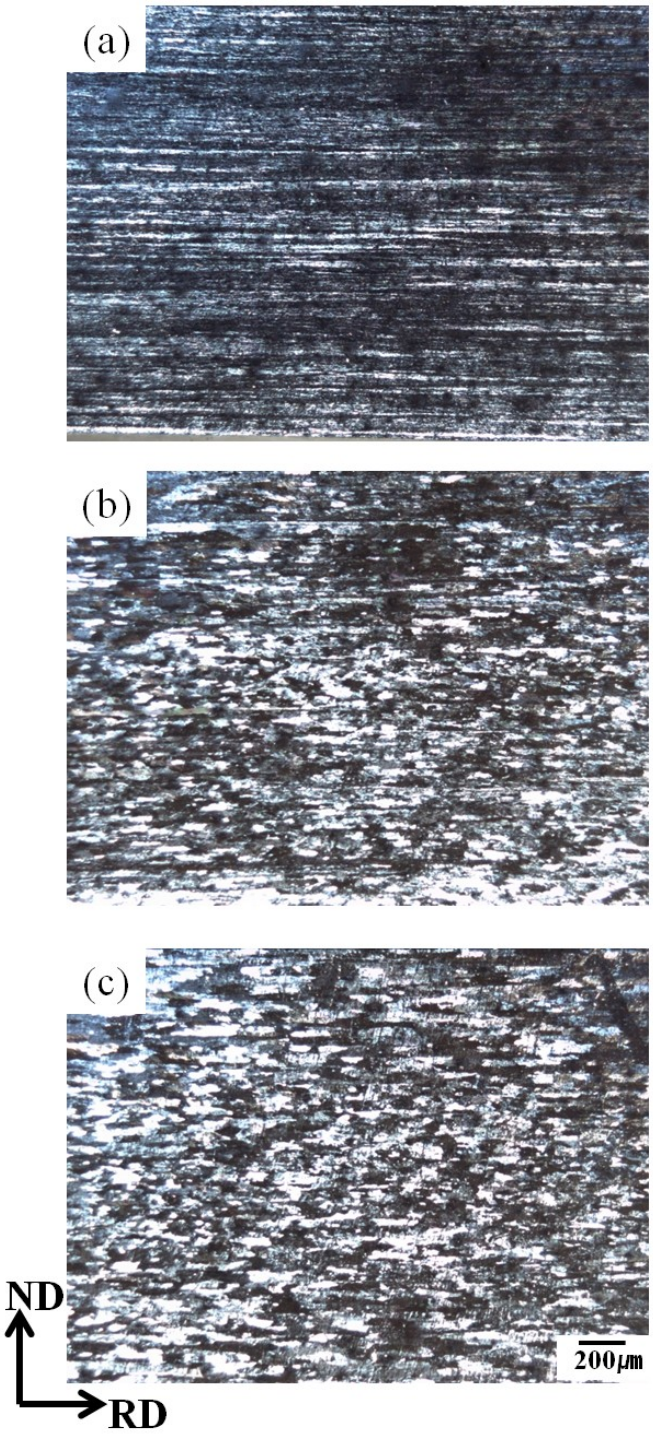

Figure 3.7 Microstructures after isothermally annealed at 350°C for (a) 60 s, (b) 300 s, and (c) 345.6ks in the Base specimen.

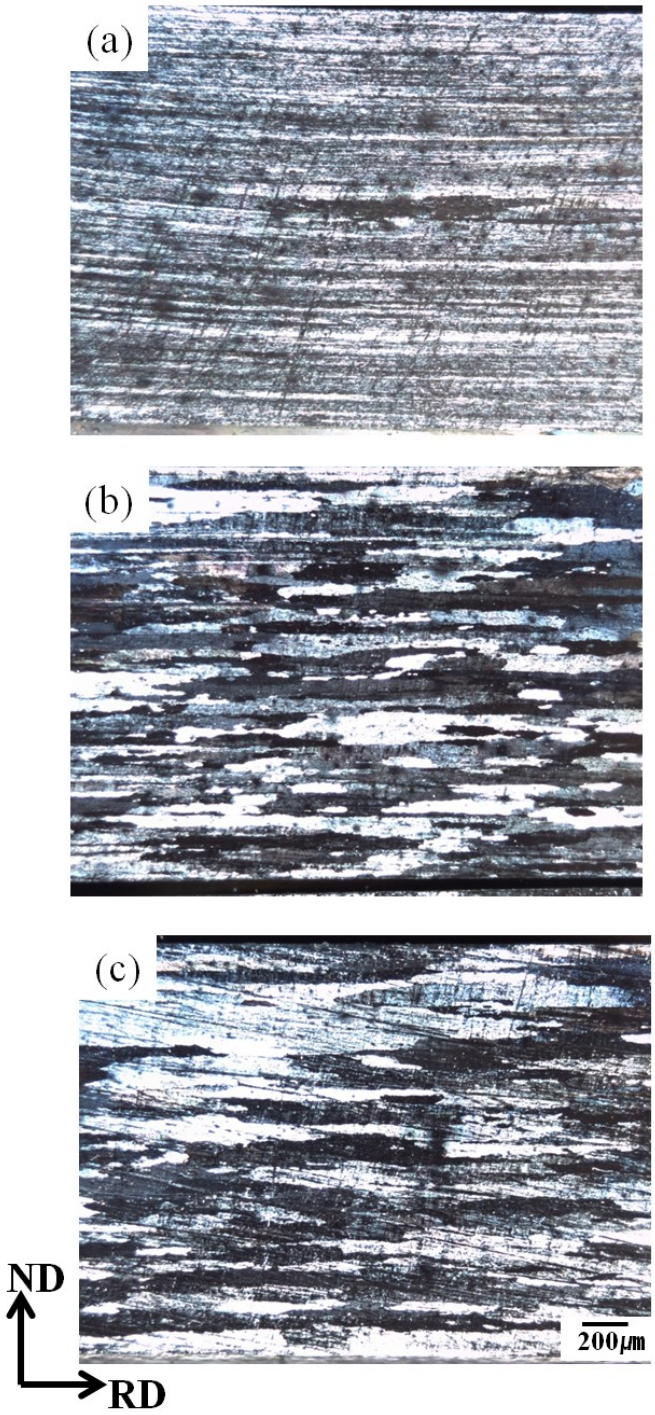

Figure 3.8 Microstructures after isothermally annealed at 350°C for (a) 1.8 ks, (b) 18 ks, and (c) 345.6ks in the No-Holding specimen.

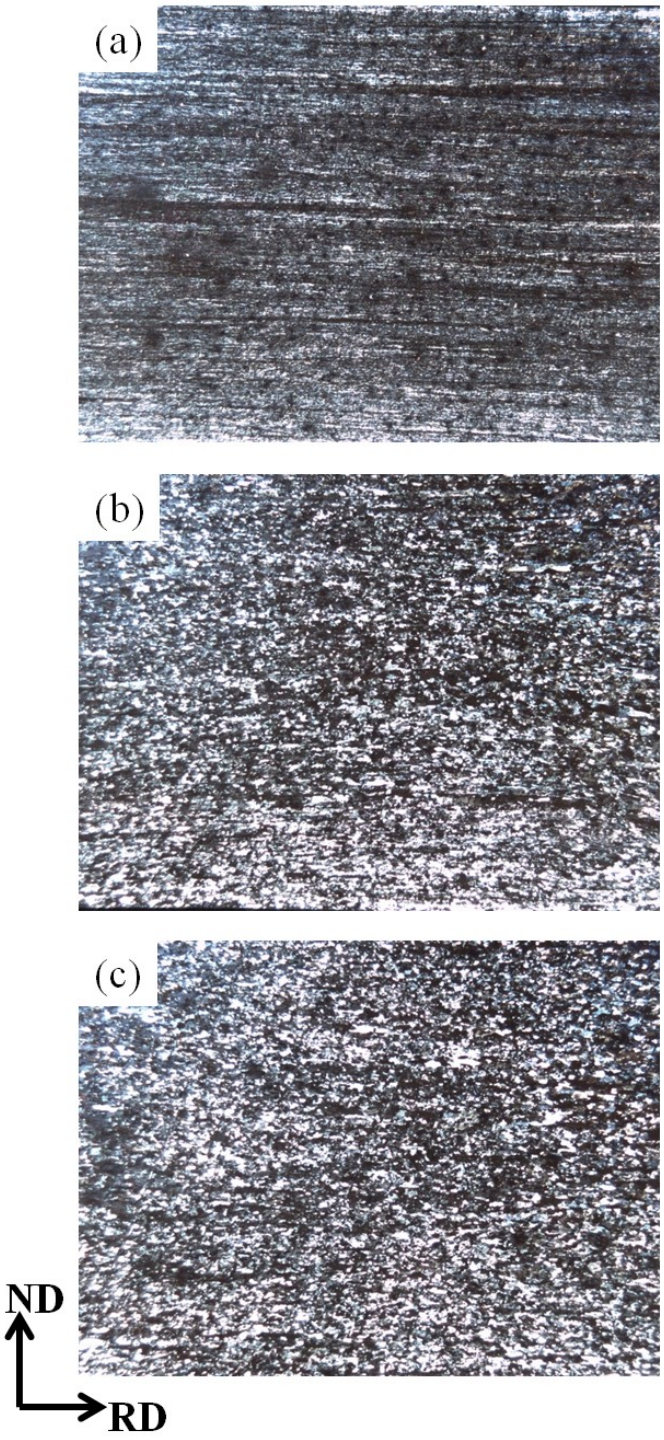

Figure 3.9 Microstructures after isothermally annealed at 350°C for (a) 10 s, (b) 60 s, and (c) 345.6ks in the Slow-Cooling specimen.

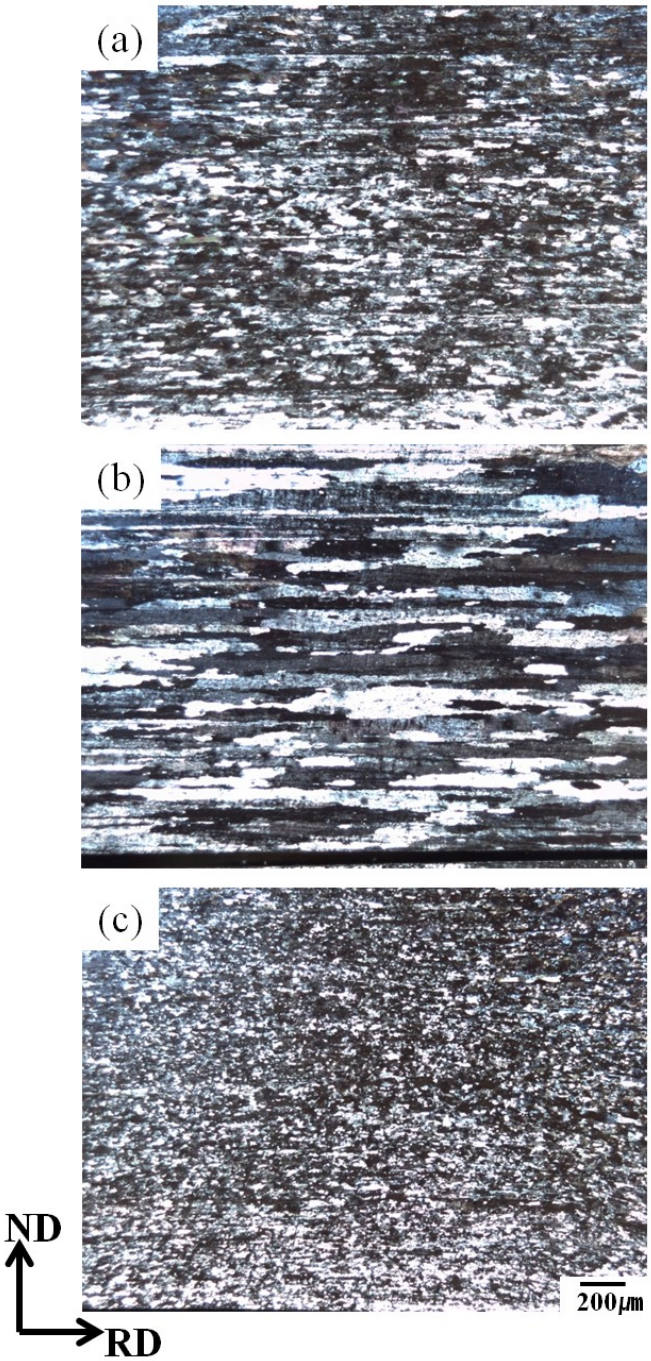

Fig. 3.10 Microstructures after isothermally annealed of (a) Base for 300 s, (b) NH for 18 ks, and (c) SC for 60 s.

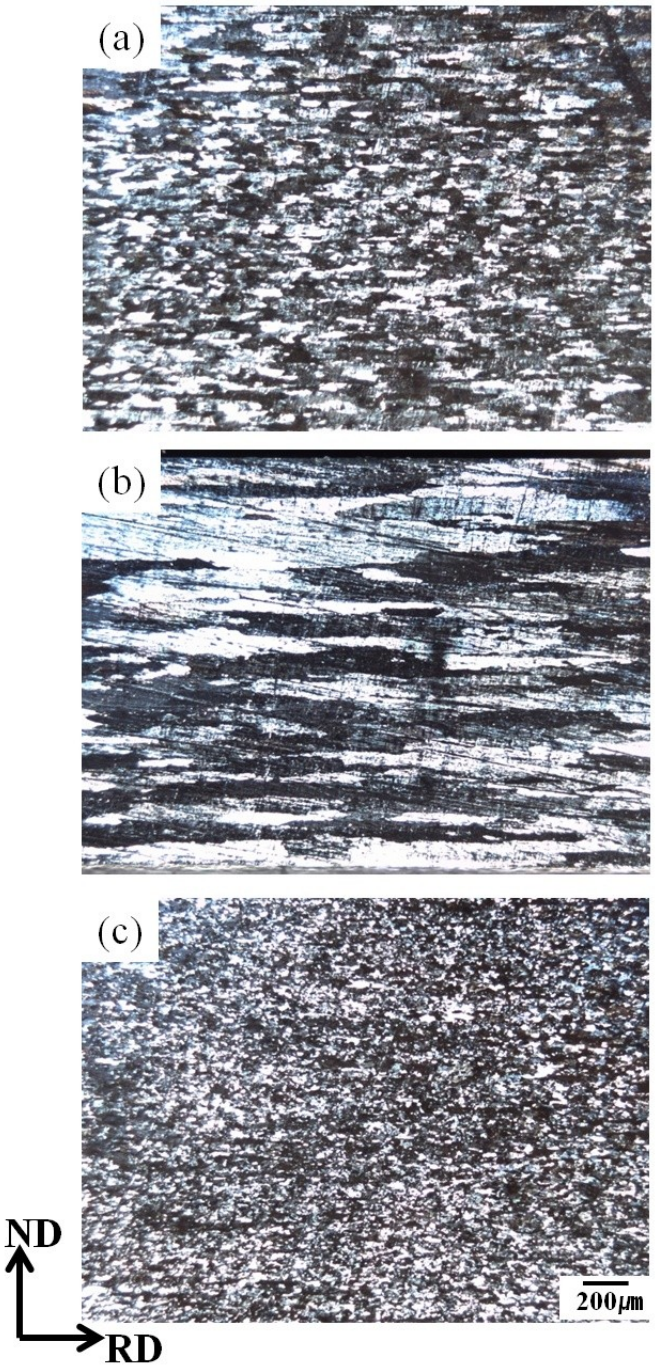

Figure 3.11 Microstructures after isothermally annealed for 345.6 ks at 350 °C (a) Base, (b) NH and (c) SC conditions.

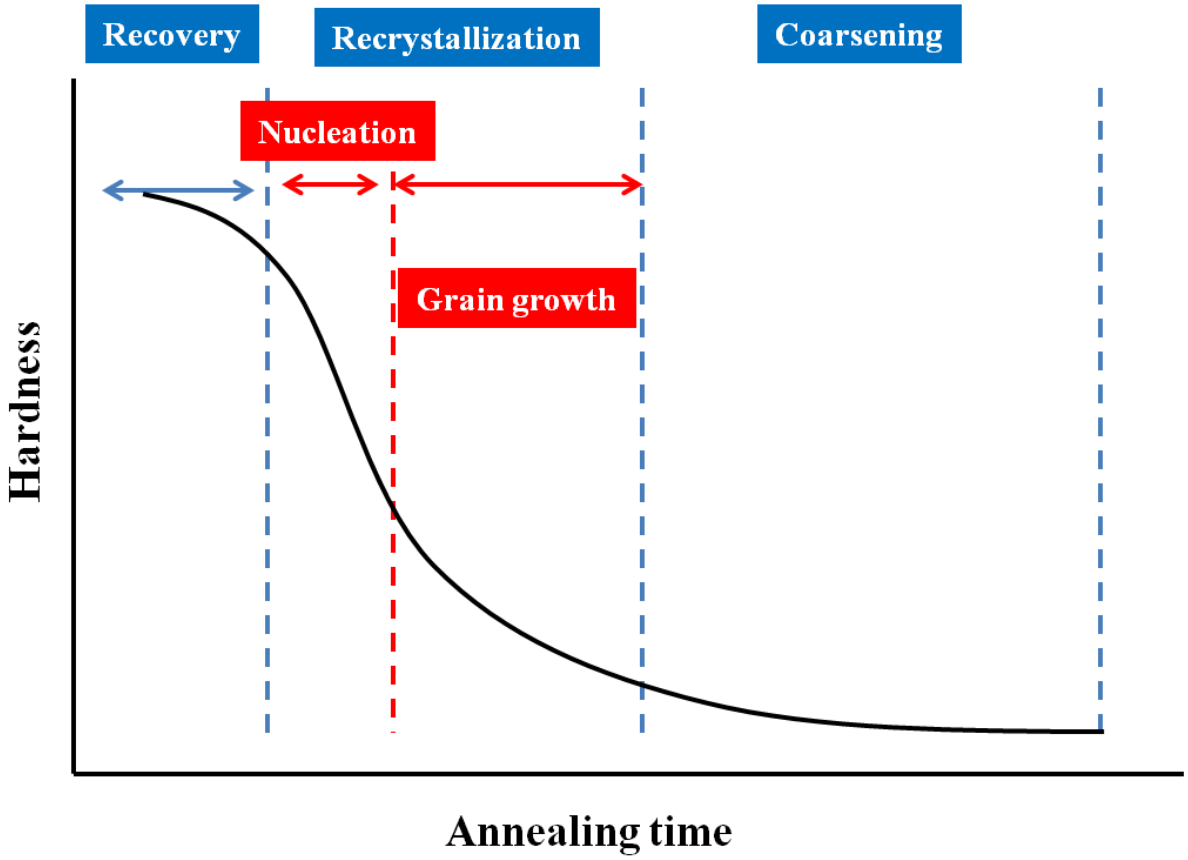

Figure 3.12 Recovery, recrystallization and coarsening stages during isothermal annealing. The recrystallization stage is divided into the initial nucleation and subsequent growth stages in the present work to understand microstructures.

Table 3.1 Summary for the stages during isochronal and isothermal annealing for the NH, Base and SC conditions.

(for 1hour)	NH	Base	SC
250 °C	Recovery	Recovery	Nucleation
350 °C	Recovery	Nucleation & Grain growth	Nucleation & Grain growth
500 °C	Nucleation & Grain growth	Coarsening	Coarsening
(at 350 °C)	NH	Base	SC
1 minute	Recovery	Recovery	Nucleation & Grain growth
5minutes	Recovery	Nucleation & Grain growth	Coarsening
5hours	Grain growth	Coarsening	Coarsening

Chapter 4

Combined effects of Mn containing dispersoids and Mn solute atoms on the recrystallization microstructures of an Al-Mn alloy

4.1 Introduction

The retardation effect by the small particles on the grain boundaries motion is called Zener pinning effect [1]. This effect has been investigated by many researchers through experimental and modeling approaches [1-11]. For a random distribution of spherical, mono-sized particles, the pinning pressure/force P_z exerted on the boundary is given by Eq. 4.1 [1].

$$Pz = \frac{3\gamma F_v}{2r} \qquad (4.1)$$

Where γ is the specific boundary energy, F_v, is the particle volume fraction and r is the particle radius. The growth of recrystallized grain is controlled by the competition of the two opposing pressures, i. e. driving pressure for growth and Zener Pining, therefore the sum of these two parts (positive or negative) is sometimes used to roughly determine whether recrystallization would occur or not [1]. It is clearly shown in Eq. 4.1 that the ratio of F_v/ r is a critical parameter. In fact, the size / spatial distribution, volume fraction, morphology of the particles also affect the recrystallization [12-19].

The deformation zones formed around large particles (1~2μm) can act as nucleation sites for

recrystallization grains because they have high dislocation density and large lattice orientation [20]. This phenomenon is termed as particle stimulated nucleation (PSN). The critical particle parameter for PSN to occur depends on temperature and strain. As shown in Figure 4.1, during high temperature deformation, the PSN may not occur, i.e. deformation zones around particles are not formed, and the process is nucleation limited while during low temperature deformation it is growth-limited. When there is a bimodal size distribution of particles in the material, both the pining effect and PSN may operate concerning both nucleation and recrystallization kinetics [21]. In this Chapter, the effects of constituent particles, especially precipitates, on the recrystallization behavior and microstructures, especially the size of recrystallized grains, are focused. Also, the effect of Mn solute atoms on the rate of recrystallization and determination between continuous and discontinuous recrystallization will be discussed.

4.2 Experimental procedure

Same alloys after designed homogenization treatments are used in this study. In order to investigate the recrystallization behavior of homogenized specimens, the isochronal annealing treatment was conducted at temperatures from 250 to 500 °C for 1 h in the salt bath after cold-rolled. The isothermal annealing treatment was also conducted at 350 °C. The thermo-mechanical processes in this study are schematically illustrated in Figure 4.2. Microstructure observations, electrical conductivity, and hardness measurements are performed in a same way with Chapter 2.

4.3 Results

Figure 4.3 shows the microstructures after annealing treatment for 1 hour at 500 °C. At the high temperature, the recrystallization behavior finished completely. The size of recrystallized grains is different with different homogenization conditions. The No-Holding specimen has large recrystallized grains while Slow-Cooling specimen has small recrystallized grains compared with the Base specimen.

Figure 4.4 shows the change of electrical conductivity after isochronal annealing treatment for 1 hour. From as-cold rolled, the conductivity is increased slightly with annealing temperature in the Base and Slow-Cooling specimens. However, the conductivity is drastically increased in the No-Holding specimen. It indicates that the precipitation behavior occurs strongly with increasing annealing temperature in the No-Holding specimen compared with other specimens.

Figure 4.5 shows the microstructures after annealing treatment at 350 °C for 300 s, 18 ks, and 60 s of the Base, No-Holding, and Slow-Cooling specimen, respectively. The recrystallization behavior is already finished in the Base and Slow-Cooling specimen. However, the No-Holding specimen generated elongated grains.

Figure 4.6 shows the microstructures after annealing treatment at 350 °C for 345.6 ks of all specimens. The recrystallized grains of the Base and Slow-Cooling specimens grow up slightly while the elongated grains of the No-Holding specimen grow up drastically. It indicated that the recrystallization behavior between the No-Holding and other specimens occurred by different mechanisms. The continuous recrystallization behavior occurred without nucleation of new grains in the No-Holding specimen while the discontinuous recrystallization behavior occurred with nucleation of new grains in the Base and Slow-

Cooling specimens.

Figure 4.7 shows the change of electrical conductivity after isothermal annealing treatment at 350 °C. The conductivity is increased slightly in the Base and Slow-Cooling specimen from as-cold rolled. However, the conductivity is drastically increased in the No-Holding specimen. This result is also assumed to be the same trend as that shown in Figure 4.4. It indicates that the concentration of Mn solute atoms is assumed to play an important role to determine the continuous or discontinuous recrystallization.

4.4 Discussion

The characteristic of precipitates were mentioned in Chapter 2. Figure 4.8 shows the microstructure after each homogenization treatment at high magnification and summarized in Table 4.1. The number density of precipitates is higher in the No-Holding and Slow-Cooling specimens compared with the Base specimen. According to the Zener pinning effect, the No-Holding and Slow-Cooling specimens must has small recrystallized grains. However, the No-Holding specimen has large recrystallized grains at high annealing temperature and large elongated grains at low annealing temperature. In other words, the recrystallization behavior of the No-Holding specimen is influenced by another factor. It is due to the Mn solute atoms. Furthermore, Mn solute atoms may influence on the rate of recovery before the recrystallization behavior.

4.4.1 Effect of Mn solute atoms on the recrystallization behavior.

It is known that the electrical conductivity of the alloy has a linear relationship with the reciprocal of the concentration of an alloying element in the solid solution. The AA3003 alloy

contains Mn, Fe and Si elements. However, the electrical conductivity is not particularly influenced by Fe and Si because the amount of contained Fe and Si is small in the present alloy. Therefore, the change of electrical conductivity is mainly due to the variation of Mn in the solid solution. The electrical conductivity, resistance and Mn concentration are shown in Table 4.2. The concentration of Mn solute atoms is the highest in the No-Holding specimen. The Slow-Cooling specimen contains the lowest Mn concentration among the homogenized specimens. These results of the Mn concentration in the matrix are correlated with the micro Vickers hardness and microstructure. It is, then, concluded that the recrystallization temperature, T_R, and time t_R, decrease with decreasing concentration of Mn solute atoms. Moreover, even though the hardness is decreased, the elongated grains appeared in the No-Holding Specimen at 350 °C. It is indicated that the concentration of Mn solute atoms strongly influence on the rate of recovery and recrystallization and determination of the continuous and discontinuous recrystallization behavior. During annealing treatment, the recovery and recrystallization mainly occur. However, the precipitation also occurs in the case of the high concentration of Mn solute atoms in the matrix such as the No-Holding specimen.

Consequently, the concentration of Mn solute atoms strongly causes the retardation of recovery with decreasing annealing temperature due to the precipitation.

4.4.2 Effect of constituent particles on the recrystallization behavior.

The Zener pinning effect strongly influenced on the recrystallization microstructure in the Base and Slow-Cooling specimens. However, in the Slow-Cooling specimen the recrystallization behavior is quickly finished compared with the Base specimen. This means that the role of precipitates is not only the Zener pinning effect but also the particle stimulated

nucleation (PSN). The size of precipitates in the Slow-Cooling specimen is around 0.18μm. However, the number density of precipitates is higher compared with that in the Base specimen based on the Table 4.1. When many nuclei are formed by the particle stimulated nucleation at the initial stage, these nuclei cannot grow up largely due to the Zener pinning effect by precipitates. Thus, the Slow-Cooling specimen has smallest recrystallized grains compared with other specimens. The role of primary particles is the same as nucleation sites in all specimens.

Consequently, the distribution of precipitates strongly influences the size of recrystallized grains. Also, the precipitates contribute the particle stimulated nucleation (PSN) even though the size is smaller than 1μm. However, when the high Mn solute atoms remain, the role of precipitates becomes less important.

Based on the results, Figures 4.9 and 10 show the schematic illustration of the recrystallization behavior at high and low temperatures, respectively.

4.5 Conclusions

The effects of constituent particles and Mn solute atoms on the recrystallization behavior were investigated in the Al-Mn alloy with different thermo-mechanical processes using micro Vickers hardness, electrical conductivity measurements and microstructure observation. The obtained results are summarized as follows.

1. The No-Holding specimen had the high number density of precipitates after the homogenization treatment. However the recrystallization behavior occurred very slowly compared with other specimens by micro Vickers hardness. In addition, the elongated grains

were observed at low annealing temperature and large recrystallized grains were observed at high annealing temperature due to the high Mn solute atoms in the matrix.

2. The Slow-Cooling specimen showed the most rapid recrystallization behavior and finest recrystallized grains. It contained large amount of precipitates after the homogenization treatment compared with other specimens.

3. The concentration of Mn solute atoms strongly causes the retardation of recovery with decreasing annealing temperature due to the precipitation. The distribution of precipitates strongly influences the size of recrystallized grains. Also, the precipitates not only case the Zener pinning effect but also contribute the particle stimulated nucleation (PSN) even though the size is smaller than 1μm.

References

1. F. J. Humphreys, and M. Hatherly, Recrystallization and Related Annealing Phenomena (Second Edition) (Elsevier) (2004).

2. H. E. Vatne, O. Engler, and E. Nes, Mater. Sci. Technol., **13** (1997), 93.

3. T. Gladman, Proceedings of the Royal Society of London. Series A, Math. Phys. Sci., **294** (1966), 298.

4. T. Gladman, Scr. Metall. Mater., **27** (1992), 1569.

5. F. J. Humphreys, Acta Metall., **25** (1977), 1323.

6. B. N. Kim, and T. Kishi, Acta Mater., **47** (1999), 2293.

7. H. Zhang, E. V. Konopleva, and H. J. McQueen, Mater. Sci. Eng. A, **319** (2001), 711.

8. M. J. Jones, and F. J. Humphreys, Acta Mater., **51** (2003), 2149.

9. W. Liu, and J. Morris, Metall, Mater. Trans. A, **36** (2005), 2829.

10. F. J. Humphreys, and M. G. Ardakani, Acta Mater., **44** (1996), 2717.

11. A. Harun, E. A. Holm, M. P. Clode, and M. A. Miodownik, Acta Mater., **54** (2006), 3261.

12. M. Hillert, Scr. Metall., **18** (1984), 1431.

13. E. Nes, N. Ryum, and O.Hunderi, Acta Metall, **33** (1985), 11.

14. W. B. Li, and K. E. Easterling, Acta Metall. Mater., **38** (1990), 1045.

15. Y. Liu, and B. R. Patterson, Scr. Metall. Mater., **29** (1993), 1101.

16. F. J. Humphreys, and M. G. Ardakani, Acta Mater, **44** (1996), 2717.

17. E. Rabkin, Scr. Mater., **39** (1998), 1631.

18. A. Harun, E. A. Holm, M. P. Clode, and M. A. Miodownik, Acta Mater, **54** (2006), 3261.

19. G. Gottstein, and L. S. Shvindlerman, Scr. Mater., 63 (2010), 1089.

20. R. D. Doherty, D. A. Hughes, F. J. Humphreys, J. J. Jonas, D. Juul Jensen, M. E. Kassner, W. E. King, T. R. McNelley, H. J. McQueen, and A. D. Rollett, Mater. Sci. Eng. A, **238** (1997), 219.

21. X. Song, and M. Rettenmayr, Comput. Mater. Sci., **40** (2007), 234.

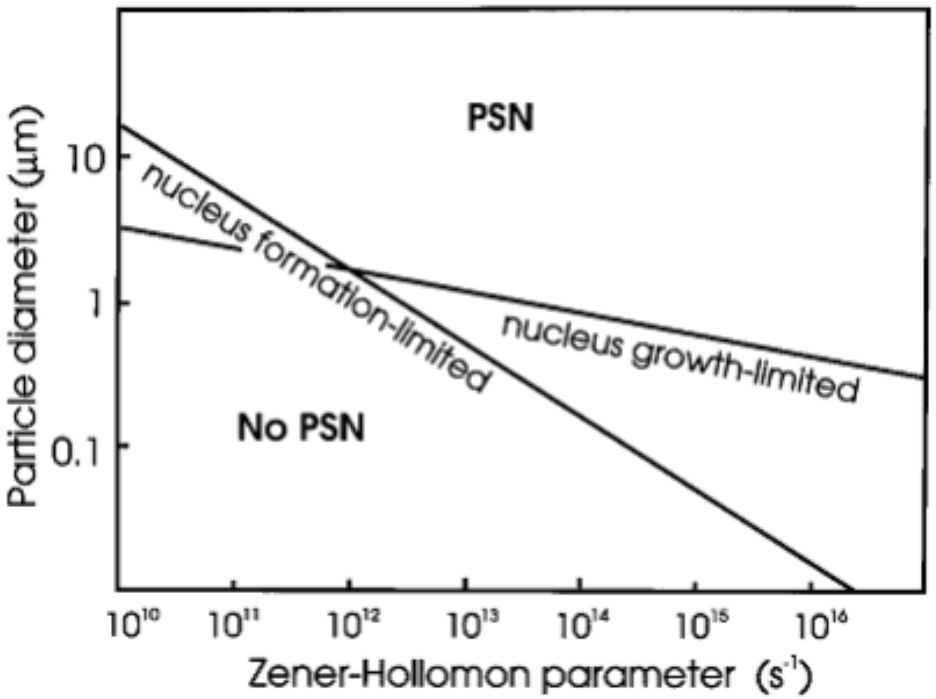

Figure 4.1 Effect of deformation on PSN [1].

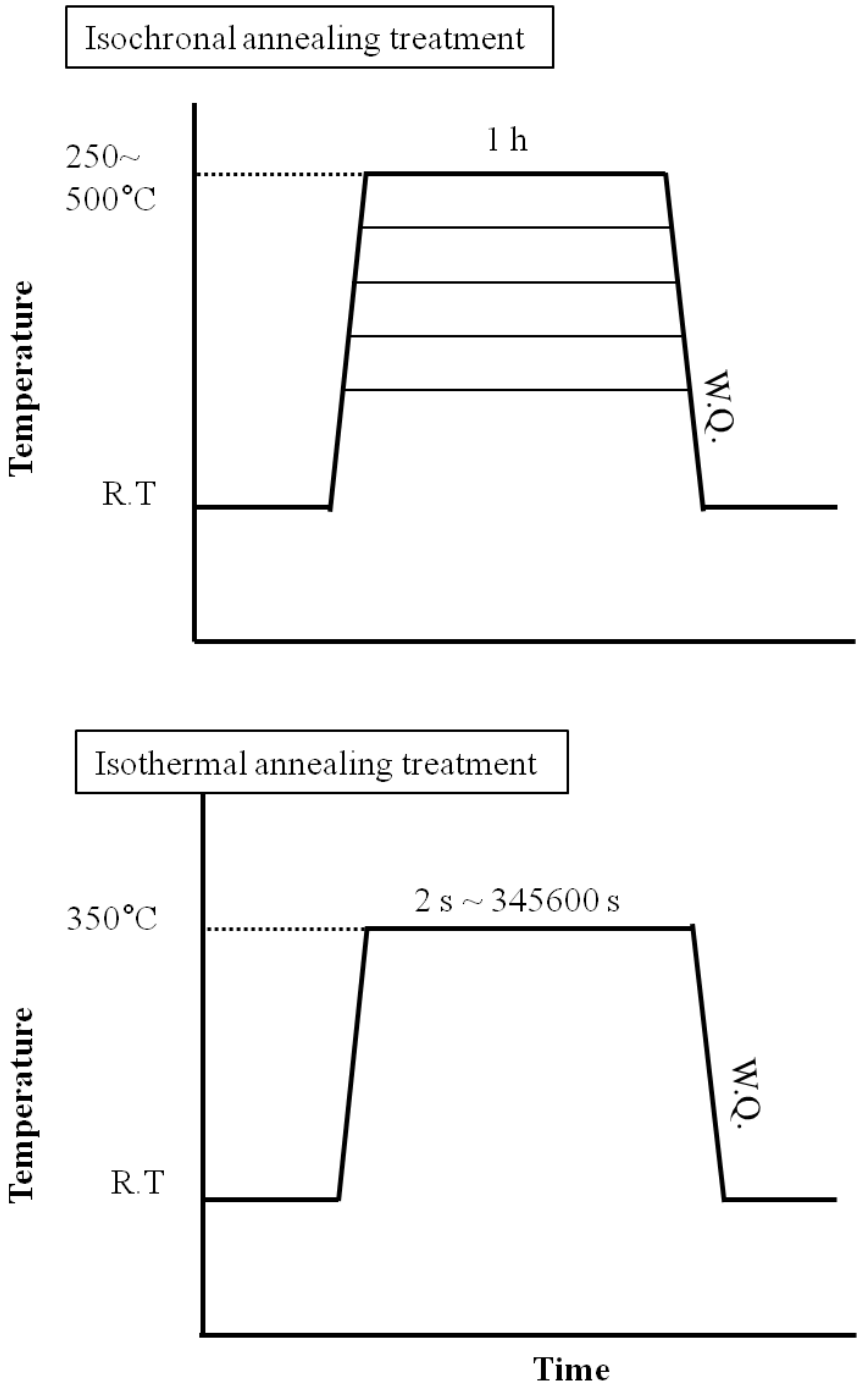

Figure 4.2 Schematic illustrations of annealing treatments.

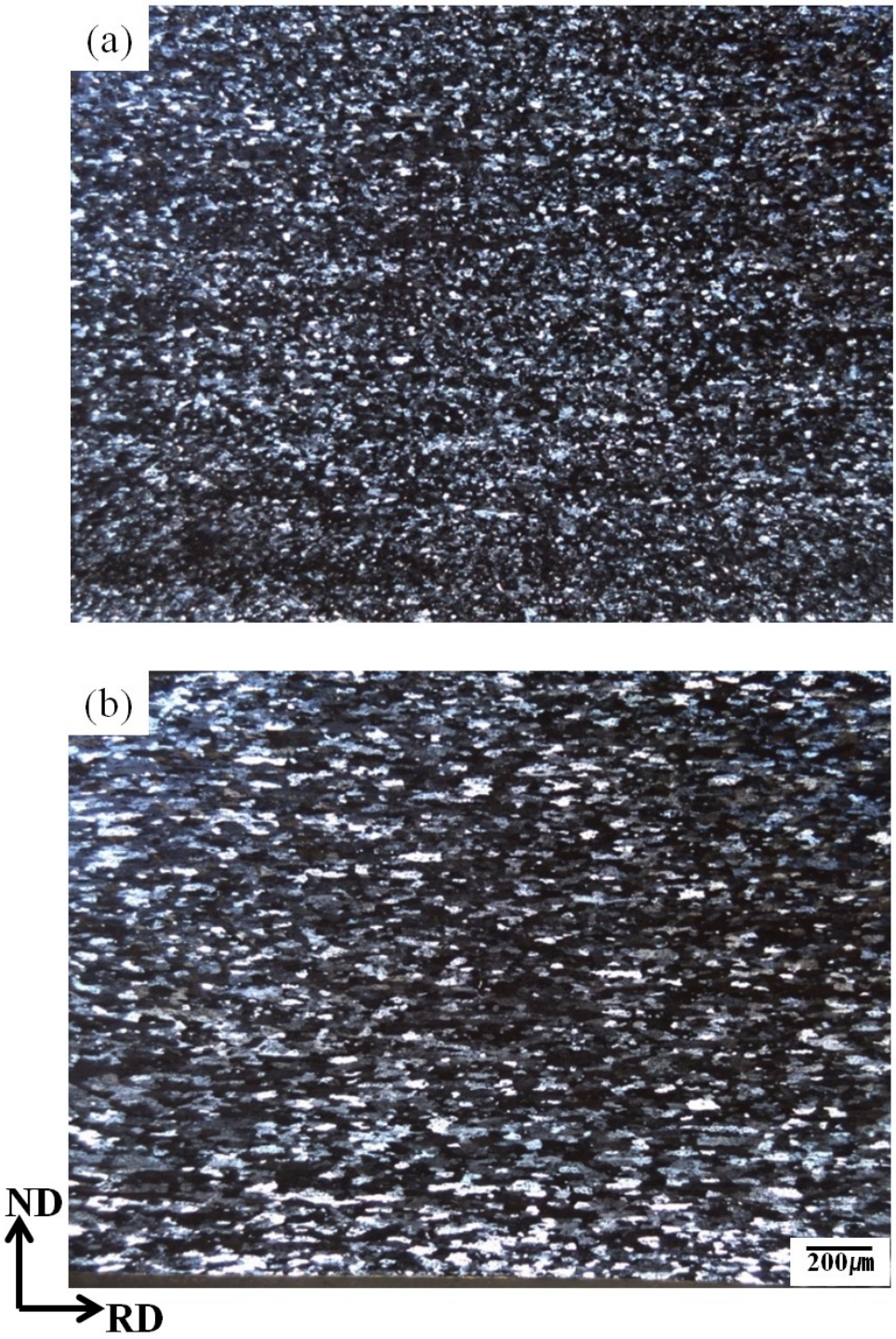

Figure 4.3 Microstructures after isochronally annealed for 1 h at 500 °C, (a) Base, (b) No-Holding, and (c) Slow-Cooling conditions.

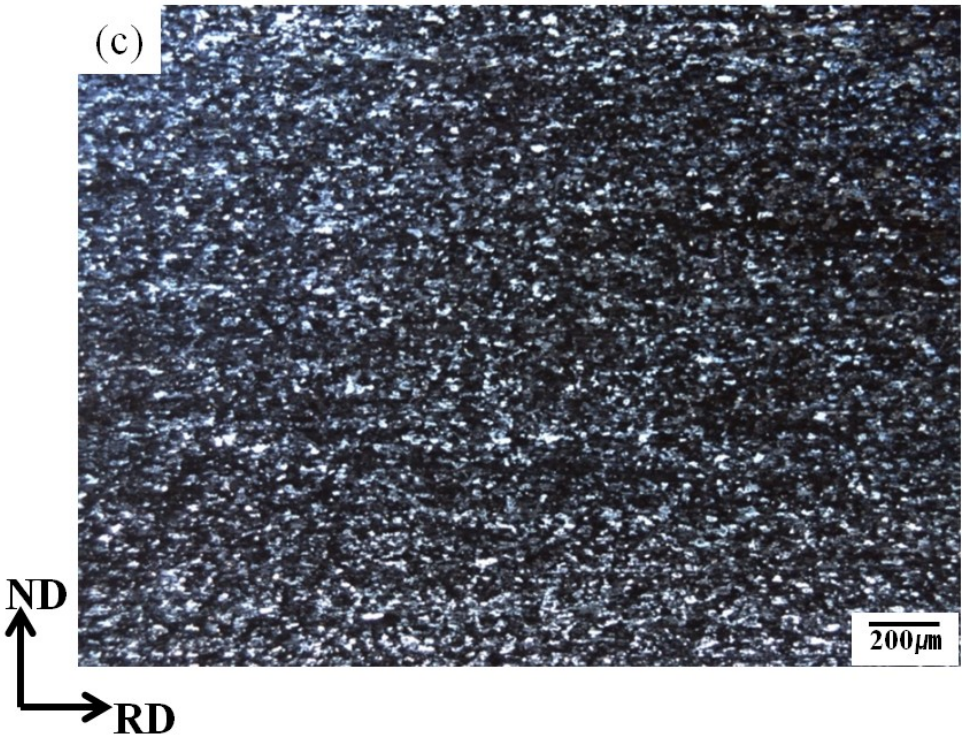

Figure 4.3 Continued.

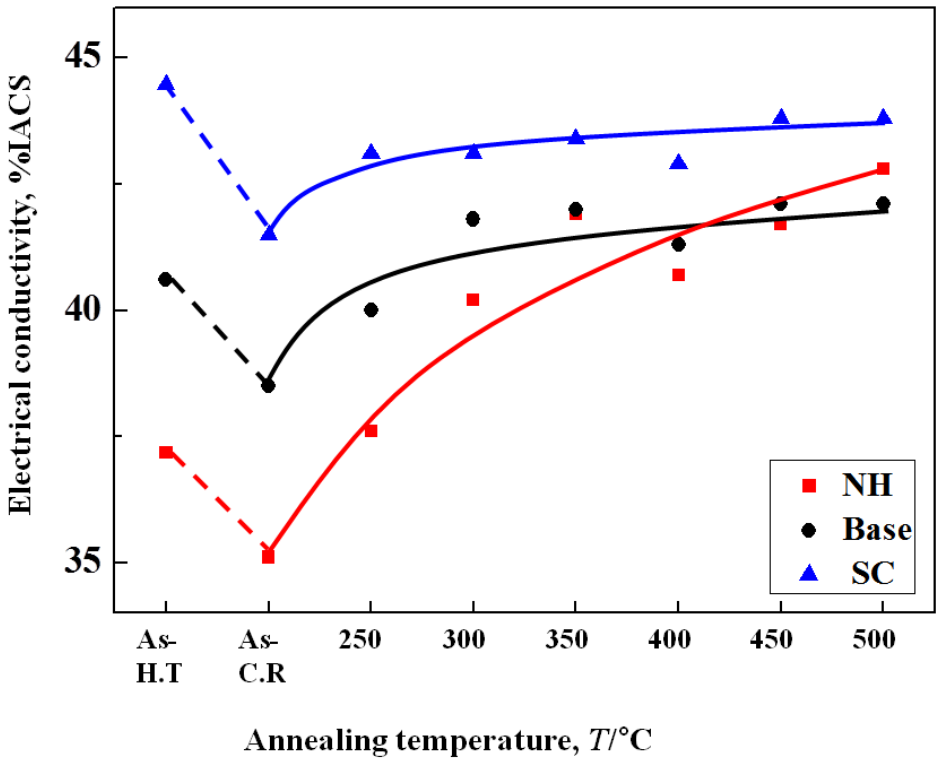

Figure 4.4 Changes of electrical conductivity during isochronal annealing for 1 hour.

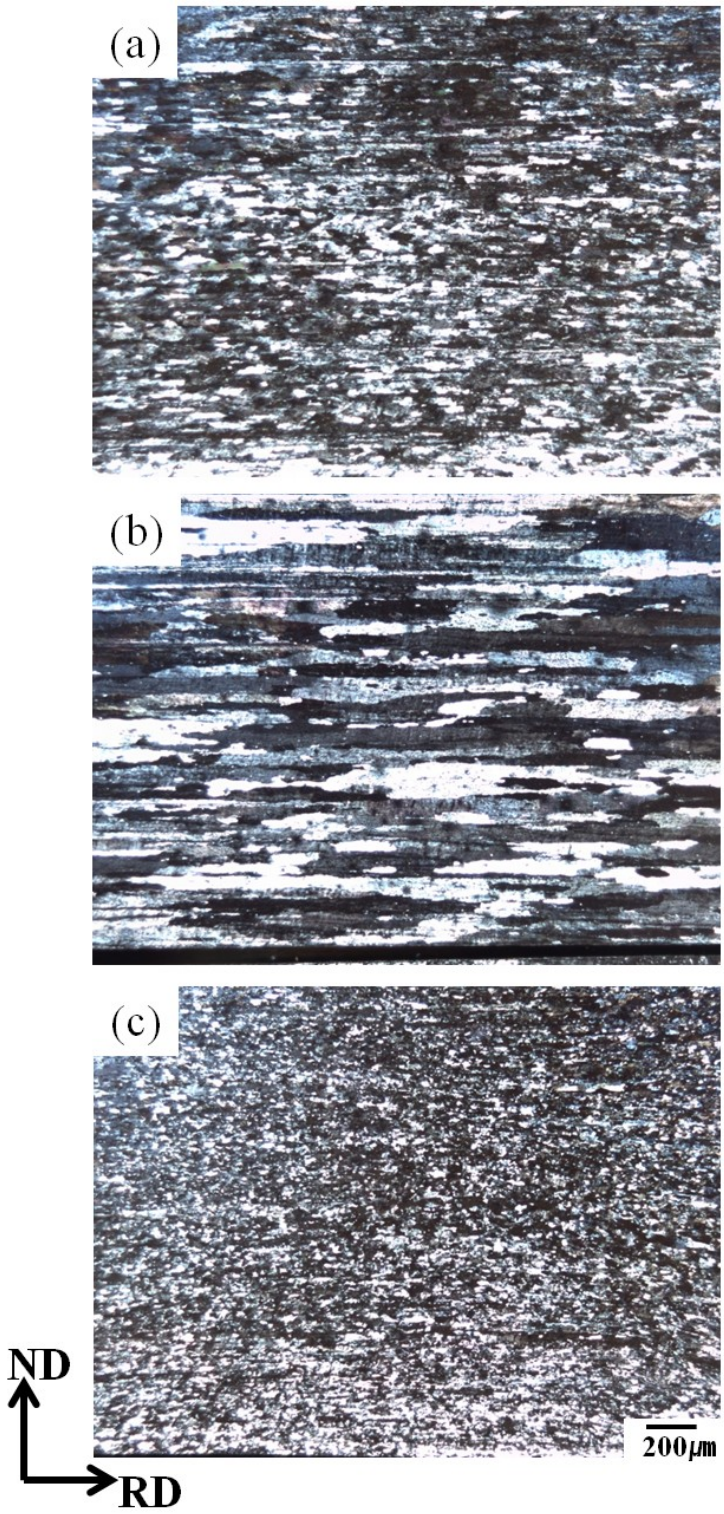

Figure 4.5 Microstructures after isothermally annealed at A area (partial recrystallized) of (a) Base of 300 s, (b) NH of 18 ks, and (c) SC of 60 s.

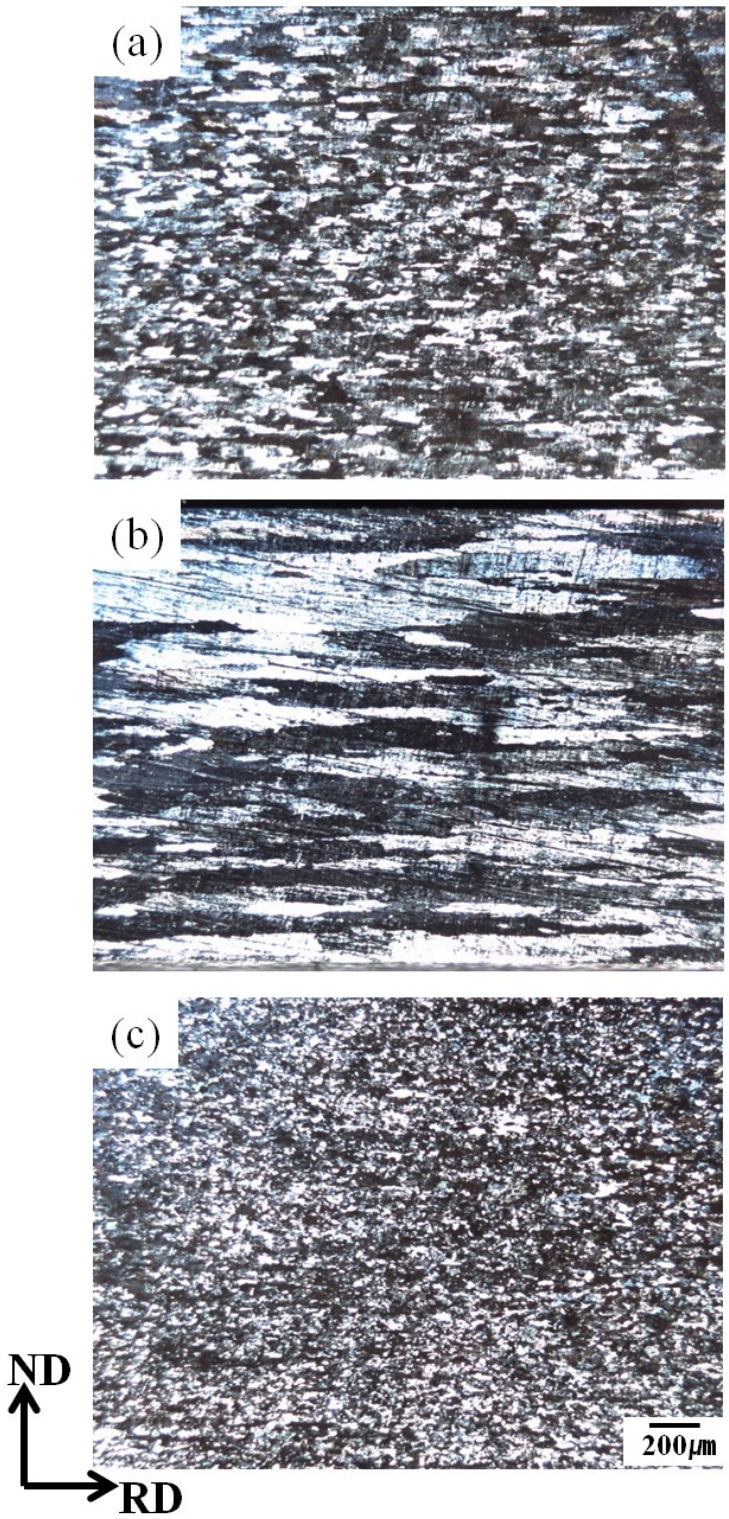

Figure 4.6 Microstructures after isothermally annealed for 345.6 ks at 350 °C (a) Base, (b) NH and (c) SC conditions.

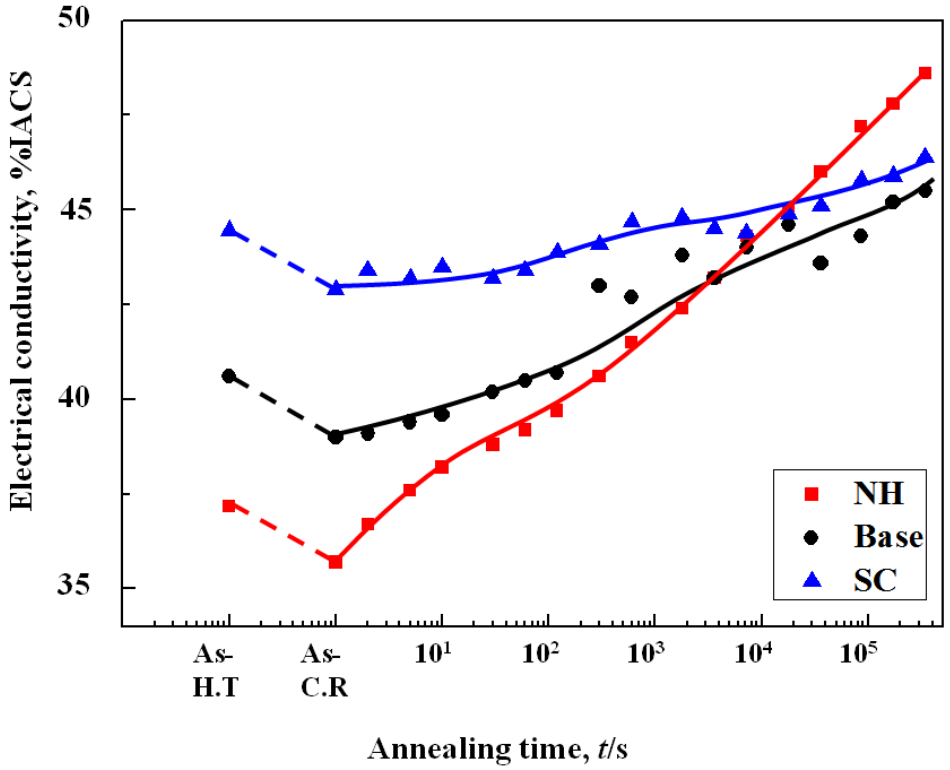

Figure 4.7 Changes of electrical conductivity during isothermal annealing at 350 °C.

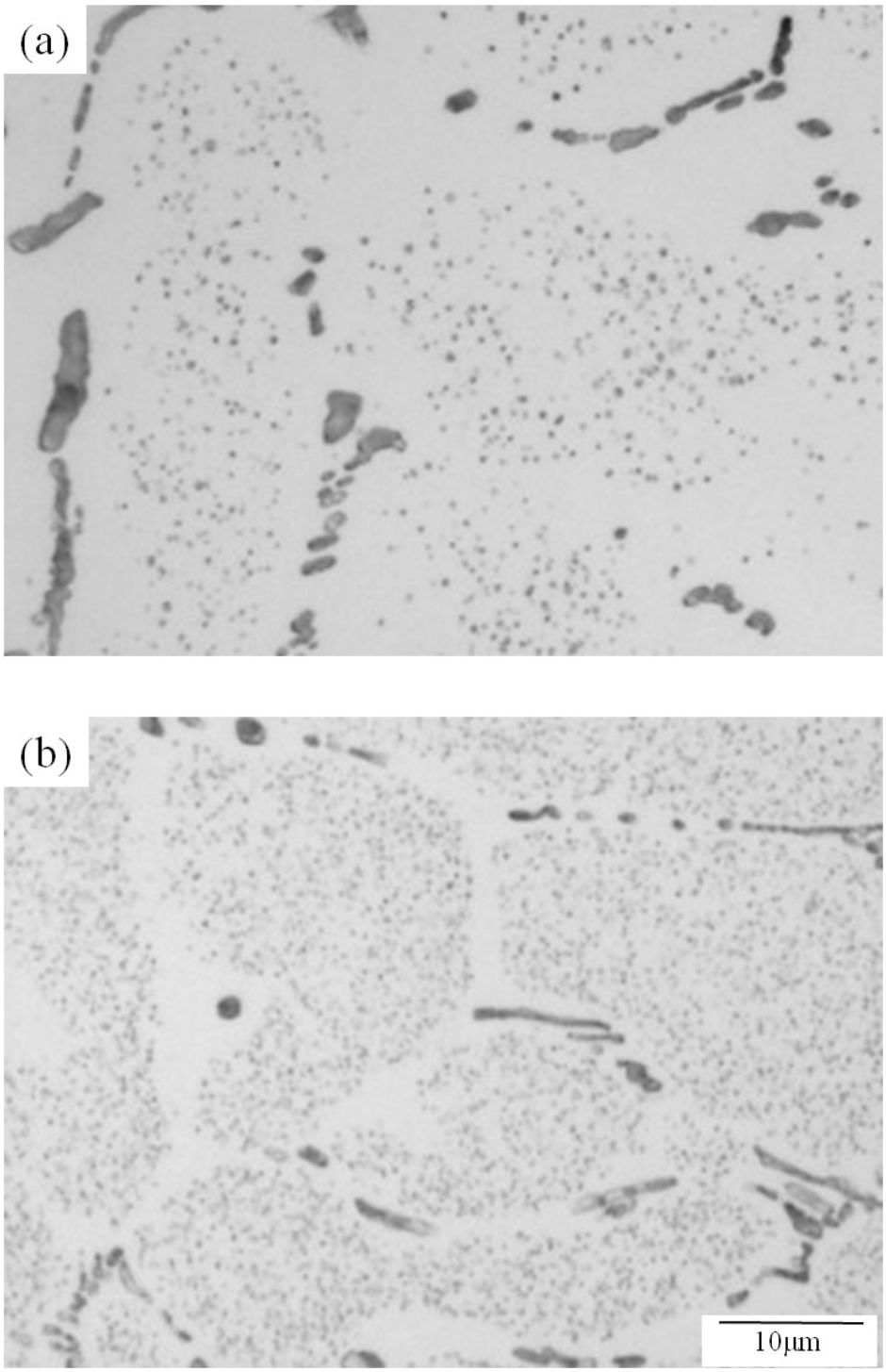

Figure 4.8 Microstructures of specimens after homogenization treatment with (a) Base, (b) No-Holding, and (c) Slow-Cooling conditions.

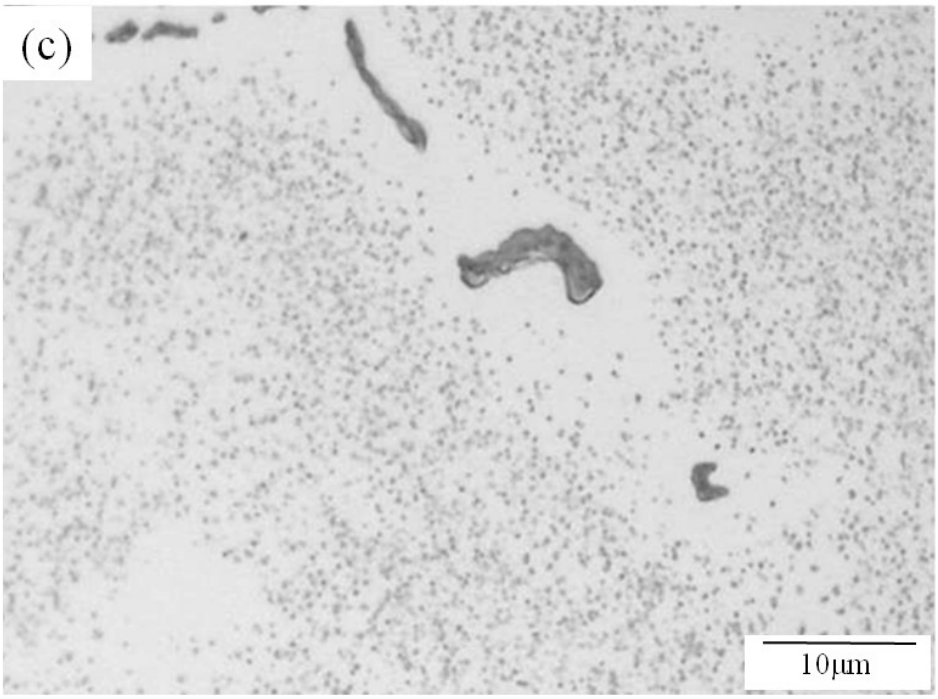

Figure 4.8 Continued.

Table 4.1 Characteristic of precipitates with each homogenization treatment.

	Base	NH	SC
Volume fraction	Medium	Low	High
Number density	Low	High	High
Average size (μm)	0.22	0.14	0.18

Table 4.2 Values of the electrical conductivity, resistivity and concentration of Mn solute atoms after homogenization treatments.

	Electrical conductivity (%IACS)	Electrical resistivity (nΩm)	Mn concentration (wt %)
Base	39.1	44.1	0.57
NH	37.1	46.5	0.64
SC	44.5	38.8	0.40

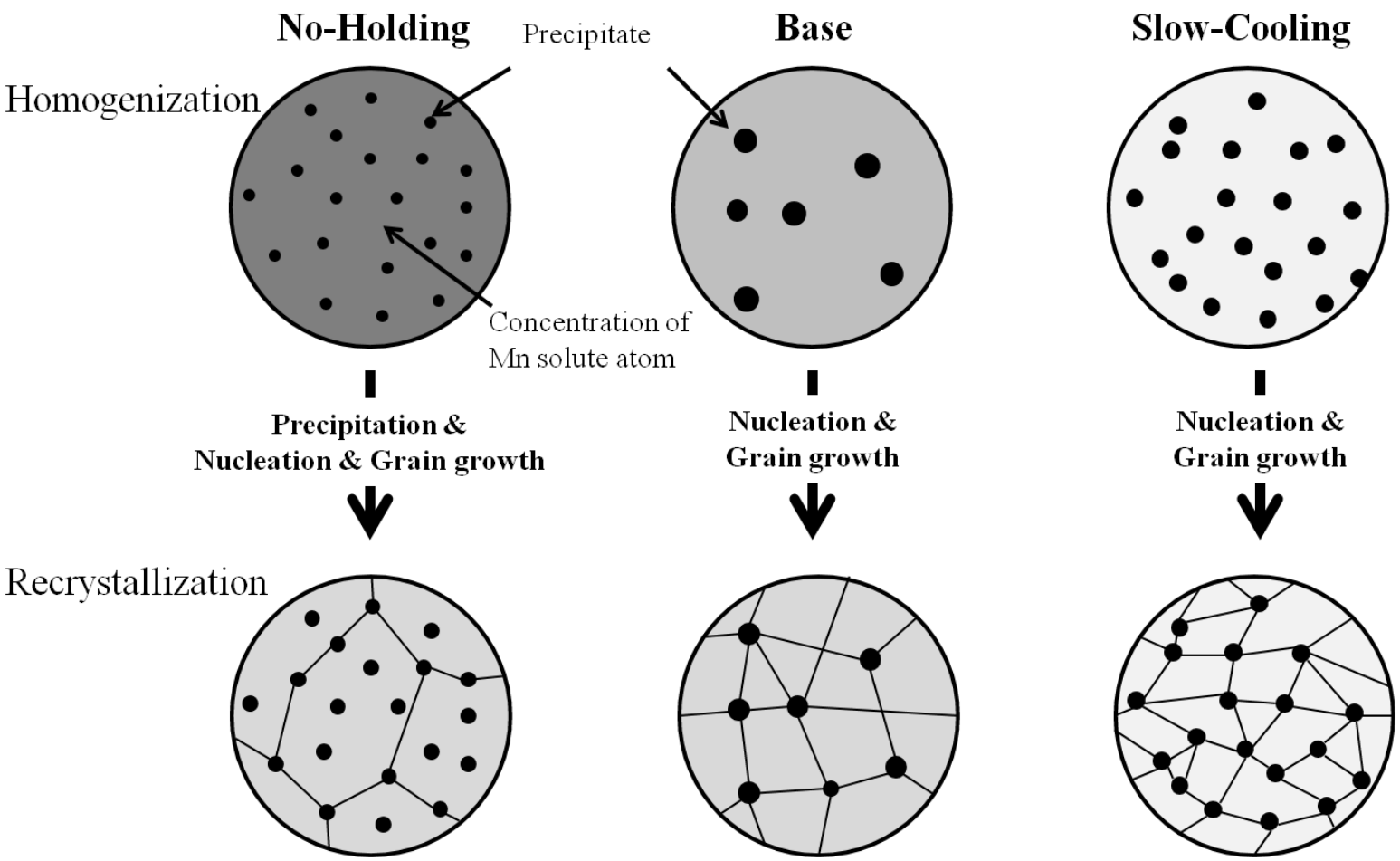

Figure 4.9 Schematic illustrations of recrystallization behavior at high temperature (500 °C)

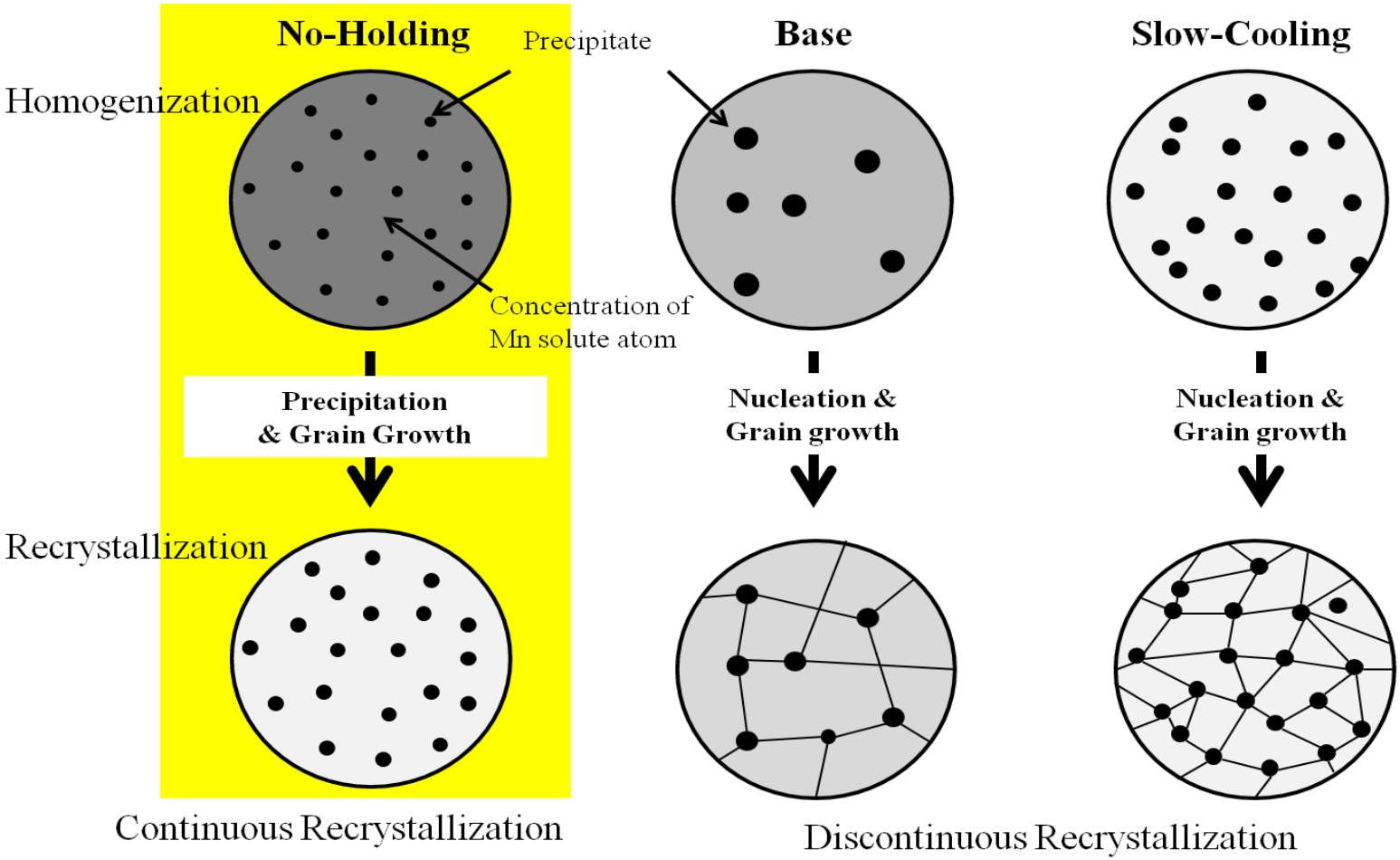

Figure 4.10 Schematic illustrations of recrystallization behavior at low temperature (350 °C)

Chapter 5

Mechanical properties of specimens with different recrystallization microstructures in an Al-Mn alloy

5.1 Introduction

Generally, the principal strengthening agents in 3xxx alloys were primary alloy additions and relevant constituent particles [1-2]. In the conventional Al-Mn alloys, such as the 3003 aluminum alloy, Al_6Mn, α-Al(Mn,Fe)Si and Al_6(Mn,Fe) particles were the main constituent particles [3-4]. The size and amount of intermetallic Mn-containing particles affect the grain structure development during thermo-mechanical processing by stimulating or retarding recrystallization. Strengthening of the material by solid solution hardening is another way; Mn solute atoms influence material properties [5].

The effects of homogenization conditions, Mn containing dispersoids and Mn solute atoms on the recrystallization behavior are discussed in the Chapter 2, 3, and 4.

In this Chapter, the mechanical properties of the specimens with the different homogenization conditions after isothermal annealing treatments at 350 °C are evaluated by the tensile test. Through the evaluation of mechanical properties, the effects of above mentioned factors will be discussed.

5.2 Experimental procedure

The specimens with the No-Holding, Base and Slow-Cooling conditions then cold-rolled by 90 % reduction and annealed at 350 °C for 18 ks, 300 s, and 60 s respectively were prepared. The shape and size of the tensile test sample is shown in Figure 5.1. The tensile tests were performed with a SIMADZU AG-X plus tensile test machine at a strain rate of 0.001 s^{-1}.

5.3 Results

Figure 5.2 shows the true stress-strain curves for the No-Holding, Base and Slow-Cooling specimens after cold-rolled. The No-Holding and Base specimens exhibit larger elongation than the Slow-Cooling specimen containing large and dense precipitates and high density of dislocations. The containing high density of dislocations means that the work hardening already strongly occurred after cold-rolling.

Figure 5.3 shows the true stress-strain curves for the No-Holding, Base and Slow-Cooling specimens after isothermal annealing treatment at 350 °C for recrystallization time as 18 ks, 300 s, and 60 s, respectively. The true stress decreased while the true strain increased in all specimens compared with the results after cold-rolled due to the softening effect.

Figure 5.4 shows the changes of UTS (Ultimate tensile strength) for the No-Holding, Base and Slow-Cooling specimens. The value of UTS is decreased after annealing treatment. It indicates that the specimens become softening completely by recovery and recrystallization.

Figure 5.5 shows the changes of elongation for all specimens after isothermal annealing treatment at 350 °C for the recrystallization time. The values of elongation are increased in all specimens. Especially, the elongation of the Slow-Cooling specimen is increased

drastically while the Base specimen is increased slightly.

The UTS and elongation of all specimens after cold-rolled and annealing treatment are represented in Table 5.1.

5.4 Discussion

5.4.1 Effects of homogenization conditions on the mechanical properties after cold-rolling

The UTS and elongation of all specimens are presented in Table 5.1. The UTS of the No-Holding specimen is higher than that of the other specimens. The hardness of the No-Holding specimen is also higher than that of the other specimens. As a result, the No-Holding specimen is strengthened with solute strengthening and precipitation strengthening. The contribution of dispersoids to the yield strength of alloys, σ_D, due to the Orowan bowing mechanism can be calculated from the Ashby-Orowan equation [6]

$$\sigma_D = \frac{0.84 M G b}{2\pi(1-\upsilon)^{1/2}\lambda} \ln\frac{r}{b} \qquad (1)$$

M is the Taylor factor, G the share modulus of the Al matrix, *b* the Burgers vector of dislocations in Al and υ the poison ratio. The interspacing of dispersoids λ depends on the radius γ and volume fraction f of dispersoids:

$$\lambda = \gamma\left(\frac{2\pi}{3f}\right)^{1/2} \qquad (2)$$

According to the Eq. (1) and Eq. (2), the yield stress due to the precipitation strengthening

increases with increasing volume fraction and decreasing size of precipitates [7]. The No-Holding specimen is quite corresponding to these required conditions. Moreover, the No-Holding specimen contained high concentration of Mn solute atoms compared with other specimens.

5.4.2 Effects of homogenization conditions on the mechanical properties after annealing treatment

After annealing treatment, the UTS decreases with increasing elongation compared with as cold-rolled. It indicates that the softening phenomena occurred during annealing treatment totally at all specimens. Especially, the elongation is drastically increased in the No-Holding and Slow-Cooling specimens. According to the results after annealing, the Slow-Cooling specimen has small recrystallized grains by the discontinuous recrystallization with high number density of precipitates and the No-Holding specimen has elongated large grains by th e continuous recrystallization. The Slow-Cooling and No-Holding specimens certainly exhibit different phenomena. In case of the Slow-Cooling specimen, precipitates with about 0.18 μm are contained with high number density and the concentration of Mn solute atoms in the matrix is lowest after the homogenization treatment. During annealing treatment, the grain refinement is achieved by recrystallization. The grain refinement is an important factor to increase mechanical properties. The fine equiaxed grains cause the increased work hardening due to the generation of dislocations homogeneously, resulting in the increasing the durability for the fracture.

On the other hand, in case of the No-Holding specimen, precipitates with about 0.14 μm are

contained with high number density and the concentration of Mn solute atoms is highest after the homogenization treatment. After the annealing treatment, the elongated grains appeared by the continuous recrystallization at the low temperature as 350 °C. However, the excellent mechanical properties, especially fracture elongation, are obtained. Muggerud et al. reported that a significant dispersion hardening effect can be achieved in 3xxx alloys by low temperature annealing [7]. Based on the electrical conductivity, the precipitation occurred during the annealing treatment. It means that the volume fraction of precipitates is increased after annealing treatment in the No-Holding specimen and the tensile test conducted to the elongated direction of grains. Therefore, the No-Holding specimen exhibits high elongation with high strength due to the precipitation hardening and anisotropy.

5.5 Conclusions

Through the evaluation of mechanical properties, the effects of homogenization conditions, constituent particles and Mn solute atoms on the recrystallization behavior was investigated in the Al-Mn alloy with different conditions such as after cold-rolled and after annealing treatment. The obtained results are summarized as follows.

1. The values of the UTS of the No-Holding, Base and Slow-Cooling specimens are 241.14, 228.60 and 220.21 MPa, respectively. The values of the elongation of the No-Holding, Base and Slow-Cooling specimens are 12.14, 13.65, and 5.50 %, respectively after cold-rolled.

2. After the annealing treatment, the values of the UTS of the No-Holding, Base and Slow-Cooling specimens are decreased, about 175.14, 170.31, and 158.36 MPa, respectively. However, the values of the elongation of the No-Holding, Base and Slow-Cooling specimens

are increased to about 31.13, 16.61, and 34.57 %, respectively.

3. During the annealing treatment, the grain refinement occurred by recrystallization in the Slow-Cooling specimen and the dispersoid hardening, and anisotropy of grain direction occurred by precipitation and the continuous recrystallization in the No-Holding specimen. Especially, the grain refinement has a strong influence on the fracture elongation.

Reference

1. T. Öz, E. Karaköse, M. Keskin, Mater Des **50** (2013), 399.

2. R. S. Rana, R. Purohit, S. Das, Int J Sci Res Pub, **2** (2012), 1.

3. S. P. Chen, N. C. W. Kujipers, S. V. D Zwaag, Mater Sci Eng A, **341** (2003), 296.

4. J. P. Martins, A. L. M. Carvalho, A. F. Padilha, J Mater Sci **44** (2009), 2966.

5. P. C. M. Haan, J .V. Rijkom, J. A. H. Söntgerath, Mater.Sci.Forum **217** (1996), 765.

6. M.F. Ashby, in: AIME Conference Proceedings, New York Meeting Society, New York, (1966).

7. A. M. F. Muggerud, E. A. Møtsell, Y. J. Li, R. Homestad, Mater. Sci. Eng. A, **567** (2013), 21.

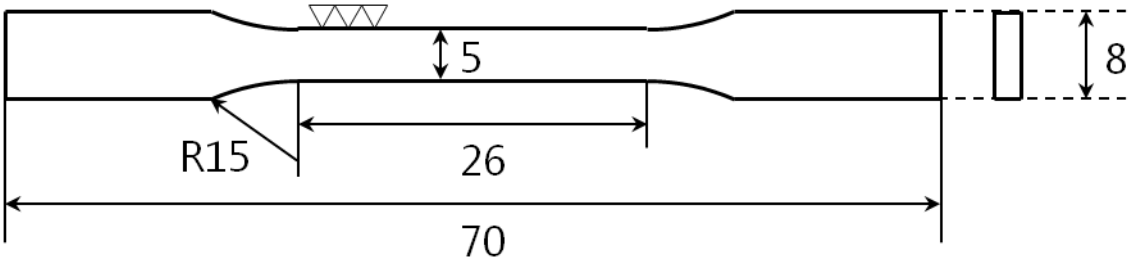

Figure 5.1 Schematic illustration of a tensile specimen.

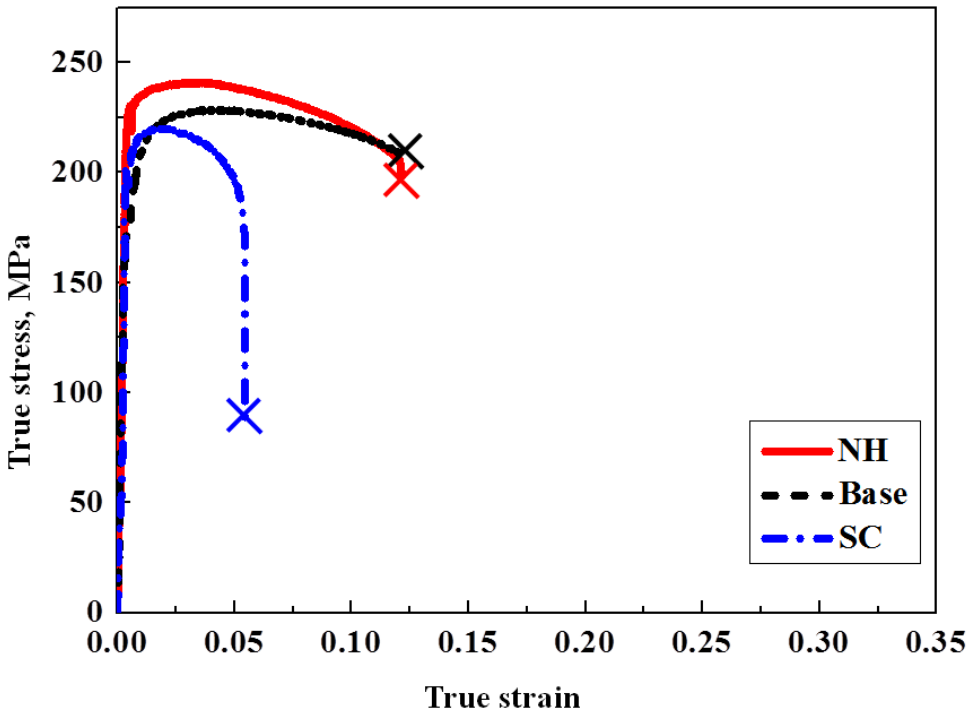

Figure 5.2 Stress-strain curves for the No-Holding, Base, and Slow-Cooling specimens after cold-rolling.

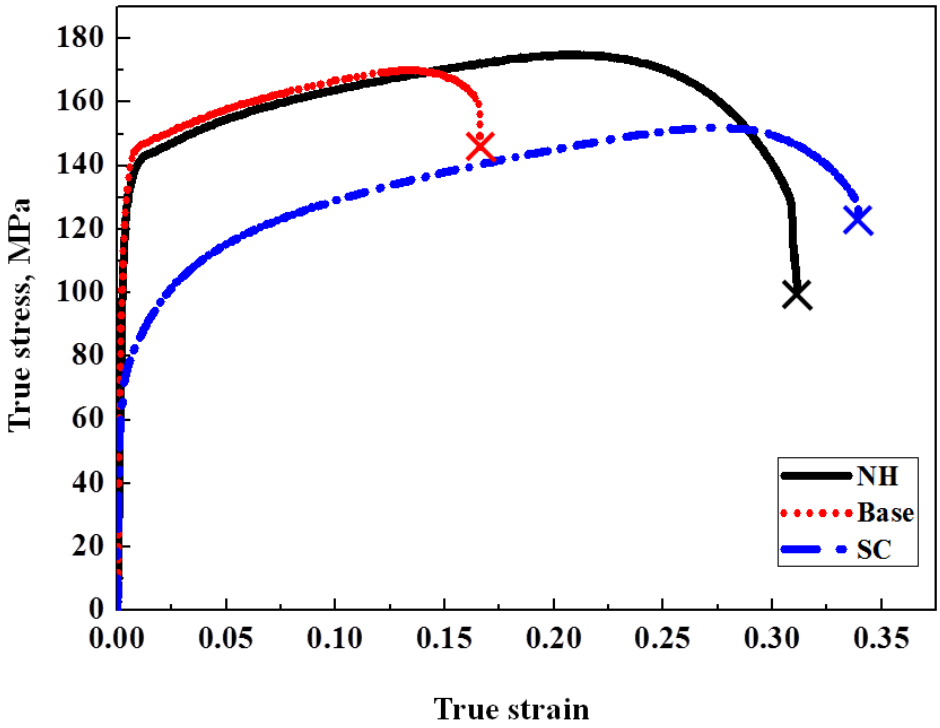

Figure 5.3 Stress-strain curves for the No-Hodling, Base, and Slow-Cooling specimens after annealing treatment at 350 °C for 18 ks, 300 s, and 60 s, respectively.

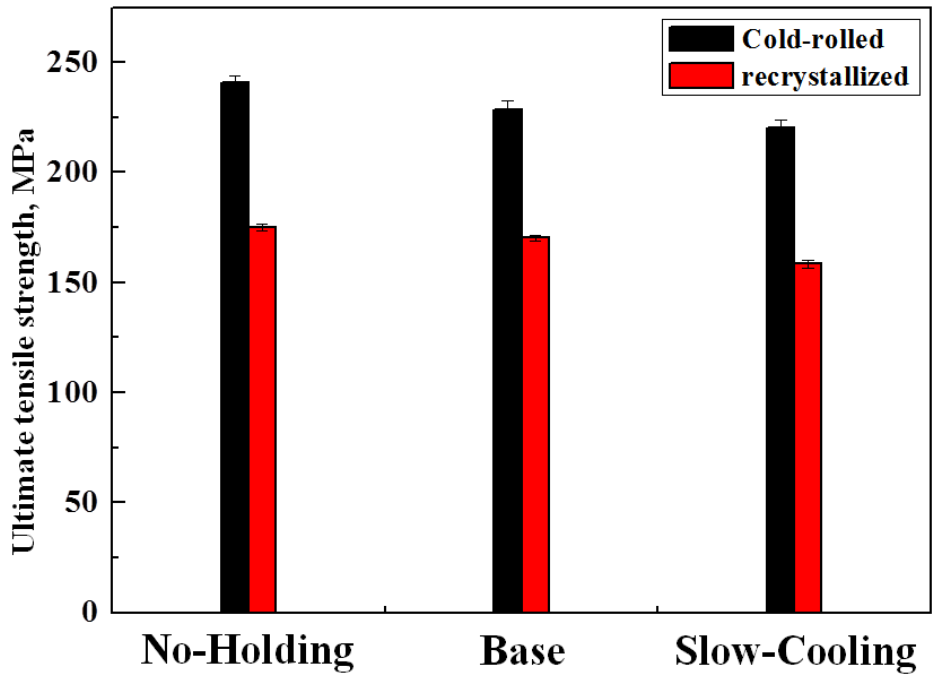

Figure 5.4 UTS values of No-Holding, Base, and Slow-Cooling specimens after cold-rolling and annealing treatment at 350 °C for 18 ks, 300 s, and 60 s, respectively.

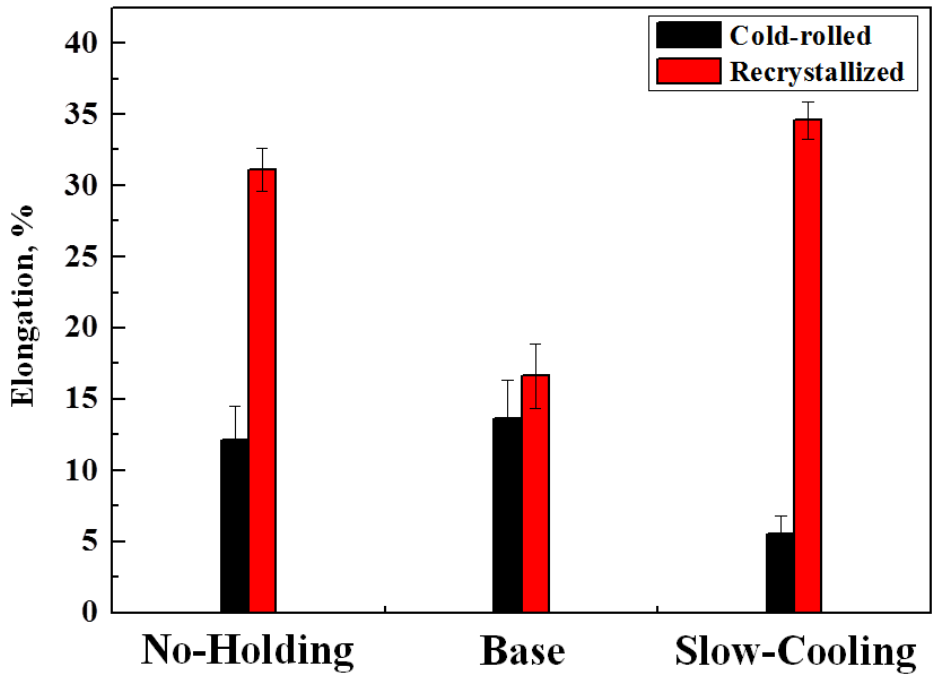

Figure 5.5 Fracture elongation values of No-Holding, Base, and Slow-Cooling specimens after cold-rolling and annealing treatment at 350 °C for 18 ks, 300 s, and 60 s, respectively.

Table 5.1 Values of UTS and fracture elongation for all specimens after cold-rolling and recrystallization.

	Ultimate tensile strength, (MPa)			Elongation, (%)		
	NH	Base	SC	NH	Base	SC
Cold-rolled	241.1	228.6	220.2	12.14	13.65	5.50
Recrystallized	175.1	170.3	158.4	31.13	16.61	35.08

Chapter 6

General conclusions

Al-Mn alloys have a good combination of strength, ductility, formability, corrosion resistance and thermal conductivity. These alloys are widely used for the heat exchanger, can body and building materials mainly in the form of sheets. In the Al-Mn based alloys, the grain size, Mn solute atoms and Mn containing dispersoids in the matrix are known to affect strongly their microstructure and mechanical properties through the thermo-mechanical processes including homogenization, deformation and annealing treatments. The present thesis focused on the effects of Mn containing dispersoids such as size and distribution and Mn solute atoms in the matrix on the recrystallization behavior of an Al-Mn alloy. The objective and mainly obtained results are summarized.

In Chapter 1 "General introduction", background, previous research work and current problems on the recrystallization behavior in Al-Mn alloys, and the objective and outline of the present thesis are presented. The importance of clarifying the relationship between the microstructure controlling by homogenization and the deformation and recrystallization behavior is described.

In Chapter 2 "Formation of Mn containing dispersoids with homogenization treatments and deformation microstructure in an Al-Mn alloy", the transitions of primary particles and precipitates during the homogenization treatment and cold-rolling are described through the microstructure observation, DSC, XRD and electrical conductivity measurements. Three kinds of homogenization treatments are designed by separated heating (No-Holding condition), heating + holding (Base condition), and heating + holding + furnace cooling (Slow-Cooling condition). The No-Holding condition, contained small precipitates with high number density and highest concentration of Mn solute atoms, Base condition, contained large precipitates with low number density and medium concentration of Mn solute atoms, and Slow-Cooling condition, contained medium size precipitates with high number density and lowest concentration of Mn solute atoms, have different dispersoids and Mn concentration produced by homogenization treatments. The primary particles are fragmented and precipitates are distributed more uniformly by cold-rolling with reduction by 90 %. Also, a number of dislocations are generated after cold-rolling. In case of the Slow-Cooling condition, dislocations are more generated due to the high number density of medium size Mn containing dispersoids.

In Chapter 3 "Effects of annealing temperature and time on the recrystallization behavior of an Al-Mn alloy", the effects of annealing temperature and time on the recrystallization behavior, especially the rate of recrystallization behavior, are described through the observation of microstructure and hardness measurement. The recrystallization temperature, T_R, and time, t_R, are different depending on the different homogenization treatments. The recrystallization behavior in the Slow-Cooling condition occurred at 350 °C

for 60 s. At the high annealing temperature, the recrystallization behavior finished completely and recrystallized grains appeared in all conditions. However, at the low annealing temperature, the elongated grains appeared in the No-Holding condition even though annealing time is prolonged. In the No-Holding condition elongated grains are clearly observed after annealing, indicating that the continuous recrystallization occurs. In the other conditions equiaxed grains are observed after annealing, indicating that the discontinuous recrystallization occurs.

In Chapter 4 "Combined effects of Mn containing dispersoids and Mn solute atoms on the recrystallization behavior of an Al-Mn alloy", the role of constituent particles, especially precipitates, and Mn solute atoms on the recrystallization behavior, such as grain size and rate of recovery and recrystallization behavior, is presented. The concentration of Mn solute atoms strongly affects the rate of recovery and recrystallization behavior. The remained Mn solute atoms affect the retardation of the recovery behavior. Thus, the recrystallization behavior is also delayed such as in the No-Holding condition at low temperature. Moreover, the Mn solute atoms are assumed to play an important role to determine the continuous or discontinuous recrystallization. The precipitates affect both the recrystallized grain size and rate of recrystallization behavior. Precipitates not only cause the Zener pinning effect but also contribute the particle stimulated nucleation (PSN) even though the size is smaller than 1μm.

In Chapter 5 "Mechanical properties of specimens with different recrystallization

microstructures in an Al-Mn alloy", the evaluation of mechanical properties before and after the annealing treatment is described through the tensile test. The UTS after cold-rolling is higher than that after annealing treatment due to the softening effect during annealing treatment. Also, the elongation is increased drastically after annealing treatment. After annealing treatment, two types of strengthening mechanism work in the Slow-Cooling and No-Holding conditions, respectively. The grain refinement occurred by the recrystallization in the Slow-Cooling condition and the dispersoids hardening occurred by precipitation at low annealing temperature in the No-Holding condition.

In Chapter 6 "General conclusions", conclusions obtained in each Chapter are summarized. Accordingly, the control of the size, distribution of Mn dispersoids (precipitates) and concentration of Mn solute atoms by using homogenization treatment strongly influence the recrystallization behavior and mechanical properties.